Islet Extracellular Matrix: Characterization & Digestion

Di Shen

Christ Church

University of Oxford

A thesis submitted for the degree of

Doctor of Philosophy in Engineering Science

Trinity 2019

Islet Extracellular Matrix: Characterization & Digestion

Di Shen

Christ Church, University of Oxford

A thesis submitted for the degree of *Doctor of Philosophy in Engineering Science*

Trinity 2019

Abstract

Islet isolation is a minimally invasive treatment that has the potential to reverse Type 1 diabetes mellitus (T1DM) in selected patients. However, the variability of human islet isolation remains a limiting factor in making this treatment more widely available. Considering the shortage of suitable pancreas organ donors and the ongoing increase in incidence of T1DM, research to understand and optimise the islet isolation procedure needs to be made a priority. This forms the basis of the research outlined in this thesis.

This study started with detailed characterization of proteins within the pancreatic matrix at the islet-exocrine interface. These studies demonstrated that the amount of collagen I and laminin decreased with increased donor age and body mass index (BMI) while perlecan increased with these two donor characteristics. These results suggested that tailored digestions are required in order to optimise islet isolation from different donor groups.

Time-dependent characteristics of the dynamic digestion process was then studied. To achieve real-time observation, a post-labelling technique and a specially designed perfusion system were developed and optimised. Focusing on collagen IV and collagen VI, a three-phase digestion profile was revealed.

To further exploit the newly developed system, impacts of enzyme combinations and age-related variations on the digestion phase were also studied. Perfusion experiments confirmed significant difference in enzymatic digestion with different donor ages. The results recommend that a change in enzyme dose or a prolonged digestion time should be conducted in younger donors in order to obtain consistently higher islet yields.

Based on above results, a new digestion system involving an early separation system was therefore developed. Using porcine pancreases for ‘proof-of-principle’ experiments, the new system demonstrates a superiority in islet protection compared with the traditional Ricordi chamber.

Acknowledgement

First of all, I would like to take this opportunity to thank my supervisors Professor Zhanfeng Cui and Professor Paul RV Johnson. Without Prof. Cui, I would never be able to become part of the Oxford family. During my study here, both of them gave me countless help and useful suggestions not only for practical research work but also for critical thinking. Meetings with them have always been efficient and inspiring.

A very special appreciation goes to Dr. Paul Bateman from Nuffield Department of Surgical Sciences, for his valuable and constructive suggestions through my Oxford life. I would never forget his encouragement outside the Natural History Museum. Those words lit my student life and endowed me with courage to continue my research and study in the most difficult time of my DPhil study.

I am so grateful to China Regenerative Medicine International Limited for funding me through my DPhil study. I am also deeply thankful to my present and previous colleagues. I wish to acknowledge the help by Dr. Julian George in engineering design and lab work. Assistance and suggestions on cell-related problems provided by Dr. Chih-Yao Chui and Dr. Sharlayne Waller were greatly appreciated. Advices given by Dr. Shaoyang Yeh, Dr. Cheng Ge, Dr. Xin Liu and Dr. Bo Zhang have been a great help

in my experimental design. I am also grateful to Mr. Haoyu Wu, for his help and support during my time here in Oxford.

I would also like to thank the Oxford Islet Research Group for generously providing me with human pancreatic samples. It was fantastic to work with all of you in the OCDEM building. Thanks for Miss Rebecca Spiers and Miss Rebecca Vaughan, who helped me a lot in entering the islet world. Thanks for Miss Helen Brown and Miss Anju Abraham for sparing your time to provide me with perfectly sectioned tissue samples. Special thanks to Dr. Heide Brandhorst and Dr. Daniel Brandhorst for kindly lending me the Ricordi chamber, allowing me to end the project with a nice comparison.

I am especially indebted to Dr. Ruobing Huang, my great roommate and my best friend. Thank you for your companion and support both morally and emotionally. My life in Oxford would never be so delightful without your participation. Special thanks extended to Mr. Zifu Zhang, for his patience and unfailing support along the way.

Lastly, I must express my very profound gratitude to my parents, Dr. Wei Shen and Ms Yuhua Li. Without their support and love, it would be impossible for me to finish my study here in Oxford. You are and have always been my role model in my life.

Contents

List of abbreviations

2D or 3D	Two- or three-dimensional
ANOVA	Analysis of variance
BMI	Body mass index
CC1	Class I collagenase (CC1)
CC2	Class II collagenase (CC1)
CITR	Islet Transplant Registry
DBD	Donation after Brain Death
DCD	Donation after Circulatory Death
DCCT	Diabetes Control and Complications Trial
DMSO	Dimethyl sulfoxide
ECM	Extracellular matrix
ELISA	Enzyme-linked immunosorbent assay
ESC	Embryonic stem cells
GAG	Glycosaminoglycans
HAS	Human serum albumin
HBSS	Hank's buffer solution

HSPG 2	Heparin sulphate proteoglycan 2
HbA1c	Glycated haemoglobin
IEQ	Islet equivalents
IF	Immunofluorescence
IHC	Immunohistochemistry
ITA	Islet transplant alone
LSM	Laser scanning microscopy
MPM	Multi-photon microscopy
MSC	Mesenchymal stem cells
PDMS	Polydimethylsiloxane
PAK	Pancreas after kidney
PTA	Pancreas transplantation alone
ROIs	Region of interests
SHG	Second-harmonic generation
SPK	Kidney transplantation
T1DM	Type I diabetes mellitus
T2DM	Type II diabetes mellitus
WHO	World Health Organization

List of Figures

List of Tables

List of Publications

Publications

1. Development of a novel perfusion chamber for studying islet ECM digestion in real-time. Di Shen, Paul Bateman, Thomas Griffiths, Paul Johnson, Zhanfeng Cui. Xenotransplantation, 2015 vol: 22 (S1) p: S109.

2. Characterization of pancreas islet-extracellular matrix with multiphoton microscopy. Di Shen, Paul Bateman, Hua Ye, Paul Johnson, Zhanfeng Cui. ***Manuscript in preparation***

3. An *in vitro* study for the time-course effects on pancreatic matrix Digestion. Di Shen, Paul Bateman, Hua Ye, Paul RV Johnson, Zhanfeng Cui. 2018. ***Manuscript in preparation***

Conferences

1. 5th European Pancreas and Islet Transplant Association (EPITA) Winter Symposium & 34th Artificial Insulin Delivery, Pancreas and Islet Transplantation (AIDPIT) Workshop

   Igls, Austria; January 2015

   Poster presentation on *Three-dimensional characterization of the islet-exocrine interface and method development of real-time islet ECM digestion determination*.

2. International Pancreas & Islet Transplant Association (IPITA) ·International Xenotransplantation Association (IXA) ·Collaborative Transplant Study (CTS) Joint Congress

   Melbourne, Australia; 12-23 November 2015

   Poster presentation on *Development of a perfusion chambers for real-time islet ECM digestion observation*.

3. IPITA 16th International Congress

   Oxford, the United Kingdom; 20-23 June 2017

   Oral presentation on *Development of a purpose-designed system for studying real-time digestion of the pancreatic matrix*

   Poster presentation on *Development of a method for characterization of pancreas islet-extracellular matrix with multiphoton microscopy*

Chapter 1

Introduction

1.1 Clinical motivation

Type 1 diabetes mellitus (T1DM) is a metabolic disorder resulting from the autoimmune destruction of the insulin-producing cells within the pancreas [1], [2]. Exogenous insulin administration is the mainstay treatment for maintaining stable glycaemia [3]. Over the last decade, insulin delivery has become more sophisticated, with mechanical insulin pumps being increasingly used. However, for a subset of patients, fluctuating glycaemia is associated with the development of chronic complications and more frequent pulmonary-edema, cerebra-edema, infarctions of the brain and cervical spinal cord even with tight glucose control [4]–[6]. Part of the reason is attributed to the failure in restoring the precise glucose homeostasis [7].

One treatment approach for reversing life-threatening hypoglycaemia unawareness is to replace the insulin-producing beta cells through transplantation. This can either be in the form of a whole pancreas transplant or a selective islet cell transplant [8], [9]. Compared to whole pancreas transplantation, islet transplantation is particularly safe and, with a wide range of applicability [8].

Outcomes for this treatment method have improved dramatically since the first clinical islet transplantation in 1977. Insulin independence, enduring graft function and most importantly, the reduction of life-threatening hypoglycaemic episodes have been reported [10]. Nevertheless, the application of this technique is limited by a shortage of transplantable islets. The relatively low isolation yield with ongoing variability of human islet isolation has long been discussed [11]. One of the primary reasons for this is that the methods currently used are generic for all donor pancreases, rather than

targeted or tailored based on various donor groups. Research in this area is limited by several challenges:

1. A lack of detailed understanding of the correlation between pancreatic structure and donor characteristics in healthy subjects [12]. More specifically, studies conducted in pancreatic extracellular matrix (ECM) analyses are based on 2-dimensional (2D) images obtained from 8-15μm thick sections, while the 3-dimensional (3D) structure of ECM surrounding an entire islet is currently absent. Moreover, most research focused on the impacts of donor age while the effects of BMI have been overlooked;
2. A lack of detailed understanding of the dynamic tissue dissociation process. Previous studies have been conducted on static digestions and as clinical isolation is a continuous process [13], it is desirable to investigate the process in a similar environment;
3. The apparatus used in current clinical isolation was designed based on a grinding mechanism [14], which may result in damage of islets [15] and therefore affect their viability and functionality. Although 30 years have passed since its proposal, there were few modifications and the apparatus remained unchanged.

To address the challenges above, this thesis aims to use biological and engineering techniques to investigate and improve islet isolation with respect to donor-rated variables. The main objective seeks to deepen the understanding of digestion phase and to develop engineering tools promoting research on the improvement of isolation yield

for specific donor groups. More specifically, this includes:

1. To improve current understanding of pancreatic ECM in relation to donor age and BMI and development of a tool enabling 3D analysing the peri-islet ECM structure in its native state. This not only helps to answer donor-related variations faced by islet isolation but also forms a solid base for further analyses.
2. To investigate the dynamic digestion process of this substrate at molecular level. This includes development of a specific tool enabling real-time observations and proof-of-concept experiments using this novel system;
3. Based on previous results, to develop a new bioreactor with better fitting to islet isolation process for younger donors. This includes reducing fragmentation for prolonged isolations and proof-of-concept experiments using porcine pancreases.

1.2 Thesis structure

To approach the proposed aim, the thesis is divided into 4 sections.

Chapter 2 presents a detailed literature review of current research on islet transplantation and related topics. The chapter starts with an overview of diabetes and its economic and social impact. With a focus on type 1 diabetes mellitus, discussions on its current management methods are discussed. This chapter also includes pancreas and islet anatomy, with an emphasis on the substrate of islet isolation, the pancreatic extracellular matrix (ECM). Compared with insulin therapy and pancreas transplantation, the history and outcomes of clinical islet transplantation are described. One of the ongoing challenges, the shortage of transplantable islets, is highlighted with

discussions on improving isolation yield from donor related variables, dissociation enzymes and apparatus.

Chapter 3 presents an investigation of pancreatic ECM and its variation with respect to donor characteristics. The 3D structure of pancreatic ECM surrounding an intact islet was studied using a multi-photon microscope. For this purpose, a new protocol for staining an intact islet was developed. Based on an established method using immunofluorescent staining [13], [16], the presence of common ECM proteins, including collagen I, collagen III, collagen IV, collagen VI, laminin and perlecan, were studied within donors of different age and BMI. Through measurement of fluorescent intensity, quantification analyses were conducted to reveal the effects of these two donor characteristics.

Chapter 4 reports the development of a novel system designed for the study of time-course effects of enzymatic dissociation process. This was achieved by developing a post-labelling technique for the digestion of specific pancreatic ECM proteins. A specifically designed perfusion chamber was used in connection with a recirculating pump and proper temperature control. The system was optimized in terms of temperature and perfusion speed while its application in observing the digestion of collagen IV and collagen VI was present.

Chapter 5 further exploits this designed perfusion system in observing real-time digestion of collagen IV and collagen VI. Based on findings from Chapter 3, the impact of donor age was studied using different enzyme combinations. The characteristics of the digestion phase were shown with discussions on the competing nature between

collagenase and neutral protease. Based on the results, prolonged digestion for pancreases from younger donors was proposed.

Chapter 6 shows the development process of a new bioreactor for prolonged islet isolation, as suggested in Chapter 5. An early-separation system was proposed and built. To reveal the performance of this device, animal tests using juvenile pig pancreas were conducted with analyses on the morphology, yield and purity of isolated islets. The performance of this new device compared to the original Ricordi chamber was also investigated.

Chapter 7 concludes the contribution of this thesis. Findings and relevant clinical applications were further discussed. Improvements and potential future work were subsequently suggested.

Chapter 2

Literature review

2.1 Type 1 Diabetes mellitus: burden and management

2.1.1 The burden of diabetes mellitus

Diabetes mellitus is a metabolic disease characterized by long-term hyperglycaemia which leads to severe complications. As discovered by Gepts [17], it is clear that two primary forms of diabetes exist: Type 1 diabetes mellitus (T1DM), which is caused by the loss of insulin-producing β-cells under autoimmune attack [1], [2], and Type 2 diabetes mellitus (T2DM), caused by insulin resistance and insulin deficit [1], [18]–[20]. As the main anabolic hormone in human metabolic system [21], the consequence of insulin deficiency is hyperglycaemia with characteristic symptoms such as thirst, polyuria and weight loss. Without glycaemic control or effective treatment, a non-ketotic hyperosmolar state or ketoacidosis can be developed, leading to stupor, coma or even death [22].

Despite the acute symptoms, progressive insulin deficiency can lead to dysfunction and eventually failure of many organs. The long-term effects include life-threatening conditions like diabetic ketoacidosis and other chronic complications in the forms of nephropathy, retinopathy, neuropathy and cardiovascular disease. These would not only severely affect the patient's health condition, increase the cost for treatment and health care, but may lead to mortality. Studies have shown that an increase of 1% glycated haemoglobin (HbA1c) level, a form of haemoglobin that could covalently bound to blood glucose, is linked with an 15-17% increase in the risk of cardiovascular events [23], a 17-36% increase in the risk of overt nephropathy, a 8-33% increase in the

risk of heart failure and a 5-19% increase in the risk of death [24].

In the United Kingdom, the diagnostic criteria follow the standard published by the World Health Organization (WHO): diabetes symptoms plus a random venous plasma glucose concentration ≥11.1mmol/l (200mg/dl), or a fasting plasma glucose concentration ≥7.0mmol/l (126mg/dl) or a 2-hour plasma glucose concentration ≥11.1mmol/l (200mg/dl) 2 hours after an oral glucose tolerance test [25].

Diagnosis using the HbA1c tests is also adapted. As the average life span of red blood cells is about 120 days, tests of HbA1c could reflect the patient's average blood glucose level for the past 2-3 months [26]. The diagnostic criteria according the 2011 WHO report is ≥48mmol/mol (6.5%) [27].

Of all the diabetes patient, about 10-15% are diagnosed with T1DM. With an incidence rates up to 50,000-100,000 population per year in western countries, it is also the most common metabolic disease in childhood [28]. To achieve normal glycaemic control, these patients require exogenous insulin administration. Due to the lack of autopsy studies, current understanding of the disease progression is fragmentary. Some report the process is caused by a $CD8^+$ T cell-mediated autoimmune reaction against islet β-cells antigens in genetically susceptible individuals [29]. The reaction may be initiated by certain environmental triggers [1], [29], possibly due to protection against infectious agents [30], resulting in an increasing trend for T1DM.

Being the cause of 382 million patients and 5.1 million deaths in 2013 [31], diabetes has already become a worldwide concern. Until 2016 there were 415 million patients diagnosed worldwide [32] and according to International Diabetes Federation,

this number will continue rise to 592 million in 2035 [33]. In the United Kingdom the number of diabetes patients has doubled to 3.8 million since 1996 [34], costing the NHS about £10 billion each year [35]. For T1DM, the prevalence rate increased at 4% each year for the past 20 years [36]. Among 400,000 T1DM patients, over 29,000 of them are children [36]. Direct patient care for these patients has cost NHS £1 billion with another £0.9 billion spent for indirect cost such as increased illness and death [37]. Nevertheless, these numbers were estimated to be £1.8 billion and £2.4 billion, respectively, in 2035 [37]. This booming trend, together with the huge economical cost, lead to an urgent requirement for a proper and efficient treatment method.

2.1.2 Management of type 1 diabetes mellitus

Glycaemic control of T1DM is balanced between diet, exercise and exogenous insulin administration. Consumption of food leads to a direct increase of blood glucose level, where carbohydrates are broken down into monosaccharide and transported to portal vein in the small intestine [38]. Healthy diet is therefore essential for glucose homeostasis. Exercise and sport, however, have diverging effects depending on the utilization of energy substrate [39], [40]. For T1DM patients doing prolonged aerobic exercise, hepatic glucose production fails to match muscular glucose disposal, leading to hypoglycaemia. On the other hand, during intense anaerobic exercise, glucose production by the liver exceeds glucose utilization of the working muscles. With a failure in circulating insulin level, hyperglycaemia can occur. Consequently, to achieve glucose homeostasis, the amount of exogenous insulin administration needs to be

carefully adjusted. Nevertheless, even with insulin therapy, morbidity and mortality caused by long-term complications are still inevitable [41].

In 1993, the benefits of strict glycaemic control were reported from a 5-year study carried out by Diabetes Control and Complications Trial (DCCT) Research Group. It is reported that compared to less-strict insulin administration (≤2 daily insulin injections), intensive management (≥3 daily insulin injections) significantly delays the onset and slows the progress of renal failure, blindness and heart disease in T1DM patients [41]. Follow-up studies confirmed their findings in terms of glomerular filtration rate, risk of cardiovascular disease and risk of progressive retinopathy [42], [43]. Therefore, at present, most patients employ intensive exogenous insulin regimens to mimic physiological insulin release. This involves daily subcutaneous injections of long-acting and rapid-acting insulin, or the use of a subcutaneous insulin pump.

Despite its advantages in delaying chronic complications, intensive insulin therapy relies on artificial insulin and fails to restore the intricate balance of normal glucose homeostasis [44]. Part of the reason is due to a lack of continuous blood glucose level monitoring and prompt insulin release. Further to this, using the HbA1c tests, a persistent gap between attained and target glucose level was reported in several multicentre studies [45].

The complexity of islet structure, synergetic effect among different islet cells and its connections with surrounding vascular and nerve network also aids in this process, which is unfeasible in exogenous insulin administration. This leads to an imbalance between insulin and physiological needs, resulting in frequent and severe

hypoglycaemia. A 2- to 3-fold increase of life-threatening hypoglycaemia episodes has been reported for patients undertaken strict glycaemic control [46] and the rate is even higher among adolescent patients [45]. On average, T1DM patients experience two hypoglycaemia episodes a week and one disabling hypoglycaemia episode a year [47], [48]. The mortality of T1DM patients caused by this adverse event is estimated to be 2-4% [49]. To avoid severe organ or brain damage, hypoglycaemia requires prompt recognition and treatment. However, recurrent hypoglycaemia results in impairment of counter-regulatory system and may lead to impaired hypoglycaemia awareness [50], vascular disease, brain damage and significantly impair the patients' quality of life. For children with T1DM, severe hypoglycaemia increases the risk of cognitive dysfunction, brain abnormalities and structural brain changes [51].

Improvements in technology have enabled a closed-loop system with continuous sensor and computerized program for insulin dosage to be developed. Different prediction regimes have been proposed and preliminary results seem to be promising. In a recent study, a fully closed-loop insulin-only system could reduce 50% of hypoglycaemia events [52]. Nevertheless, the intrinsic glucose homeostasis is not restored and glucose control relies heavily on sensor accuracy [7]. These together with the inherent risk of pump failure limit its application. Treatment methods to achieve precise restoration of glucose homeostasis with a more physiological approach are highly demanded.

Further to this, even with tight control, the blood glucose level for certain T1DM patients can be severely unstable. These patients experience unpredictable blood

glucose swings from hyperglycaemia to hypoglycaemia. These episodes cause disruptions to patients' quality of life and the patients are termed as "brittle" diabetes patients. Stressful life circumstances are often accompanied with these patients, resulting in a higher prevalence rate of psychiatric disorders [6]. Compared to the "stable" cohort, brittle diabetes patients are associated with more frequent pulmonary-oedema, cerebra-oedema, infarctions of the brain and cervical spinal cord [6]. Extreme cases of permanent disability and higher risk of death have been reported [4], [5]. For those patients, an accurate and real-time continuous glucose monitoring system is highly desirable. Considering limitations of current monitoring system mentioned above, restoring endogenous insulin secretion provides a promising alternative to treat brittle diabetes patients. In fact, a study comparing intraperitoneal insulin infusion through an implantable pump and intraportal islet transplantation for brittle diabetes patients reported better metabolic results were obtained with the latter method [53].

Despite many regimens developed for T1DM management, the glucose control of endogenous islet cells has yet to be replicated. Replenishment of insulin-releasing β-cells in diabetic patients is one way to achieve tight glycaemic control. However the replication of these cells peaks in gestation and is rarely observed in mature adults [54]. Consequently, transplanting insulin-producing tissue from an organ donor is highly desirable.

2.2 Anatomy of the human pancreas

2.2.1 Pancreas

Human pancreas is a yellow-pinkish gland located in the upper left part of the abdomen, connecting the duodenum in the head region and the spleen in the tail region. The anatomy of pancreas is shown in **Figure 2.1**. It has an elongated shape with a length of 14-20cm and an average weight of 80g (range 45-120g) for healthy adults. The pancreas develops from two endodermal buds on the dorsal and ventral side of the duodenum. The two buds are then rotated and fused in the later stage of embryonic development to form dorsal and ventral pancreas [21], [22]. Part of pancreas head arises from ventral part while dorsal part develops into body, tail and the rest of the head part. Blood supply for ventral pancreas is from the mesenteric artery while celiac artery irrigates the dorsal part.

The gland is composed of small lobules, and secretes both endocrine hormone and exocrine digestive enzymes. Exocrine cells comprise 98% of pancreatic cells and are arranged into acini surrounded by small intercalated ducts, which fuse into intralobular ducts, interlobular ducts and finally the main pancreatic duct that connects to the duodenum. Exocrine cells secret proenzymes that are cleaved and activated in the duodenum to aid the digestion of food. These includes protease like trypsin for protein digestion, amylase for carbohydrate digestion and lipase for lipid breakdown [57]. Endocrine cells comprise only 2% of the parenchyma [1] but are of extreme importance to glucose homeostasis.

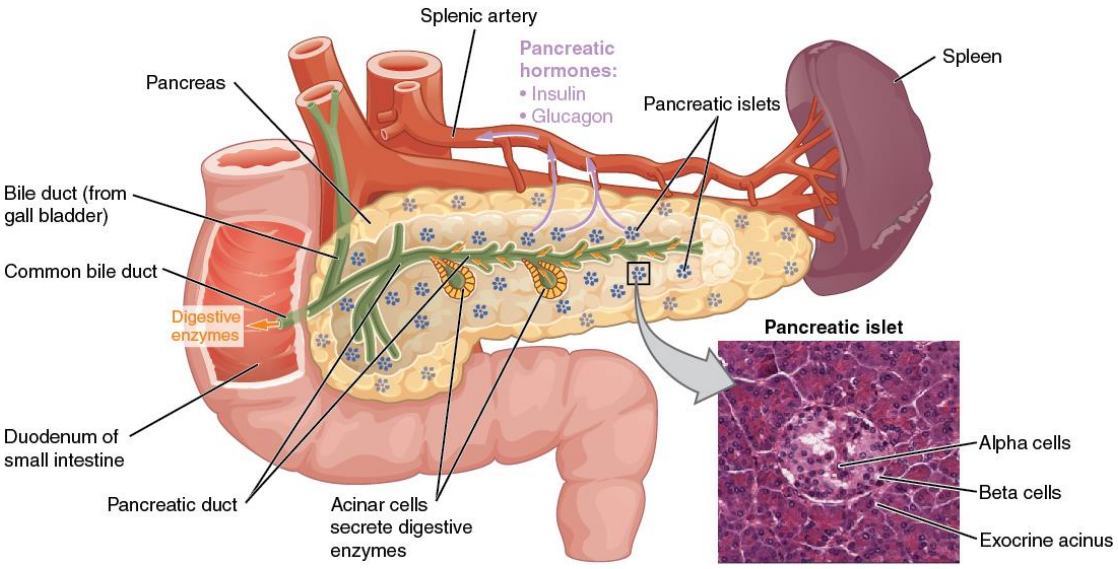

Figure 2.1 Anatomy of pancreas. The pancreatic exocrine function involves the acinar cells secreting digestive enzymes that are transported into the small intestine by the pancreatic duct. Its endocrine function involves the secretion of insulin (produced by β-cells) and glucagon (produced by α cells) within the pancreatic islets. The micrograph reveals pancreatic islets. (Micrograph provided by the Regents of University of Michigan Medical School © 2012). Image adapted from OptenStax College [58]

2.2.2 Islet of Langerhans

Islets of Langerhans are formed by endocrine cell aggregates and are circumscribed by thin layers of basement membranes and a glial sheet [59], which separate them from the exocrine cells. The size of islets varies significantly, ranging from few micrometres to more than 1mm. The average diameter is around 140 to 200μm [60]. These micro-organs are dispersed throughout the exocrine component and there is a tendency of increasing number towards the tail region [61]. It is estimated that there are more than 1 million islets in a healthy human adult.

Five different types of cells have been found in human islets: glucagon-secreting α-cells, insulin-secreting β-cells, pancreatic polypeptide-secreting PP cells,

somatostatin-secreting δ-cells and ghrelin-secreting ε-cells [62]–[65]. The presence of these cells, as well as the surrounding vascularization and innervation are different in the dorsal and ventral part of the pancreas, due to the divergence of its origin. **Table 2.1** lists the presence of cell types and their excreted hormones in adult human endocrine pancreas.

TABLE 2.1 Cell types and excreted hormones in the adult human endocrine pancreas. Adapted from In't Veld and Marichal [1].

	Cell type				
	α	**β**	**δ**	**PP**	**ε**
Volume % (adult)					
Dorsal	15-20	70-80	5-10	<1	1
Ventral	<1	10-20	2	80	1
Total	15-20	70-80	5-10	15-25	1
Peptide hormone	Glucagon	Insulin	Somatostatin	Pancreatic polypeptide	Ghrelin
Molecular weight	3500	5800	1500	4200	3400
No. of amino acids	29	51	14	36	28
Function	Increase blood glucose level	Decrease blood glucose level	Regulate the endocrine system	Self-regulate pancreatic activities	Regulate appetite

The majority of pancreatic endocrine cells are β-cells, which secret insulin through a nutrient-induced pathway. Insulin is stored in the small secretory granules and is the prime hormone down-regulating blood glucose level through inhibition of gluconeogenesis and stimulation of glucose uptake in tissues, while glucagon promotes glycogenolysis and gluconeogenesis to increase blood glucose levels [66]. The secretion activities are regulated by many factors including hormones released by other

pancreatic endocrine cells [1], [67]. For instance, somatostatin could inhibit the release of both insulin and glucagon [68] while ghrelin, secreted by ε-cells, could inhibit insulin secretion by selectively activating δ-cells and promoting somatostatin release [69]. Little is known about pancreatic polypeptide but its function is found to be related with insulin sensitivity [70].

The cell arrangement may have a significant impact on islet signalling and function. In rodents, most islets show a rosette structure, with β-cells present in the core and all other types of cells present in the periphery [71]. Such organization is not observed in human islet, which has scattered α-cells with central β-cells [72], [73] (**Figure 2.2**). Therefore the differences between species may limit the application of findings from mice [74].

The onset of T1DM is characterized by the presence of inflammatory infiltrates in the islets [17]. With the progression of disease, although the pancreas remains normal in appearance and weight, β-cell mass is significantly reduced. Islets in T1DM patients were largely pseudoatrophic, where only non β-cells remained, as shown in **Figure 2.3** [1], [17].

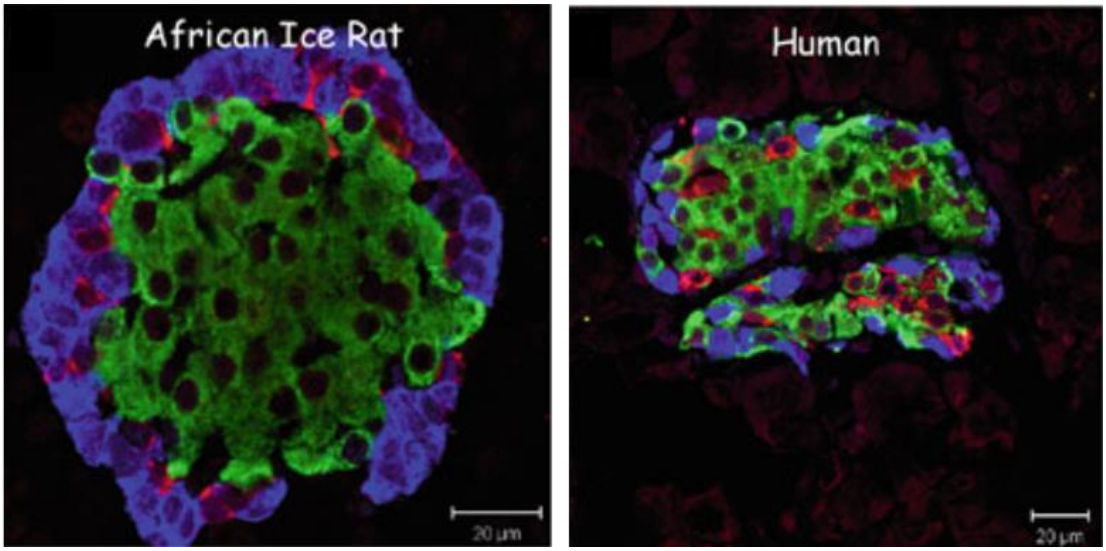

Figure 2.2 The anatomy of islets in African ice rat and human. Unlike the rosette structure in mice islets, human islets show a scattered pattern. Sections were stained for insulin (green), somatostatin (red), and glucagon (blue) and scanned with a Zeiss LSM 510 confocal microscope. Scale bar = 20µm. Image adapted from Heller [75].

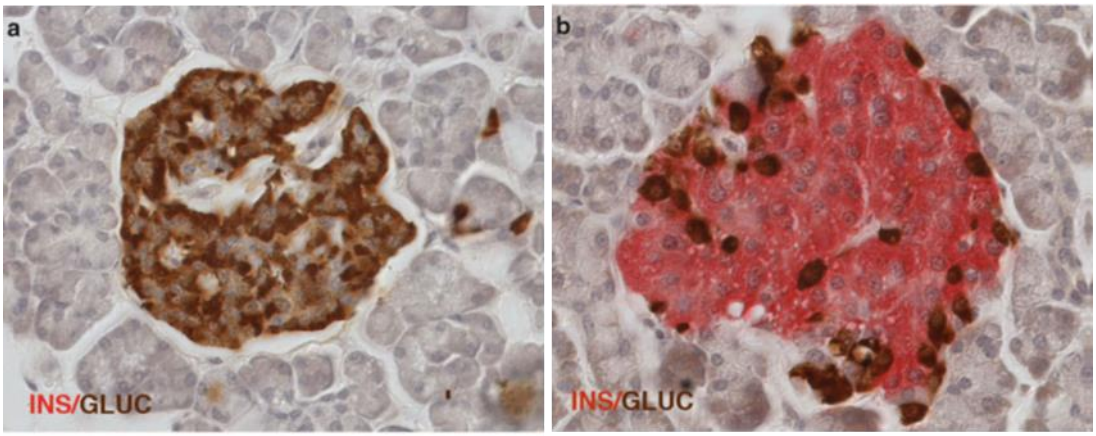

Figure 2.3 Comparison of islets from chronic T1DM patients (A) **and normal control** (B). Islet stained for insulin (red) and glucagon (brown). Islets from chronic T1DM patients are pseudoatrophic and consist primarily of α-cells while islets from a normal control islet with both α- and β-cell. Images taken from In't Veld and Marichal [1].

2.2.3 Extracellular matrix

Due to its biochemical and structural properties, the ECM can be divided into two groups: the basement membrane and the interstitial/stromal ECM. Basement membrane

is a highly dynamic sheet-like structure separating cells from mesenchyme. It plays a vital role in structure supporting and tissue homeostasis [76], [77]. The stromal/interstitial ECM, on the other hand, is produced by mesenchymal cells [78].

The composition and arrangement of extracellular matrix (ECM) proteins in pancreas is of great interest for islet isolation as well as scaffold design for 3D cell culture. The composition of ECM changes with species and age [77], [79], but primarily consists of water, polysaccharides and proteins [80]. Human pancreatic ECM proteins are mainly structural proteins, like collagen, and adhesive proteins, such as laminin and fibronectin [81].

Collagen is a trimeric molecule consists of three twisted α-chains, which then assemble into a stable structure with extensive crosslinking based on their macromolecular arrangement [82]. The repeating X-Y-Gly amino acids arrangement results in a triple helical conformation with hydrogen bonding between α-chains [83], [84]. Different amino acid compositions give rise to various α-peptide chains, resulting in 28 different types of collagens [83]. Even for collagens from the same type, isoforms of α-chains are also observed, resulting in an increased diversity [85].

Depending on their supermolecular conformations, collagens are grouped into fibrillar collagens, such as collagen I, collagen III and collagen V, as well as non-fibrillar collagens, such as collagen IV and collagen VI [86]. **Table 2.2** summarizes the distribution and composition of some collagens found in vertebrate [83]. **Figure 2.4** and **Figure 2.5** show the assembly process for a fibrillar collagen (collagen I) and a network collagen (collagen IV), respectively.

TABLE 2.2 The distribution and composition for some of the vertebrate collagens. Isoforms of α-chains are used to indicate the composition of different collagen subtypes. Taken from Shoulders [83].

Type	Class	Composition	Distribution
I	Fibrillar	$\alpha1[I]_2\alpha2[I]$	Abundant and widespread: dermis, bone, tendon, ligament
III	Fibrillar	$\alpha1[III]_3$	Skin, blood vessels, intestine
IV	Network	$\alpha1[IV]_2\alpha2[IV]$ $\alpha3[IV]\alpha4[IV]\alpha5[IV]$ $\alpha5[IV]_2\alpha6[IV]$	Basement membranes
V	Fibrillar	$\alpha1[V]_3$ $\alpha1[V]_2\alpha2[V]$ $\alpha1[V]\alpha2[V]\alpha3[V]$	Widespread: bone dermis, cornea, placenta
VI	Network	$\alpha1[VI]\alpha2[VI]\alpha3[VI]$ $\alpha1[VI]\alpha2[VI]\alpha4[VI]$	Widespread: bone cartilage, cornea, dermis

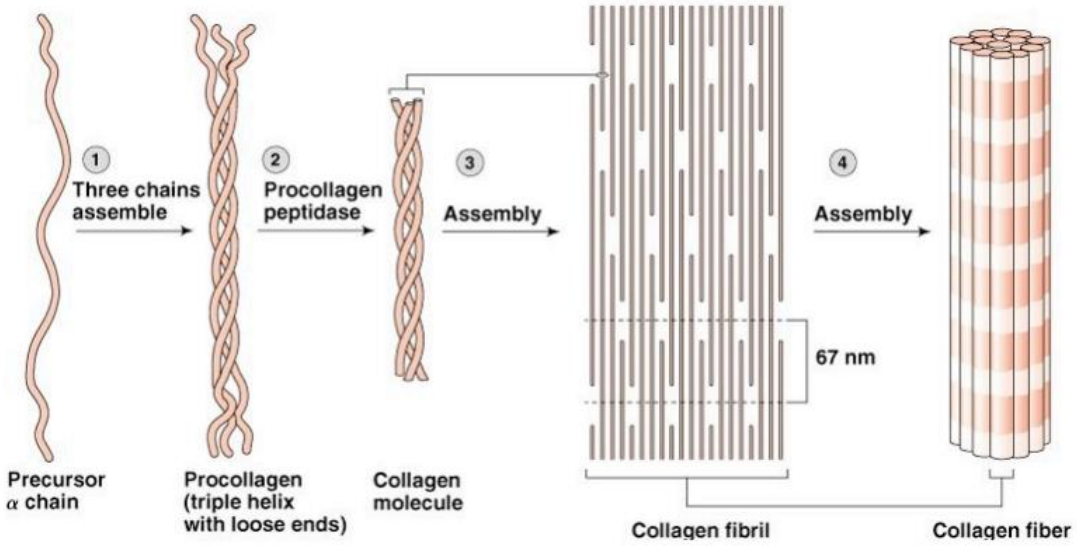

Figure 2.4 Schematic representation of collagen I assembly. (1) Precursor α-chains are assembled to form triple-helical procollagen molecules; (2) Procollagen is converted to collagen by enzymatic cleavage of the propeptides; (3) The collagen molecules self-assemble into collagen fibrils; (4) The fibrils assemble laterally into collagen fibres. Image taken from Friedrichs [87].

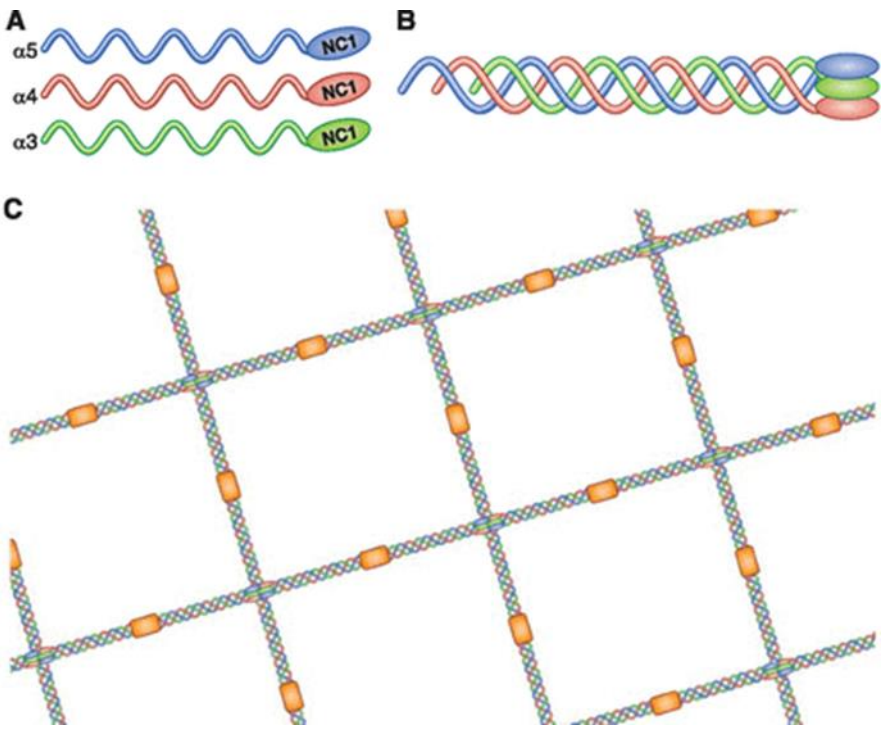

Figure 2.5 Schematic representation of collagen IV assembly. (A) Triple-helical protomers of α3, α4, and α5 chains; (B) Precursor α-chains are assembled to form triple-helical structure; (C) Binding through 7s domains (shown in orange) completes the lattice-like structure of the type IV collagen network. Image taken from Stephen and Pusey [88].

In human pancreatic ECM, collagen IV and collagen VI are two of the most abundant proteins [80], [89] while collagen I, collagen III and collagen V have also been detected. Collagen IV has been reported as the main component of the basement membrane while collagen I, collagen III, collagen V and collagen VI are interstitial collagens [90]. These proteins function as a structural support in ECM but could also regulate cell adhesion, differentiation and insulin production [79], [91].

Laminin is a cross- or T-like heterotrimer assembled from α-, β- and γ-chains [89], [92], [93]. **Figure 2.6** shows the molecular structure of laminin and its relationship with other basement membrane proteins. Different chain compositions give rise to 15 laminin isoforms [94]. In human pancreas, laminin-411/421 and laminin-511/521 have

been identified [95], [96]. However, Laminin-α4 is found only in the vascular basement membrane while laminin-α5 is found in both endothelial and endocrine leaflets, suggesting a duplex layer of basement membrane surrounding human islets [95], [96].

Laminin have receptors for integrin and nonintegrin mediators [72]. They could stabilize the ECM network and influence islet differentiation and survival [79], [91]. Studies have shown that insulin gene expression and proliferation in β-cells are promoted by laminin-411 and laminin-511 [97]. Beneficial effects of culturing isolated islets with laminin-521 in islet adhesion and spreading have also been demonstrated [98].

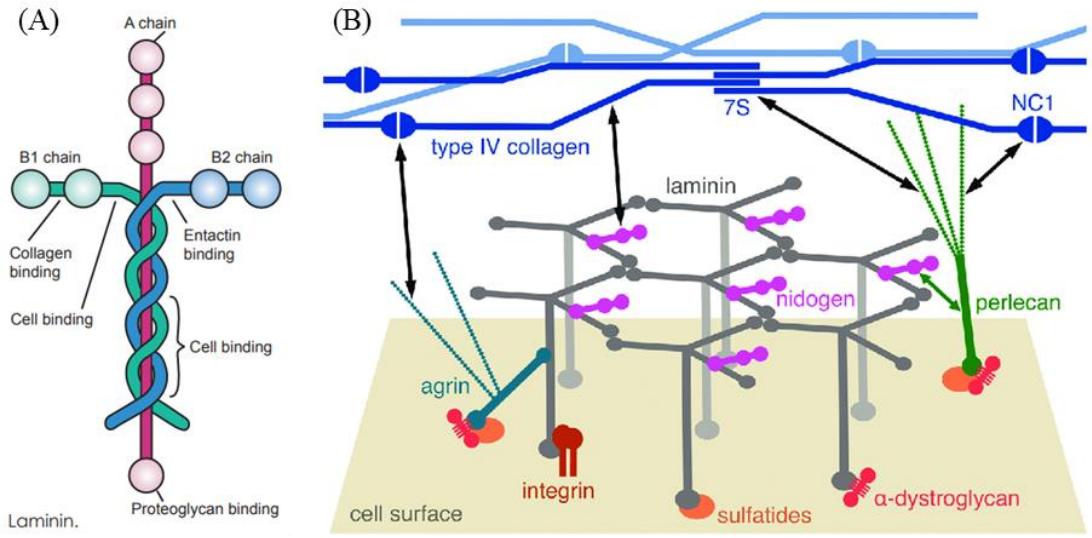

Figure 2.6 Molecular structure of laminin and its relationship with other basement membrane proteins. (A) Molecular structure of laminin; (B) Laminin in basement membrane. The laminin network is anchored to the cell surface by interactions of the long arms with cellular receptors (integrins, a-dystroglycan and sulphated glycolipids/sulfatides). Collateral interactions are made with the heparan sulphate proteoglycans agrin and perlecan. The laminin and collagen networks are linked by nidogen and heparan sulphates (black double-headed arrows). Image taken from Purdom [99] (A) and Hohenester and Yurchenco [100] (B).

In the pancreas, polysaccharides are present in the form of glycosaminoglycans (GAGs) and control osmosis [91]. It is mainly composed of heparin sulphate, which

binds to other ECM components and cell surface receptors. One of the most abundant heparin sulphate proteoglycans found in the islet basement membrane is perlecan (a.k.a. Heparan Sulphate Proteoglycan 2, HSPG2), which can interact with laminins and collagen IV to affect β-cell function.

In the human pancreas, dense capillaries pervade the islets for sufficient oxygen supply and timely response for glycaemia control [80]. Islets secret VEGF-A to attract blood vessels and this in turn results in the formation of basement membranes. Previous studies have shown that compared to other species, human islets are surrounded by two layers of basement membrane [101], which anchors to cytoskeleton via cell-surface receptors [89]. The main component is laminin [95], which are connected to the stromal collagen IV, collagen VI, laminin, nidogen and perlecan [79], [89], [91]. **Figure 2.7** shows a schematic view of the interaction between blood vessels and β-cells and the role of vascular basement membrane.

Due to its direct relationship with islets, basement membrane not only provides mechanical stability but also regulates cell behaviour as well as controlling functions of β-cells [89]. Studies of ECM digestion suggest that disrupted islet basement membrane may result in compromised islet survival [102]. Consequently, preserving its integrity might be beneficial for islet transplantation. Studies on the underlying mechanisms and links between basement membrane components and β-cell function have been carried out, with scaffolds coated with ECM proteins produced for islet culture. *In vitro* studies using matrix-protein containing medium to culture islets showed an improvement in islet viability and glucose-stimulated insulin secretion.

Similar results were also observed *in vivo*, where diabetic rodents receiving islets kept in the ECM exhibited enhanced glucose control. However, little is known of their contents within a healthy pancreas and how these vary with normal physiological changes like ageing, to facilitate islet isolation.

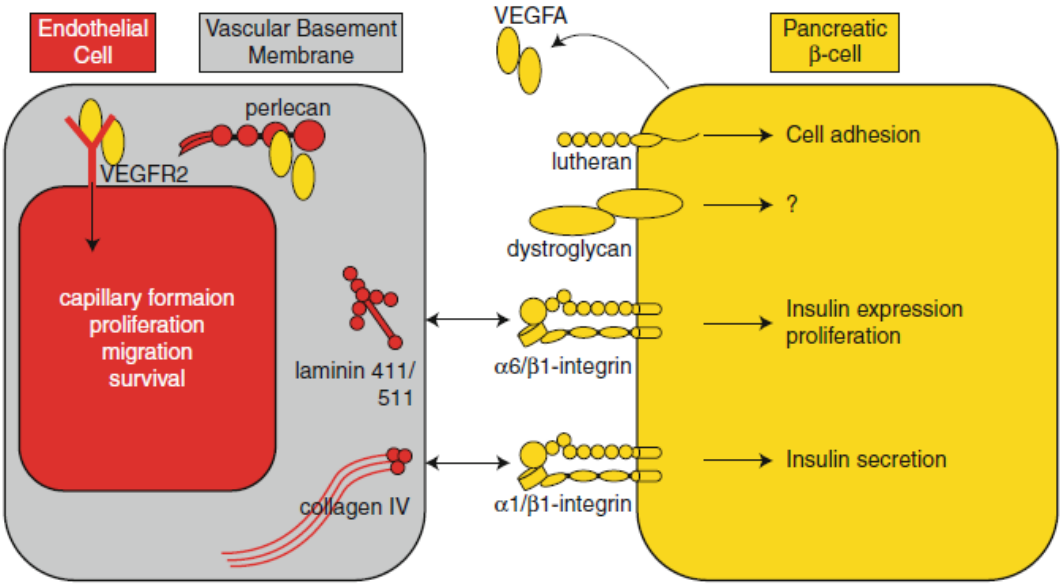

Figure 2.7 Schematic view on the interaction between blood vessels and β-cells and the role of vascular basement membrane. β-cells secret VEGF-A, which attract blood vessels to invade the islet. The presence of blood vessels in the islet is crucial for β-cell function as it depends on components of the specialized vascular basement membrane, which communicate with cell surface receptors on β-cells. The interaction between laminin and α6β1-integrin affects insulin gene transcription, whereas binding of collagen IV to α1β1-integrin influences insulin secretion. Laminin binding to β1-integrin receptors accounts for stimulation of β-cell proliferation. Image adapted from Lammert and Kragl [75].

2.3 Pancreatic islet replacement therapy

β-cell replacement can be achieved through whole pancreas transplantation or islet transplantation. Both methods result in improved glycaemia control, restoration of

normal HbA1c level, minimization of micro- and macro-disease while reducing the occurrence of the life-threatening risk of hypoglycaemia.

2.3.1 Whole pancreas transplantation

Transplanting the whole pancreas into a patient involves series of complicated surgical operations. The first successful pancreas transplantation was achieved simultaneously with a kidney graft in 1966, where insulin independence was established in a T1DM recipient [103]. However, two months later, the patient died of pulmonary embolism which might be caused by the transplantation. In the late 1970s a powerful immunosuppressant, Cyclosporine A, was introduced. This polypeptide has a specific action on lymphocytes, reducing the acute rejection and eventually leads to an increase of the graft survival rate [104]. This together with the publication of the first International Pancreas Transplantation Registry report and organization of international meetings boosted the development of pancreas transplantation [105].

Pancreas transplantation takes in the form of simultaneous pancreas and kidney transplantation (SPK), pancreas after kidney (PAK) or pancreas transplantation alone (PTA), with SPK to end-stage nephropathy patients being the most commonly performed [9]. One-year insulin independence rates for SPK, PAK and PT are 86%, 80% and 78%, respectively [106].

Although pancreas transplantation is considered a well-established therapeutic option with high success rate, the process is associated with frequent surgical

complications and technical failure. Haemorrhage, infection, graft thrombosis and graft pancreatitis have been reported [107] with a rate of relaparotomy up to 44% [108]. In addition, perioperative mortality is around 4% [109] and a comparison between patients receiving pancreas transplantation to those on the waiting list shows that this surgical process could increase mortality hazard at a ratio of 2.18, 4.63 and 4.25 for SPK, PAK and PTA, respectively, during the first 90 days after transplantation [110]. The relative high rate of morbidity and mortality, together with increased financial burden due to repeated relaparotomy limit the application of this technique, especially for children with T1DM.

2.3.2 Pancreatic islet transplantation

2.3.2.1 A historical perspective

As an alternative approach to whole organ transplantation, transplanting isolated islets provides a safer and more efficient approach and is believed to have a wider range of applicability [8]. Physically separating endocrine and exocrine component in a pancreas was first proposed in 1902 [111] but it was not until 60 years later when the separation was performed.

Isolating islets from rodent models was first achieved in 1967 with intraductal injection of Hank's buffer solution (HBSS) followed by collagenase incubation and sedimentation, where isolated islets were found to be morphologically and functionally normal [112]. Further experiments transplanting these isolated islets into chemically

induced diabetic rodent model resulted in successful correction of hyperglycaemia. However, this method failed in large animals or humans, partly due to its inability to cope with dense and fibrous gland.

It was not until 1977 when the first successful clinical islet transplantation in a human patient was performed [113]. Nevertheless the success rates in the 1970s were low, with only 10% of all recipients achieved insulin independence one-year post transplantation [114]. International Human Pancreas and Islet Transplantation Registry reported that until 1982, none of the 71 recipients achieved insulin independence from 76 islet transplantations [115]. The major cause for graft failure was attributed to rejection.

A pivotal breakthrough was made in 2000, when the Edmonton group reported a steroid-free immunosuppressive protocol with much higher islet dose could significantly improve the success rate [116]. The group used islets from multiple donors to achieve a final transplantation mass >11,000 islet equivalents (IEQ, the number of islets equivalent to that for islets of 150μm diameter) per kilogram of the recipient weight. According to their report, insulin independence was achieved in 7 consecutive T1DM patients with a history of severe hypoglycaemia over a median follow-up of 11.9 months. The protocol was adapted in many centres worldwide and similar success was achieved. Since then considerable efforts have been directed to the improvement of Edmonton protocol and substantial improvements in technical procedure, recipient management and clinical outcomes have been made.

2.3.2.2 Procedures for islet transplantation

The process of islets transplantation comprises of organ retrieval, islet isolation, islet purification, islet culture and final transplantation, with each step having a profound impact on transplantation results.

After perfusion of preservation solution, the organ is retrieved and transported to the isolation centre in cold preservation solution [117]. Duodenum, spleen, excessive fat and connective tissue are subsequently removed before the organ is washed in betadine solutions for decontamination. As efficient delivery of enzymes can reduce undigested tissue, the pancreatic duct is then securely cannulated to allow enzyme solution loading [118]. Details of enzymes used in clinical islet isolations can be found in **Chapter 2.4.2.1**. To achieve this, infusion can be achieved either manually with a syringe or automatedly with a recirculating pump, while the latter was shown to improve islet yields [119].

Following enzyme perfusion, the pancreas is dissected and placed in a digestion chamber, where recirculation of enzyme solutions at 37^{o}C takes place. Detailed operating procedures vary from centre to centre while most adapt an automated method proposed by Ricordi in 1988 [120]. In these centres, a Ricordi chamber is used, where mechanical agitation with 7-9 silicon nitride marbles accompanies enzymatic digestion to free islets from surrounding exocrine tissue and ECM network. Samples are taken intermittently from the circuit to monitor the progression of isolation. Dithizone, a sulphur-containing chemical is used to stain the zinc ions associated within insulin,

which is present in islets. When successive samples with high proportion of free islets are observed, the process switches to the collection phase.

Cold minimum essential medium (MEM) solution with human serum albumin (HAS) is used to inhibit enzyme activity and to dilute the enzyme concentration. The solution is added progressively to the circuit. The homogenized tissue is collected and purified by isopycnic density gradient centrifugation, where the less dense islets are separated from exocrine tissue. The weight of undigested tissue is recorded to assess the digestion efficiency. Purification of isolated islets not only reduces the volume for transplantation but also removes activated proteolytic enzymes secreted by exocrine tissue, which may affect islet function *in vivo* [11].

An important predictor for better graft function is transplantable islet mass [121]. To meet the requirement of 5000 IEQ/kg recipient weight for a first transplantation [122], isolations with high yield and purity are highly desirable. The criteria for a successful isolation vary from centre to centre while a requirement of yield ≥200,000 IEQ and a viability of ≥70% is applied in the UK Islet Taskforce.

Purified islets are cultured, usually for 24-48h before they are transferred to the transplant bag for hepatic intraportal transplantation into the recipient's liver [122]. Culturing islets could provide additional quality control tests and allow preparations for immunosuppressive protocol [123]. This includes viability tests using DNA-binding dye [124], [125] and functional assays such as insulin content assessments and glucose-stimulated insulin secretion assay [124]. To quantify the insulin content, an enzyme-linked immunosorbent assay (ELISA) can be applied. The ability of insulin secretion

under different glucose concentrations can therefore be performed to assess the *in vitro* function of cultured islets.

Most patients receive multiple transplantations for a large islet mass, ideally >8,000-9,000 IEQ/kg in total, to achieve and maintain sufficient endogenous insulin production, as introduced by the Edmonton protocol [116], [126]. To prevent acute rejection and maintain the graft function, lifelong immunosuppressive therapy is required for the recipients.

2.3.2.3 Clinical outcomes of islet transplantation

Since the introduction of Edmonton protocol, significant improvements in functional outcome have been achieved. According to the most recent Collaborative Islet Transplant Registry (CITR) report [127], 819 islet transplant alone (ITA) have been reported in the period between 1999 to 2013 from all 37 centres worldwide, with the insulin independence rate of 50% at 1-year post-transplantation and 28.6% after 5 years. C-peptide levels, as the measurement for graft function, was 80% at 1-year post-transplantation and 45.1% after 5 years, proving the enduring effect of this technique. The occurrence of severe hypoglycaemic episodes has dropped significantly, with 88.5% free of any even after 5 years.

Compared to death rates for those on the waiting list (30%) and recipients of pancreas transplantation (9%) [128], islet transplantation provides much more considerable survival benefits. As the process involves only minimally invasive

operations, cumulative mortality is reported as <3% 1-year post transplantation. Of all 30 deaths, 25 cases are believed to be unrelated to islet transplantation but caused by long-term complications of T1DM. Moreover, death rate has been reduced from 7.1% during 1999-2002 period to only 0.3% in 2011-2014. Life-threatening events, generally with neutropenia and abnormal liver function involved, are reported with an occurrence significantly reduced during the past decades. Other adverse events post-islet transplantation could be divided into infusion-related and immunosuppression-related groups. The majority of the adverse events, such as abnormal lymphocyte count and abnormal liver function, are not unexpected and the many have also declined over the era.

The improved success in functional results and minimal complications has made islet transplantation an attractive approach for T1DM patients with unstable glycaemic control. In fact, although it is still deemed as an experimental and investigational therapy in the United States, this technique is reimbursed by health insurance providers in Canada, mainland Europe and Australia.

2.4 Challenges for islet transplantation: shortage of transplantable islets

Although significant improvements for long-term graft function has been made, islet transplantation has long been challenged by limited organ source and graft attrition over time.

Compared to the continuous booming trend in T1DM, the number of available healthy donated pancreas is relatively limited, not to mention the competition with pancreas transplantation. As a newly emerging therapy, islet transplantation is usually discriminated against by most organ allocation schemes. Pancreases for islet transplantation are usually from obese and older donors, which are linked with inferior function compared to those from young and lean donors [101]. Although the superiority of using higher-grade pancreases remains to be shown, the relatively poor graft survival rate of islet transplantation might be the direct result of using lower grade pancreases.

Since the steroid-free immunosuppressive therapy proposed by Edmonton group, a large array of relevant agents and immunosuppressive regimes have been developed [45]. Sirolimus and tacrolimus, the two agents used in the Edmonton protocol, are reported to impair both β-cells and kidney [129]–[131]. Since then, new therapy with alemtuzumab, mycophenolate mofetil and etanercept in combination with prednisone, daclizumab and rabbit antithymocyte globulin, have emerged with promising preliminary results [45]. However, reduction of islet graft function is also observed in autotransplantations, where the isolated islets are transplanted to the patient him/herself due to chronic pancreatitis and no further immunosuppression regimen is applied [132]. This suggests that innate immune reactions such as instant blood mediated inflammatory reactions are not the only reason causing long-term graft attrition. In fact, it has been proposed a series of reasons, including low islet yield, lack of islet vascularization and suboptimal transplant site might all contribute to the gradual loss

of graft function [133], [134]. Clinical trials aiming at solving above-mentioned obstacles have been carried out.

To compensate for the large loss of β-cell mass in the early post-transplant period and the long-term graft attrition, multiple infusions with large islet numbers are commonly conducted during routine islet transplantations, as suggested by the Edmonton group [116], [126]. This in turn calls for an expansion of cell numbers, either from isolation of donor pancreas, or *in vitro* generation of islet cells.

2.4.1 Expanding sources for islets

Expanding the donor pool is probably the most direct approach to increase available islets for transplantation. This could be achieved by encouraging pancreas donation and improving pancreas allocation scheme. Changing of the current donation system in the United Kingdom to an opt-out system, which makes donation a default option unless otherwise stated or registered, is expected to come into effect in early 2020.

Identifying pancreas suitable for islet transplantation but suboptimal for pancreas transplantation may also benefit the expansion of organ source for this technique. In 2010, a new national Pancreas Allocation Scheme was introduced in the United Kingdom, which provides islet transplantation equal access to donated pancreases. Significant increase in islet transplants was observed, with >20 islet transplantations conducted annually ever since [135].

Using marginal donors for islet transplantation has been studied. Pancreases for islet transplantation can be retrieved from both Donation after Brain Death (DBD)

donors and Donation after Circulatory Death (DCD) donors. A study systematically comparing 15 DCD and 418 DBD donors in terms of islet transplantation was carried out by Edmonton group in 2016 [136]. Islet yield, metabolic function and mean decrease in insulin requirements were found to be similar between the two groups, supporting the using of DCD donors.

Another method to overcome the scarcity of islets is xenotransplantation. Animal donors like pigs have been proposed, as their insulin structural properties are similar to those from human [137]. With cell encapsulation, the ability of porcine islet in blood glucose level control and even for achieving insulin independence were reported [138]–[141]. Although many reports successful results using xenotransplantation, there are still concerns regarding ethical and safety issues. Scientific hurdles like virus safety, donor age, transplant sites and the intrinsic differences between pig and human islets have also been pointed out, requiring further investigations to be taken [142].

In vitro expansion of β-cells or islets has also been proposed as an alternative source of cells for transplantation. This includes differentiation from stem cells, transdifferentiation, de- and re-differentiation of differentiated cells [143], [144]. At the current stage, production of islet-like clusters from differentiated cells involves complicated gene engineering *in vitro*, where genes of crucial transcription factors are over- or under-expressed in tested animals to direct differentiation towards pancreas endocrine [145]–[147]. The process is under relatively poor control while its applicability in humans remains unknown. On the other hand, studies on differentiation from embryonic stem cells (ESC) and mesenchymal stem cells (MSC) to insulin-

producing cells have proved to be achievable although not all β-cell attributes have been present [143], [148], [149]. Nevertheless, a recent review of 16 clinical trials shows that the c-peptide and HbA1c level are improved in T1DM patients receiving stem cell therapy [150], confirming the feasibility and safety of this technology. Although researchers agree the potential of stem cells in diabetes treatment, technical hurdles like maturation and optimisation of the differentiated cells remains to be solved [151], [152].

Compared to relatively immature techniques like *in vitro* islet expansion and xenotransplantation, the most immediate approach to overcome islet shortages is to improve current islet isolation results. Although decades have passed since the publish of Edmonton protocol, the isolation yields are still relatively low and unstable. With only 30-50% of transplantable islets could be isolated from a healthy pancreas, improving the isolation process itself could provide an efficient solution [11], [44], [153], [154].

2.4.2 Factors influencing the isolation success rate

2.4.2.1 Donor age & BMI on islet isolation success

Studies have shown that islet isolation outcome is linked with many donor-related variables [153], [155]–[158]. Among the numerous factors affecting a donor pancreas, donor age and BMI have been found to be the most common ones [159]–[161]. A massive study of isolation variables and islet yield and successful isolation was carried out in 2005 [158]. 437 islet isolations were analysed with some of the donor variables

summarized in **Table 2.3**. Using univariate analyses, it was found islet yield correlated with donor age and BMI. Moreover, isolation success was found to be significantly associated with donor BMI in univariate but not multivariate analyses. Another study analysed 171 islet isolations and found islet yield was significantly associated with donor age ($p<0.005$) and BMI ($p<0.05$) in univariate analyses [157]. Age was also found to be associated with isolation success (IEQ⩾250,000) in multivariate analyses ($p<0.05$).

TABLE 2.3 Univariate analyses between donor variables and islet number and successful isolation. Data expressed as median value with interquartile ranges in parentheses. P-values are given to indicate statistical significance, with asterisks represent $p<0.05$ (*), $p<0.01$ (**) and $p<0.001$ (***) respectively. Successful isolations were defined as ⩾250,000 IEQ with ⩾20% purity. Taken from Nano *et al*. [158].

Isolation variables	Individuals	Characteristics	Islet number	Successful isolation
Sex	431	261 males; 170 females	0.0981	0.0708
Age (years)	430	42 (30-52)	0.0009***	0.0204*
BMI (kg/m^2)	338	24 (22-26)	0.0004***	0.0074**
Cause of death	398	140 traumatic; 258 non-traumatic	0.1195	0.8957
Intensive care unit days	272	2 (1-4)	0.4797	0.8652
Blood glucose (mmol/l)	205	7.8 (6.1-9.9)	0.8916	0.8717
Amylase level (U/I)	191	90 (51-195)	0.4942	0.48859
Dopamine dose (kg^{-1} min^{-1})	185	6 (3-8) µU	0.6344	0.7190

Noradrenalin dose ($\mu g\ kg^{-1}\ min^{-1}$)	155	0.000 (0.000-0.001)	0.2252	0.4017

People with high BMI but normal glycaemia level are believed to be ideal donors, due to the fact that pancreases from those donors are generally larger and can cope with higher metabolic demand [44], [159]. It is also proposed that the enzymatic digestion is more efficient with the accumulation of acinar fat in obese donors (BMI>24) [162]. Nevertheless, there is controversy regarding the effect of fat accumulation on islet viability, as it may lead to β-cells lipotoxicity [163]. An analysis of 104 islet isolations reported that although not statistically significant, islets from lean donors (BMI<21) resulted in better islet recovery and viability [164]. This, however, was not reflected in recent studies [156]. Moreover, the isolation yield from normal and obese donors were found to be significantly higher in comparison with lean donors [165]. The glucose-stimulated insulin secretary ability of islets from obese donors with normal glucose homeostasis is reported to be comparable with lean BMI donors [156], [159], making such pancreases highly attractive.

Compared to donor BMI, there is much more debate around the impact of donor age. Many suggest that high isolation yield is achieved with older donors while others report a lower post-digestion yield followed by a comparable post-purification yield [166]. Nevertheless, most report that islets from old donors have a decreased β-cell function and proliferation ability, resulting in relatively poor transplantation results [166]–[169]. On the other hand, juvenile pancreatic islets generally result in low yield and purity, due to contaminating exocrine acinar tissues [101], [166]. Also, the islets

are generally smaller and more difficult to be efficiently purified. However, improved isolation techniques, such as changes in enzyme combination and delivery method, could enhance yield [101], [170]. In addition, there have been few investigations on the histologic features of pancreas from healthy young and older donors [12], leading to a poor understanding of the effects of ageing.

Overall, higher isolation yields could be obtained from older donors with a higher BMI. However, considering their functionality, islets from those donors may not be ideal for islet transplantation. Detailed investigations are thus required to determine the impact of those donor characteristics on the islet-exocrine interface, which acts as the substrate during islet isolation, to improve isolation yields from younger and leaner donors. Understanding the molecular ultrastructure of this interface and the impact of such donor variables on it may enable the development of tailored isolation strategies for each different donor type, resulting in improved isolation outcomes from the full range of donors available.

2.4.2.2 Enzymes for pancreas dissociation

To liberate islets from the surrounding exocrine tissue, enzyme blends are used to digest the islet-exocrine interface. As discussed in **Chapter 2.2.3**, the pancreatic ECM consists mainly of collagens and laminin. Therefore, clinical isolations use a combination of collagenase and non-collagenolytic components.

Collagenase used for islet isolation is derived from *Clostridium histolyticum*. It is a collagenolytic protease that could degrade collagen efficiently as well as remove

proteoglycans and glycoproteins [171]. During the digestion, collagenase binds to collagens and unravels their triple helical structure to initiate degradation through a step-wise process [172]. Immunohistological studies show that perfused collagenase was found to be colocalized with pancreatic collagen and the binding of collagenase to collagen was not inhibited even at room temperature [173].

There are two isoforms of collagenase. Class I collagenase (CC1) has a high activity toward native collagen while class II collagenase (CC2) has a low collagen digestion activity toward synthetic peptides. Studies with rats have shown that CC2 plays a major role in pancreas digestion while CC1 acts synergistically with CC2 [171]. Digestions of pancreases from human, however, depends more on the stability of intact CC1 [174]. Decreasing the CC2/CC1 ratio also result in better enzyme performance [175] but the digestion was more effective only when a balanced CC2/CCI ratio is presented [176], [177].

An efficient enzyme blend is desirable to achieve successful islet isolation. Digestion with collagenase alone only results in an inadequate release of islets from the exocrine tissue [171], [177]. Studies have shown that the introduction of neutral protease is necessary for pancreatic dissociation [178]. However, prolonged dissociation in the presence of neutral protease resulted in islet fragmentation [178] and a reduction in islet viability [179]. Further to this, it has been suggested that non-collagenolytic protease could degrade collagenase non-specifically, reducing collagenase activity [180]. Therefore, the amount of this enzyme used and time for islets or collagenase exposed to this enzyme needs to be carefully controlled.

The hydrolysis of collagens by collagenase starts from the Y-Gly bonds in the repeating X-Y-Gly sequences, resulting in a mixture of small peptides [181], [182]. Histochemical analyses reveal that glycoprotein and proteoglycan can also be affected by this enzyme [12]. Nevertheless, the kinetics of digestion is accelerated when neutral protease is added [12]. Currently there is little understanding on the mechanism of these two enzymes in pancreatic ECM digestion and the dynamic process at molecular level remains to be revealed.

In early 1990s, the islet community use crude enzymes like Sigma Collagenase V. The composition and activity of crude enzyme preparations vary significantly between enzyme batches, making it difficult to compare results from different centres. Some companies provide purified enzyme blend to reduce this lot-to-lot variability. In the late 1990s, Liberase HI, a product from Roche Applied Science, was introduced. In addition to CC1 and CC2, this product also contains thermolysin, a non-collagenolytic enzyme derived from *Bacillus thermoproteolyticus*. Studies show that this enzyme led to enhanced islet yield and function [183], [184] and over the next 10 years Liberase HI became the gold standard enzyme. However, in 2007 it was found that this enzyme blend potentially contained bovine neural component and might lead to prion disease transmission. Consequently, the islet community began to use other alternative collagenase sources. Many centres use products from Serva Electrophoresis: Collagenase NB1, which contains only CC1 and CC2, in combination with separately packaged Neutral Protease. Other enzymes, such as Collagenase HA (VitaCyte), Liberase Mammalian Tissue-Free (Roche) are also proposed and studied [12], [133],

[136], [185]. The group from University of Minnesota even make their own blends using intact CC1/CC2 and neutral protease [186].

Although the change of enzyme resulted in a decreased isolation outcomes worldwide [26], many centres reported successful isolations with Serva blend. Using an average of 1,600 units of collagenase and 200 units neutral protease/100g pancreas, Szot *et al.* achieved a high rate of islet isolation success rate for young donors [187]. According to their report, the amount of enzyme used were significantly lower using Serva products than with Liberase HI [187]. They also suggest that separately packaged collagenase and neutral protease also provide possibility to adjust enzyme proportion based on donor characteristics. This could potentially help to improve isolation outcomes from young and/or lean donors, as discussed in **Chapter 2.4.2.1**.

To date, considerable efforts have been put in enzyme optimization and new enzyme development. Although many have reported improved isolation results, the process still faces problems like batch-to-batch variation [157], [188]. Investigations of non-enzymatic pancreas dissociation have also been conducted. Methods like dielectrophoresis and *in situ* cryopreservation of islets while selective destruction of acinar tissue have been proposed. However, there is still a long way to go before translating these strategies into clinical islet isolation.

2.4.2.3 Apparatus used in islet isolation

During clinical isolation, a dissociation chamber, known as the Ricordi chamber, was developed to provide mechanically enhanced enzymatic digestion [120]. Although

successful and repeatable results were obtained, no further development or adaption of this device has been promoted or marketed since. **Figure 2.8** shows the schematic diagram of the digestion process using the Ricordi chamber.

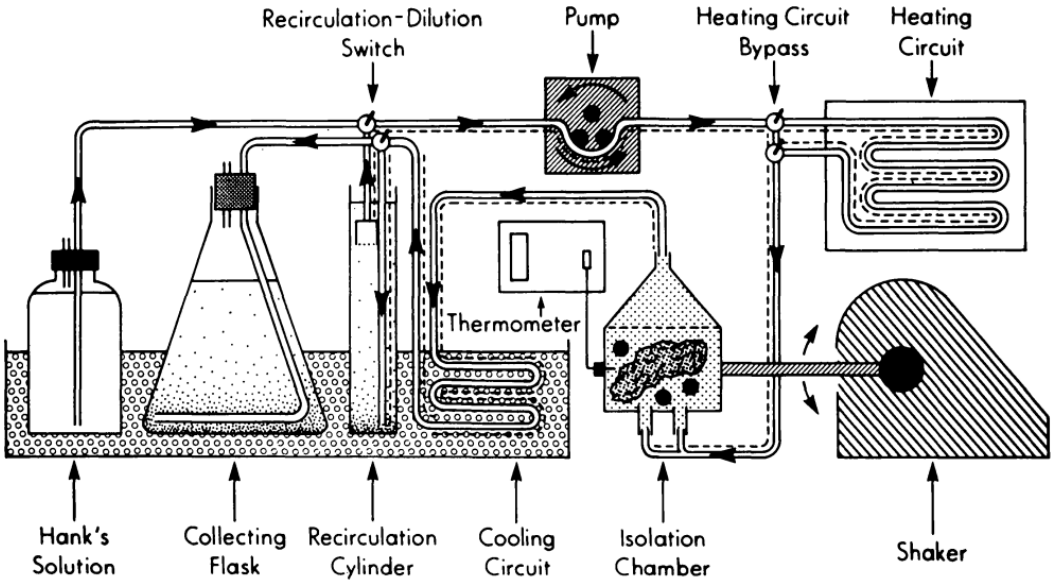

Figure 2.8 Automated procedure for isolation of human pancreatic islets. Briefly, collagenase-perfused pancreas is placed in the Ricordi chamber with 1cm glass marbles. A screen is placed to keep tissue in the lower compartment while the system is perfused with enzyme-contained recirculation media. Samples are taken from the circuit to determine the endpoint of recirculation. Once sufficient free islets are observed, the system is switched to the dilution circuit. The digest is then drawn into prepared Hank's solution and cooled at 4°C to inactivates the collagenase. Image taken from Ricordi [120].

The device Ricordi firstly introduced was a 300ml chamber made of stainless steel, as shown in **Figure 2.9 (A)**. A 280μm stainless steel mesh separated the chamber and kept pancreatic tissue in the lower compartment. Seven glass marbles with 1cm diameter were placed in the chamber. There were four openings for the chamber: one for the temperature probe, 2 for the inlets at the bottom and 1 for the outlet at the top. The two parts of the chamber were held together by screws and sealed by an O-ring. Coupled with the recirculating circuit and the collection circuit, this device has become

the gold standard for human and large animal pancreas processing. Chambers of sizes ranging from 50 to 1000ml and various materials are readily available for different purposes. Silicon nitride marbles with larger diameter were also adapted to improve mechanical dissociation of the tissue. However, as uncontrolled battering and grinding were involved in this process, the viability and functionality of isolated islets might be affected [15].

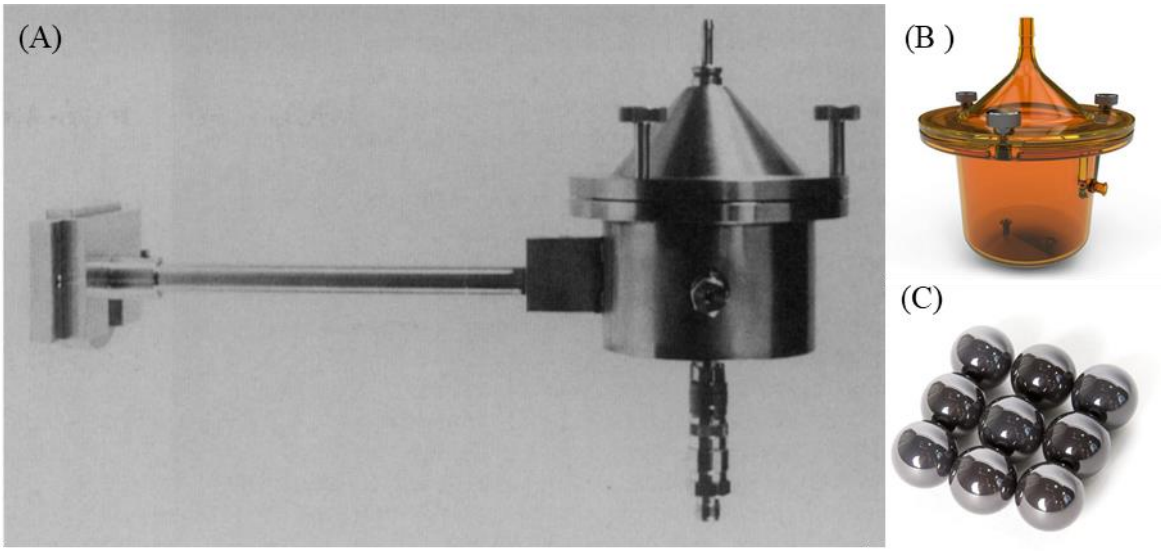

Figure 2.9 Ricordi chamber and marbles. (A) Metal chamber with shaker, taken from Ricordi [120]; (B): Ultem Ricordi chamber; (C) Silicon nitride marbles, diameter = 15.875mm. Figure (B) & (C) are obtained from Biorep®

In 2004, a modified chamber, named the Oxford chamber, was proposed by Gray [15]. The new chamber uses shear forces generated by fluid movement to facilitate mechanical agitation. As shown in **Figure 2.10**, a central threaded tie-rod with attached hooks was secured in a glass cylinder sealed with Teflon plates. A ring-shaped piston was introduced to push the fluid through the cylinder and was connected to an external handle for manual or automated operation. Vortex could then be formed with the travel of the piston, resulting in the stir of the fluid. Pancreatic tissue section could thus be

caught by the hooks and teared by the shear forces. It was proposed that tissue dissociation in this way could be less destructive and the isolation yield could be potentially increased.

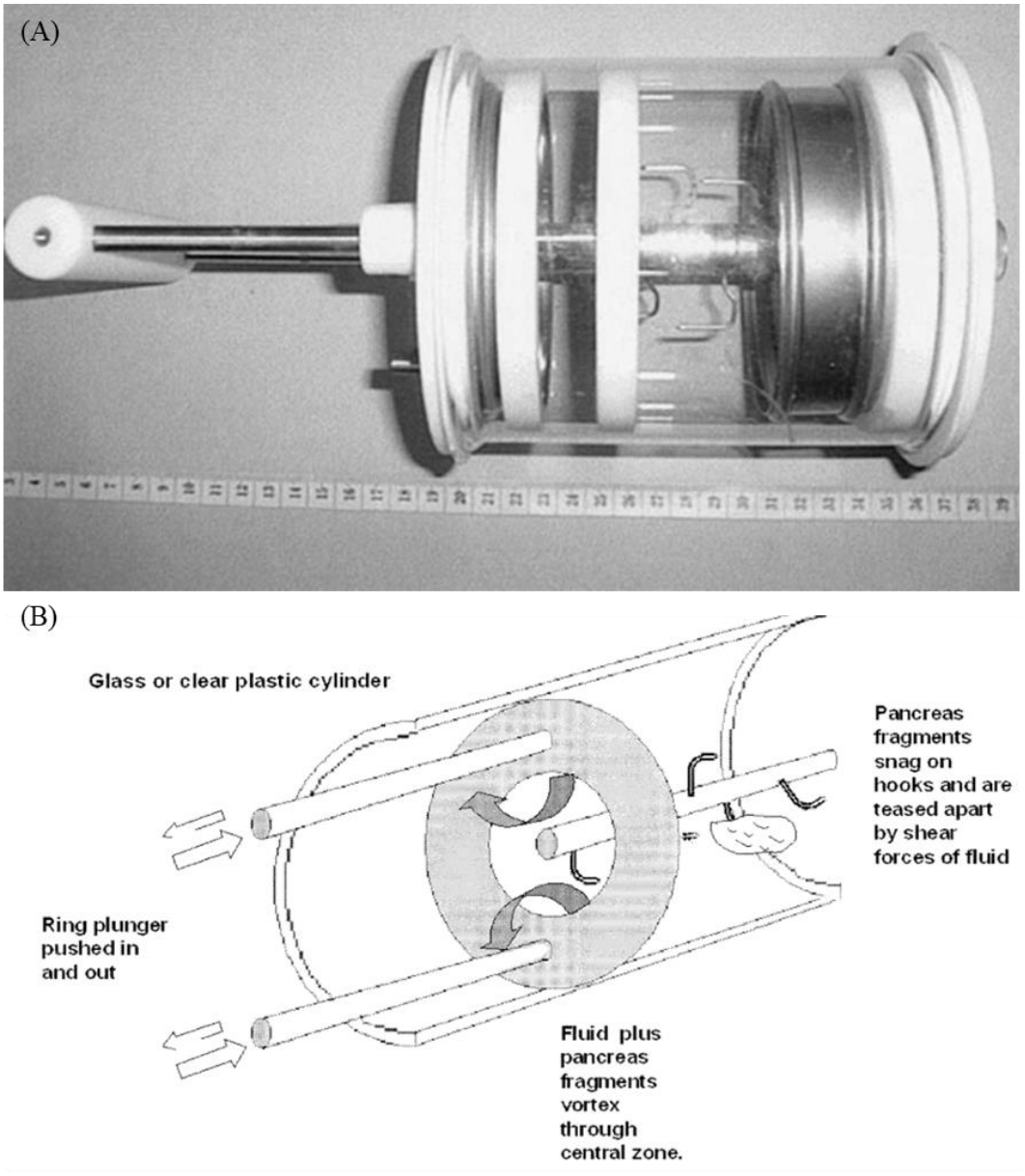

Figure 2.10 The Oxford chamber. (A): Picture of the completely assembled chamber; (B): Diagram showing the principles of operation of the new chamber. Adapted from Gray [15]

The performance of this modified chamber was assessed. For human pancreas digestion, >200,000 IEQ were obtained and intact islets were observed. For pig pancreas digestion, >5,000 islets/g pancreas were isolated from juvenile pigs (n=2)

using this modified chamber while insignificant numbers of islets were obtained with Ricordi chamber. Although the group planned parallel experiments comparing the performance of both chambers, no results have yet been reported. Further to this, islets isolated from the pancreatic tissue are still soaked in a harmful enzymatic environment and no prevention of further fragmentation could be provided.

In 2017, a method for mouse islet isolation using a multi-layer centrifuge tube (MCT) was proposed. Briefly a 50ml centrifuge tube was divided into several sections with detachable joints. Mouse pancreatic tissue sections were placed on a coarse sieve in the upper layer. After collagenase addition, the tube was incubated upside down at 37°C for 8-20min followed by thorough vortexing until the solution became slurry. The tube was then placed upright and the bottom part was carefully detached from the main tube. Isolated products were collected from the detached part while further digestion could also be performed for residual tissue to improve the isolation yield. The whole process is summarized in **Figure 2.11**.

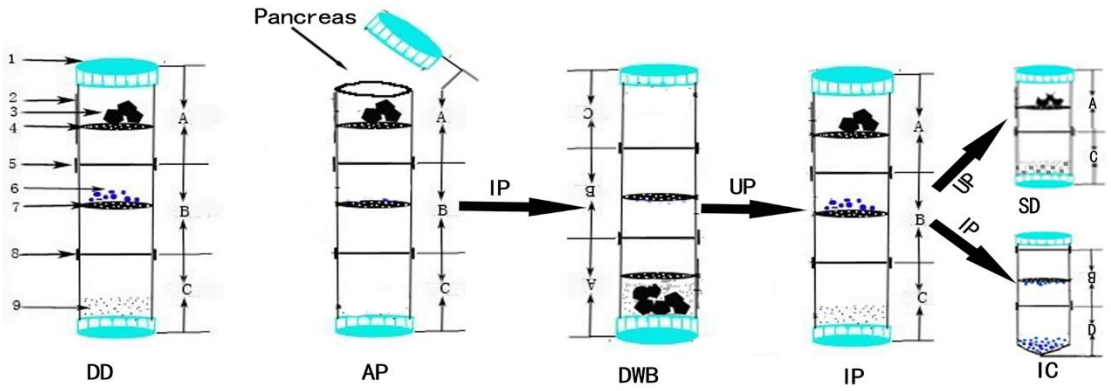

Figure 2.11 Device and flow chart of islet isolation and purification. 1: Centrifuge cap; 2: Matte surface of tube outer wall; 3: Pancreatic tissue; 4: Coarse sieve; 5 and 8: Detachable joints; 6: Islets; 7: Fine sieve; 9: Single-cell suspension; DD, device description; AP, acquisition of pancreas; IP, inverted position; DWB, digestion in water bath; UP, upright position; IP, islet purification; SD, second digestion; IC, islet collection. Image taken from Yin [189]

Compared to Ricordi chamber and the Oxford chamber, this simple device provides a protection of early-released islets by separating them from toxic enzymatic environment. Therefore, the residual tissue could be further digested to achieve complete dissociation. The purity, function and yield of islets were found to be superior than digestion using simple perfusion of collagenase while no significant differences were found in islet viability. However, the device was designed for mouse pancreas digestion and works in a batch mode. For clinical human islet isolation, an automated method with large capacity is required.

2.5 Overall summary

As a viable treatment strategy for T1DM, islet transplantation has become a clinical option for patients suffering from severe life-threatening hypoglycaemic episodes. This treatment method could significantly improve patients' blood glucose level and quality

of life. However, <50% of islets present in a healthy human pancreas can be recovered from clinical islet isolations [44], and generally multiple infusions are required for one patient to achieve and maintain sufficient endogenous insulin production [116], [126]. Considering the shortage of organs available, improving the process efficiency to enhance the isolation yield is necessary.

Human islets are surrounded by double basement membranes, which separates them from exocrine tissue. Clinical isolations use enzyme blends to degrade surrounding ECM proteins and to isolate islets for transplantation. However, large variations in isolation outcomes were found from donors of different ages and BMI. Investigations in ECM network and development of new enzyme blends were conducted but the dynamic digestion process at molecular level is yet to be elucidated. Further to this, the equipment used for current clinical isolation has remained unchanged for over 30 years. With advances in our knowledge on the structure of pancreas and islet as well as enzymatic dissociation process, modifications of this apparatus may provide a better approach to improve the isolation efficiency.

Chapter 3

An investigation of the islet-exocrine interface using high resolution MPM imaging: 3D structure, age and BMI related variations of the normal human pancreas

3.1 Introduction

As discussed in **Chapter 2.3.1**, one of the key issues limiting successful islet isolation is the lack of understanding about the substrate of the digestion enzymes, the islet-ECM interface. Imaging of the pancreas, islet and ECM could provide a better understanding and form a firm foundation for the design of tailored digestions based on donor peri-islet ECM profile. Although more than one century has passed since the discovery of islets and an enormous amount of studies have been carried out, there is still little by way of available images on the detailed microstructure of a pancreas [81]. Even for those who study the prevalence of peri-islet ECM proteins, most were carried out with 8-15μm thick samples while little focus on the intact structure.

One study involving the concept of 'entire' islet was carried out by Bosco [72], who sectioned 80 consecutive 5μm thick sections from one human pancreas sample. The sections were than stained for insulin and glucagon before imaging with an Axiokop fluorescence microscope (Zeiss, Feldbach, Germany). This method was successful in generating a semi-continuous 3D network for an entire islet, as shown in **Figure 3.1**. The group also observed empty spaces within an islet and by triple labelling with CD34, they attribute these gaps to the presence of vascular channels. However, no investigation on the peri-islet ECM was carried out and the cellular structure might have been seriously affected during sectioning. Moreover, as no analysis on the z-axis was performed, only semi-continuous qualitative analysis was reported.

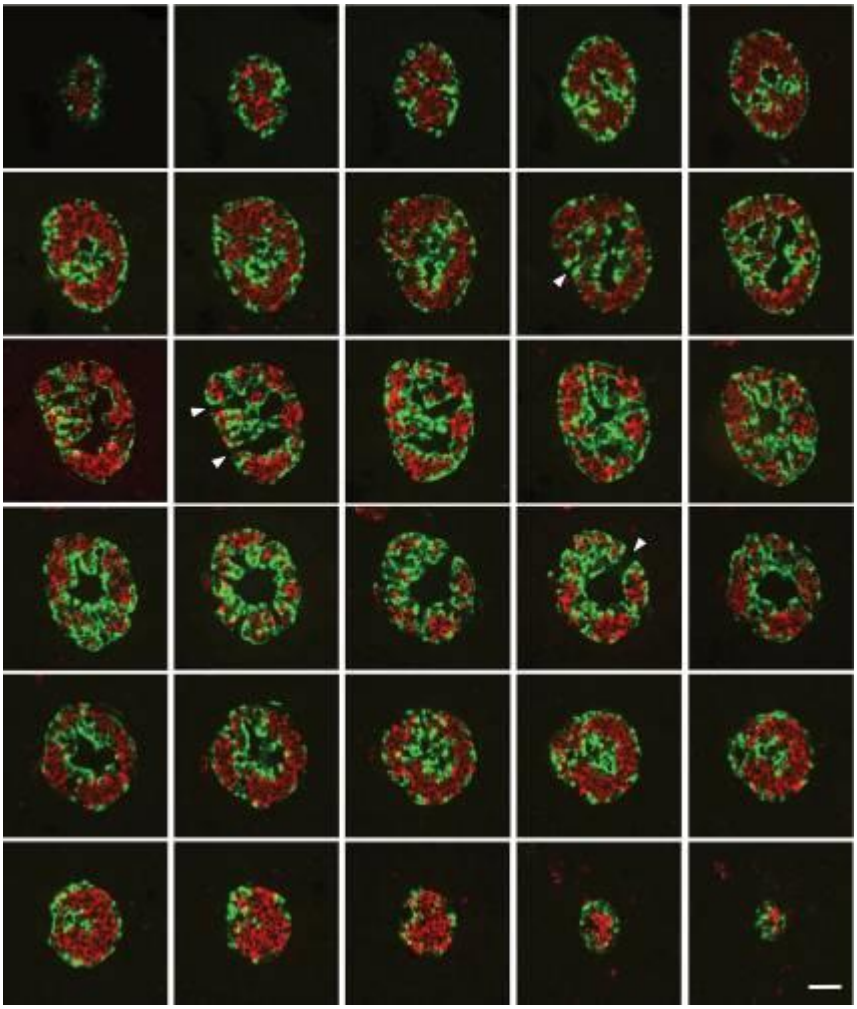

Figure 3.1 3D analysis of human pancreatic islets. Images of 80 consecutive sections show that within an intact islet, continuous 3D networks are formed by insulin (red)- and glucagon (green)-stained cells. Vascular channels were pointed as arrowheads. Scale bar = 50μm. Images were adopted from Bosco [72].

In 2007, Alenentalo *et al.* described a method to image an adult mouse pancreas using methanol for antigen retrieval with prolonged immunofluorescence staining [190]. Coupled with tomographic molecular imaging, the 3D structure within an intact adult mouse pancreas was shown for the first time. Using this technology, the group discovered a correlation between the reduction of β-cell volume and the onset of type-1 diabetes. Although the structure of an intact islet was observed (**Figure 3.2**), no studies on peri-islet ECM were carried out. Nevertheless, this is the first research on

imaging an intact islet without much disturbance to its surrounding structure.

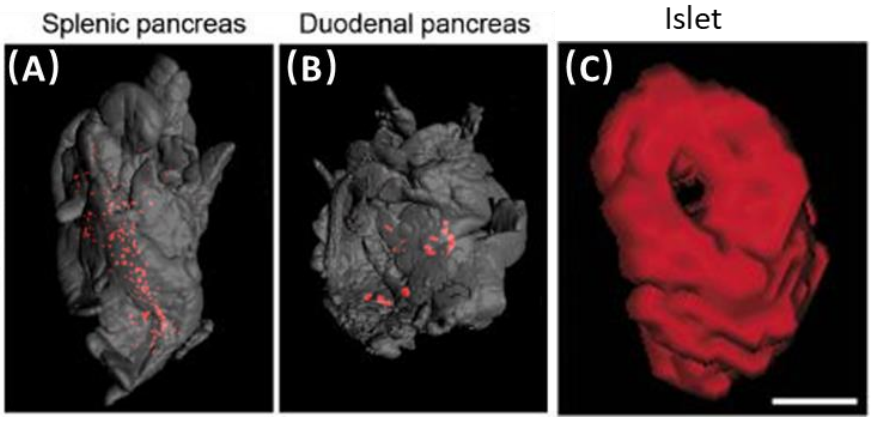

Figure 3.2 Spatial arrangement of β-cells within an adult mouse pancreas. (A), (B): spatial assessments of β-cell in interactive 3D data-visualizations. (C): example of islet, scale bar = 110μm. Images were adapted from Alanentalo *et al.* [190].

Optical devices, such as laser scanning microscopy (LSM), as well as nuclear imaging have been suggested in pancreas imaging and each technique has its own strengths and limitations [191]. Compared to other methods, 2-photon LSM, or multi-photon microscopy (MPM) has advantages in high resolution 3D imaging without out-of-focus photon-damage [192], [193]. It is also versatile to sample preparation methods thus has a wide range of applications [191], [194], [195]. MPM uses a long wavelength infrared laser to excite fluorophores which emits short wavelength laser [196]. This is achieved by restricting the probe activation to the focal plane for simultaneous absorption of two photons [191]. As photons are limited to the focal plane, longer penetration depth can be obtained allowing 3D visualization [197]. Despite its potential, the application of this technology for pancreas imaging has yet to be explored.

With LSM, an autofluorence signal, called second-harmonic generation (SHG) can be observed for non-centrosymmetrical crystalline molecules [194], [196]. An SHG signal has a wavelength which is exactly at the half that of incident light and has a sharp

and narrow peak in the spectrum, making them easily identified [193], [196], [198], [199]. Despite from SHG, autofluorescence has also been observed for both laser scanning microscopy of tissue imaging, which shows a monotonously decaying fluorescence spectral [195], [200]. Fluorophores contributing to the autofluorescence consist of both endogenous and extracellular ones. Despite the fact that autofluorescence could provide an approach to selective imaging without staining, its presence may interfere with fluorescent labelling [197], calling for extreme care in filter settings.

One of the research interests for pancreas imaging is to reveal the differences in peri-islet ECM with respect to certain donor characteristics and how these could influence islet isolation. As discussed in **Chapter 2.3.1**, donor age and body mass index (BMI) have been shown to be the most common factors affecting isolation results [159]–[161]. To date, there have been few investigations on the histologic features of pancreas from healthy younger and older donors [12], leading to a poor understanding of the effects of ageing. Moreover, isolated islets from young and lean donors are often mantled, i.e. surrounded by layers of ECM proteins, leading to higher density and poorer separating during the purification stage of isolation and thus to poor yields and low purity [101]. As donor age and BMI could potentially affect the amount and structure of peri-islet ECM, the correlation between these two factors and specific ECM proteins might be important in optimizing islet isolation.

With the aim of improving the current understanding of islet isolation for further yield improvement, this study focuses on the characterization of the islet-exocrine

interface in its native state. High resolution 3D images were obtained with MPM, where spatial arrangement and interactions of islet-ECM interface were studied. The impact of age and BMI on the islet ECM were also investigated, which may aid in the design of tailored digestions for different donors. To the best of our knowledge, this is also the first time that the islet-ECM relationship has been revealed for an intact islet in its native state.

3.2 Methodology

3.2.1 Donor pancreas characteristics

Thirty human adult pancreases were retrieved from DBD (donated after brain death) donors, with appropriate consent and ethical approval obtained. Samples were taken from the head of the pancreas and snap frozen in liquid nitrogen. All samples were stored at -20°C before sectioning.

The average donor age was 38 (ranged from 24 to 60) with an average BMI of 26 (ranged from 18 to 34). For all organs, cold ischemia time was less than 10 hours. The donor characteristics are summarized in **Table 3.1**. Due to the limitations on donor availability, there was a small positive co-linear relationship between age and BMI, but this did not reach statistical significance (**Figure 3.3**, R^2=0.068, p=0.113).

TABLE 3.1 Summary of donor characteristics. (Table to be continued in the next page)

Isolation ID	Age (years)	BMI	Imaging involved
1029	24	25	Thin sample characterization
1031	51	28.7	Thin sample characterization
1035	44	31	Thin sample characterization
1044	28	23	Thin sample characterization
1046	25	24	Thin sample characterization
1101	30	28.4	Thin sample characterization
1106	20	22.6	Thin sample characterization
1107	21	23	Thin sample characterization
1123	44	23	Thin sample characterization
1203	45	31	Thin sample characterization
1215	26	30	Thin sample characterization
1218	53	29	Thin sample characterization
1222	46	26	Thin sample characterization
1232	38	20	Thin sample characterization
1249	46	27	Thin sample characterization
1253	60	31	Thin sample characterization
1256	49	23	Thin sample characterization
1257	18	29	Thin sample characterization
1328	22	21	Thin sample characterization
1332	53	29	Thin sample characterization
1335	26	24	Thin sample characterization

(Table to be continued in the next page)

Isolation ID	Age (years)	BMI	Imaging involved
1337	54	22	Thin sample characterization
1410	41	34	Thin sample characterization
1413	42	29	Thin sample characterization
1423	33	29	Thin sample characterization
1425	35	29	Thin sample characterization
1430	56	26	Thin sample characterization
1431	46	26	Thin sample characterization
1444	53	31	Thin sample characterization
1455	39	23	Thin sample characterization
1506	50	27	Thin & thick sample characterization
1510	54	23	Thin & thick sample characterization
1524	51	26	Thick sample characterization
1525	52	29	Thick sample characterization
1528	53	28	Thick sample characterization
1536	49	25	Thick sample characterization

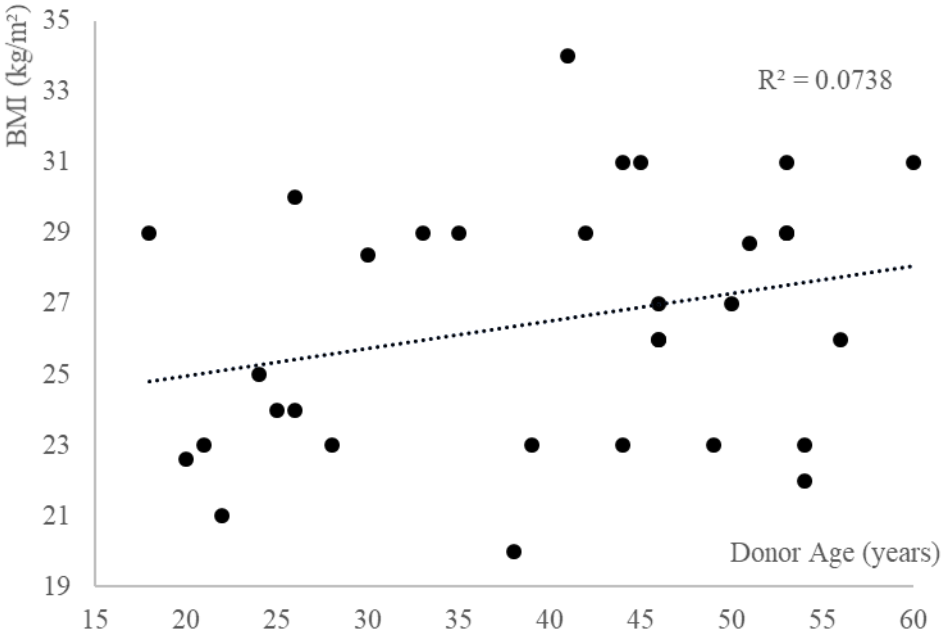

Figure 3.3 Distribution of donor age and BMI.

3.2.2 Native whole-islet staining

Because of the penetration depth achievable with MPM, it was possible to generate continuous 3D images using thicker samples, which allows the study of the islet-ECM interface, as well as their relationship with surrounding vessels in intact islets.

Samples from 6 donors were imaged for native whole-islet staining. Donors were chosen to represent standard donors for clinical isolation process. The average donor age was 52 (ranged from 49 to 54) and the average BMI was 26 (ranged from 23 to 29).

After removal of the attached spleen, duodenum, surface fat and blood vessels, samples were taken from the head of the pancreas and stored in formalin at 4°C before further treatment. As the average diameter for an islet is 140-200μm [60], 200μm thick sections were prepared with a Leica VT1000 S vibratome (Leica, Germany) and stored in PBS (Thermo) at 4°C. Unless specified, all experiments were carried out at room

temperature.

The method for sample preparation was developed based on a protocol for whole-islet staining [190]. Modifications were made to increase penetration depth of protein antibodies. To optimize parameters such as autofluorescence reduction and antibody penetration, conditions for permeabilization and incubation were tested. **Table 3.2** shows parameters tested for each step with results shown in **Section 3.3.3**.

TABLE 3.2 Parameters tested for native whole-islet staining. (Table to be continued in the next page)

Step	**Parameters Tested**	**Optimized Conditions**
Autofluorescence reduction & antigen retrieval	2:1:3 methanol: dimethyl sulfoxide (DMSO): H_2O_2/ methanol dehydration & freeze thaw/ not treated	Methanol dehydration & freeze thaw
Permeabilization	0.1% Triton X-100/ 1% Tween-20	0.1% Triton X-100
Blocking time	0.5h, 1h, 2h, 3h, 4h, 5h, 6h, 8h	8h
Primary antibody incubation Time	0.5h, 1h, 2h, 4h, 8h, 16h, 22h, 26h, 33h, 48h	33h
Primary antibody concentration	1x, 2x, 3x	2x
Secondary antibody concentration	1x, 2x, 3x	2x

(Table to be continued in the next page)

Step	Parameters Tested	Optimized Conditions
Secondary antibody incubation Time	0.5h, 1h, 2h, 4h, 8h, 16h, 22h, 37h, 48h	37h
Tris-NaCl buffer (TBS) with 0.1% Triton X-100 washing time	4min, 0.5h, 1h, 2h, 4h, 8h	4h

With above optimized parameters, tissue sections were stained. Briefly, the sections were firstly dehydrated in methanol for 1 hour with one change of solution after 30 minutes. For antigen retrieval, sections were firstly frozen at – 80°C for 1 hour and thawed at room temperature for an additional hour. The freeze-thaw cycle was repeated for three times before the sections were rehydrated back in a series of TBST (TBS with 0.1% Triton X-100) - methanol solution (33%, 66%, 100% TBST, >15min for each wash). Normal goat serum (1:20 in TBST) was used to block non-specific binding for 5 hours, followed by 33 hours of primary antibody incubation (1:50 Dako polyclonal guinea pig anti-insulin, with cue of 1:150 Abcam polyclonal rabbit anti-human pan-laminin or 1:150 polyclonal rabbit anti-human collagen IV, 1:25 Dako monoclonal mouse anti-human CD31 endothelial cell, 1:10 DMSO, all in TBST). Excess antibodies were washed off 3 times in TBST solution, each for 4 hours. Secondary antibody incubation (1: 250 Invitrogen goat anti-rabbit Alexa 488-conjugated, 1:25 Vectorlabs goat anti-guinea pig Texas Red-conjugated, 1:50 Vectorlab AMCA-conjugated horse anti-mouse IgG antibody, 1:10 DMSO, all in TBST) lasted for 37 hours in dark. Post incubation the tissue was washed as previously described.

Details of the antibodies are listed in **Appendix 7.1**. Finally, the samples were mounted (Vectorshield Hard-Setting Mounting Media) and imaged. Tissue sections incubated with only TBST and DMSO served as negative controls.

3.2.3 Thin section staining

To demonstrate the suitability of using MPM imaging to study the impact of age and BMI on the pancreatic matrisome, pancreatic tissue sections were stained for ECM proteins. Due to the difficulties in antibody penetration and extensive time requirement, thin sectioned samples (10-15μm), instead of thick samples were used.

Three 10μm samples were cryosectioned onto Superfrost Plus slides (Thermo Fisher) at -20°C. Collagens I, III, IV, VI, laminin and perlecan were chosen as the proteins of interest for their abundance and representativeness of collagenase and neutral protease substrate, as discussed in **Chapter 2.2.1**. The proteins were identified by double immunolabeling and the optimal staining conditions were determined for each protein subtype. Briefly, tissue samples were firstly blocked with normal goat serum (1:20) for 30 minutes, followed by a 1-hour incubation with primary polyclonal antibodies (1:100 Dako guinea pig anti-insulin, with one of: 1:300 Abcam rabbit anti-human pan-laminin, 1:300 Abcam rabbit anti-human collagen I, 1:300 Abcam rabbit anti-human collagen III, 1:300 Abcam rabbit anti-human collagen IV, 1:300 Abcam rabbit anti-human collagen VI, or 1:300 Abcam rabbit anti-human perlecan, all diluted in TBS). The excess antibodies were washed off in TBS solution (Thermo) 3 times, with each wash lasting for 4 minutes. Tissue sections were then incubated in secondary

polyclonal antibodies (1: 500 Invitrogen goat anti-rabbit Alexa 488-conjugated, 1:50 Vectorlabs goat anti-guinea pig Texas Red-conjugated, both in TBS) for 30 minutes in dark, followed by a similar washing process in TBS. Details of the antibodies are listed in **Appendix 7.1**. Finally, the samples were mounted (Vectorshield Hard-Setting Mounting Media) and imaged. An average of ten 3D images were taken and analysed for each specimen. To avoid interruptions from SHG signals, tissue sections incubated in TBS but not stained were imaged to determine the background signal level.

3.2.4 Imaging

Images were taken with a multi-photon dedicated laser scanning imaging system. The microscope uses a Verdi laser with Mira laser booster (Coherent UK Ltd). The imaging system comprises an upright microscope (Nikon E600FN) coupled to a multi-photon dedicated laser scanning imaging system (Bio-Rad Radiance 2100MP). The upright microscope is also equipped with a bright field microscope and mercury lamp. The spatial arrangement of the imaging system is shown in **Figure 3.4**.

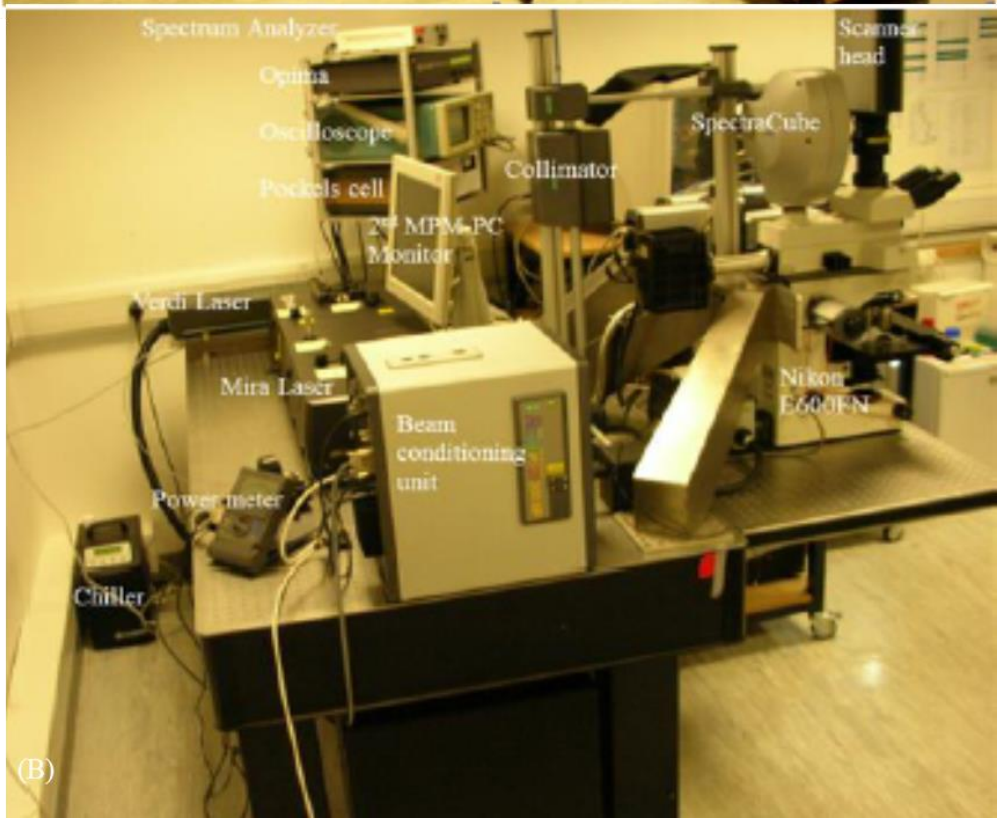

(Image to be continued in the next page)

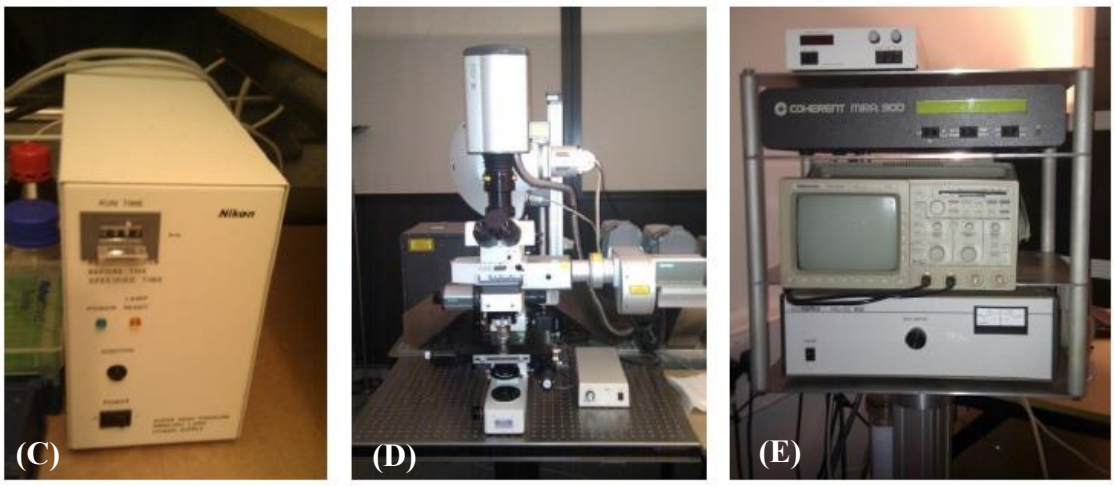

Figure 3.4 MPM set -up. (A) & (B) Overall set-up of the MPM with all associated apparatus; (C): Mercury lamp; (D): microscope; (E) oscilloscope

The objective used was a Nikon CFI Fluor 40x with water being the immersion media. The direct detectors used were non-descanned photomultiplier tubes and a spectral interferometer (SpectraCube®) was used for fluorescence signals characterization. For our experiments, the inlet laser power was around 10W with a wavelength of 800nm. The spectral interferometer divided the emission light into blue, red and green channels. However, due to the current arrangement of the spectral detection system, in which a CCD camera was used for acquiring an image, the system was not suitable for spectral characterization of fluorophore sources located deep in scattered tissue. As a result, same settings were used for both thin and thick sample imaging while for native islet staining experiments, samples were imaged from both top and bottom sides, to confirm the penetration of antibodies. Images produced from MPM were made in planes with 0.45μm intervals and processed in Lasersharp 2000 software.

3.2.5 Analysis and statistics

Qualitative and quantitative analyses were achieved with *Imaris* (Bitplane) and *Fiji* software, respectively. Both *Imaris* and *Fiji* were used to build 3D images and incorporate information from individual channel colours. *Imaris* was used for its set-up functions, like iso-surfaces building or volume calculations. However, it was time-consuming for users to select their own region of interests (ROIs) based on signal intensity. In contrast, *Fiji* is open-source thus easier for users to write their own operations. To make the most use of the software, qualitative analysis was achieved with *Imaris*, which clearly showed islet-exocrine interface in 3D. Images obtained with MPM were first deconvolved to enhance contrast then iso-surfaces were built which could provide more clarity of the interface.

Difficulties were encountered when trying to conduct quantitative analysis with *Imaris* software, where full or semi-automatic ROI selection of islet boundary based on image intensity proved to be difficult. For this purpose, a method was developed for 3D quantification based on a method developed by the Islet Transplant Research Group [13]. The full test of operations is listed in **Appendix 7.2**, which is divided into preparation, islet area and intensity measurement and protein area and intensity measurement. Briefly, the 3D images were first reconstructed to a series of 2D images, with the space the same as laser scanning (0.45μm). Islets were identified based on an automatically detected threshold value and were measured for their area on each plane. Since the research interests were placed on the islet-exocrine interface, ideal ROIs were slightly larger by 5% than the islet boundary. The principle was to draw, select and

measure ROIs based on automatic or user-defined threshold. Therefore, the extent of the area and intensity of proteins surrounding each islet (105% of the islet area) were quantified.

Montages of islets and proteins signals in ROI, as well as the outlines of islet and proteins measurement are shown in **Figure 3.5** and **3.6** as examples. The numbers at the bottom of images are slides number in *z-axis*.

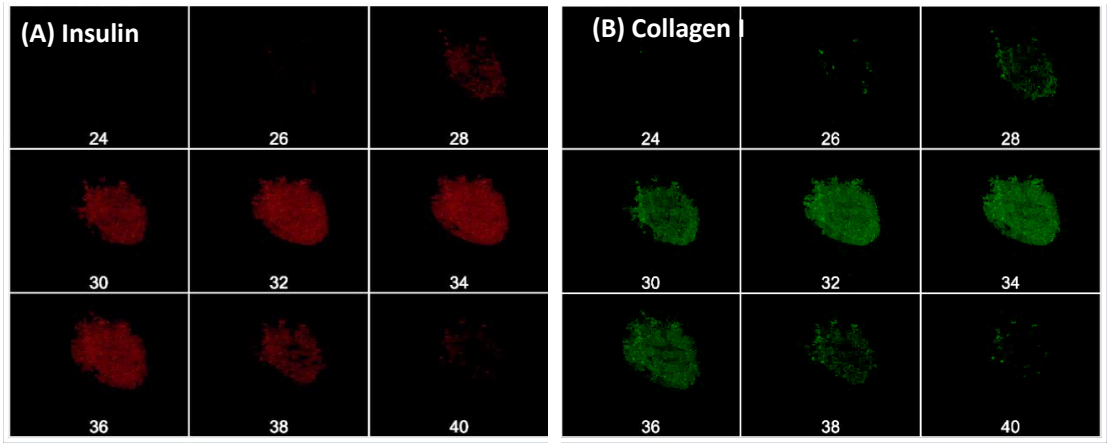

Figure 3.5 Insulin (A) and Collagen I (B) signals in ROI (HP 1249 Coll I)

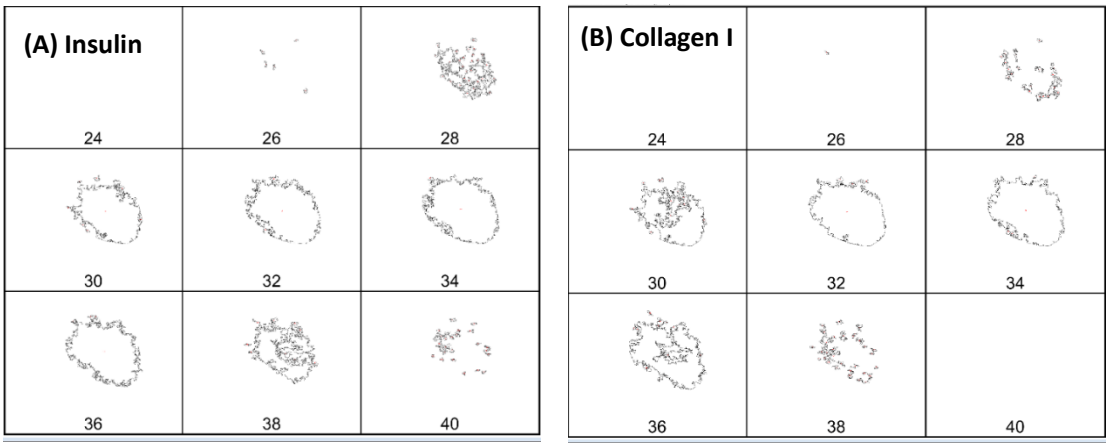

Figure 3.6 Outline of insulin (A) and collagen I (B) measurement (HP 1249 Coll I)

During the analysis, brightness and contrast were first adjusted for all images for optimal analysis. Background noise was measured and subtracted from the whole image. The threshold of the islet channel was then adjusted, and the ROIs were automatically

selected based on this. The ROIs were then expanded where islet and protein signals were measured. The protein signals are normalized with those of islets to enable comparisons among samples of different islet size.

Data were expressed as the sum of the area times the intensity of protein on each plane surrounding the islet over the sum of islet area on each plane, as shown below:

$$\text{Ratio} = \frac{\sum(Intensity_{protein} * Area_{protein})}{\sum Area_{islet}}$$

This normalization was applied to exclude the effects of islet size. Data were expressed as mean±SD and statistical analyses were achieved with analysis of variance (ANOVA), mixed linear modelling or multiple linear regression (p<0.05 for significant), with IBM SPSS version 24 (Chicago, USA). The analysis included 'donor' as a co-variant to determine the effect of potential confounders.

3.3 Results

3.3.1 Whole-islet staining

Thick pancreas sections (150-200μm) were imaged from 6 donors (age 51±3 years, BMI 29±2 kg/m^2, CIT<10h). The donors were selected to represent standard donors for clinical islet isolation. The protocol used was adapted from whole-organ staining using tomographic molecular imaging [190]. The method was optimized to reduce autofluorescence as well as increase penetration depth of the antibodies. Variables tested are summarized in **Table 3.2**. **Figure 3.7** illustrates the effects of two autofluorescence reduction methods in comparison to untreated samples. As shown,

freeze-thaw cycles after methanol dehydration resulted in the best image quality and was conducted for further experiments. **Figure 3.8** shows the effects of antibody concentration, where a direct improvement on image quality was observed by doubling the antibody concentration. Further increase the antibody concentration resulted in little improvement of the antibody penetration depth and was therefore abandoned. Similarly, prolonging the incubation time resulted in a significant improvement of the antibody penetration depth, as illustrated in **Figure 3.9**.

Collagen IV, insulin and CD31+ endothelial cells were labelled to study the islet-ECM interface and vessel distribution surrounding the whole islet. With optimum staining conditions, the penetration depth of antibodies could reach the whole section, which was confirmed by double imaging from both sides of the section. However, further than 70μm, photons were relatively insufficient to excite attached fluorophores. Nevertheless, data-rich 3D images were obtained for all 6 donors, proving the applicability of this optimized protocol.

The protein distributions for thick sections could be seen as a stack of thin section series with improved tissue continuity (**Figure 3.10**). For small islets (<50μm) or tips of large islets, proteins form a sheet-like structure surrounding them while for large islets they also intrude into the centre. Vessels, as represented by endothelial cells, showed a similar structure. They are prevalent in exocrine tissue, periphery of islets, or intruding into the centre of large islets, which were in accordance to previous thin-section studies [72]. Careful examination showed that within an islet, vessels were always juxtaposed with ECM proteins, possibly due to the structural support and cell

communication function provided by the latter. The observed structural features were found to be consistent among all 6 donors.

Compared to conventional 2D images, 3D imaging of an intact islet enables detailed investigations at peri-islet interface. Unlike image sets obtained from serial sections, 3D imaging allows continuous observation of the structural features at arbitrary region. Furthermore, as the structural integrity is preserved, it allows analyses for the spatial arrangement and porosity of ECM proteins.

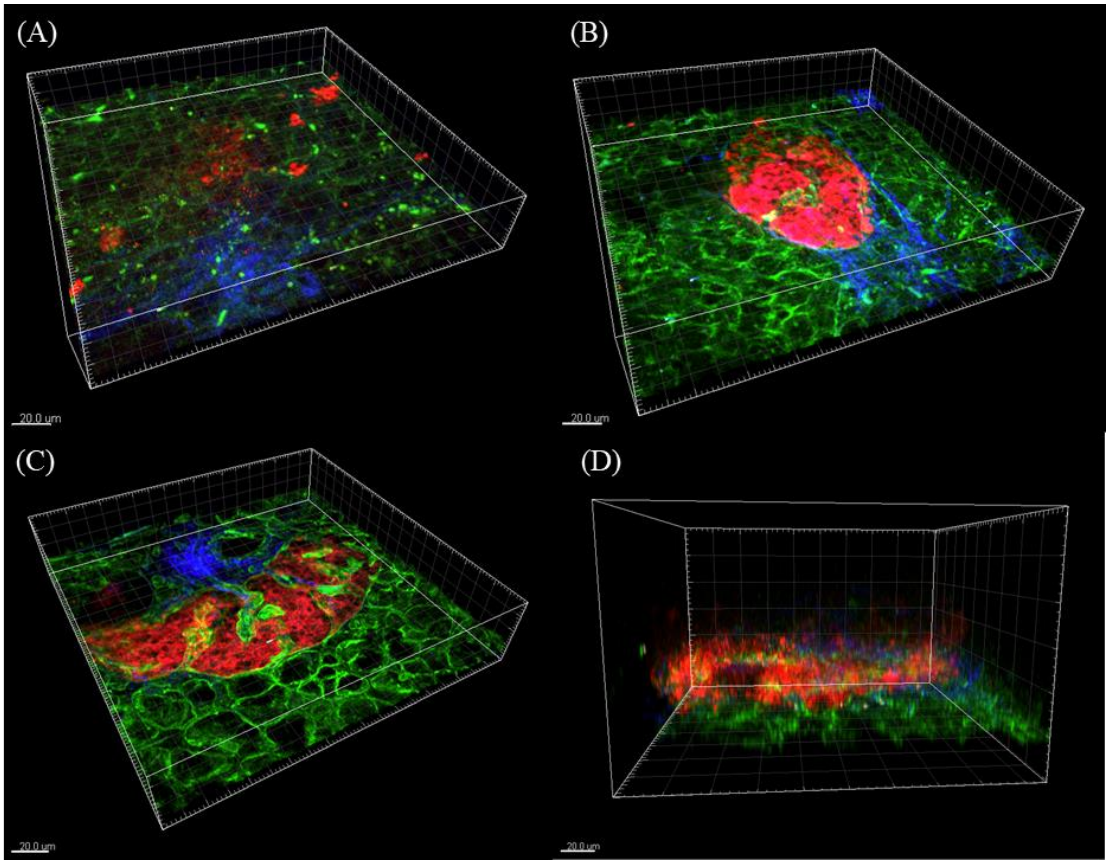

Figure 3.7 Impacts of different autofluorescence reduction methods. (A): non-treated; (B): 2:1:3 methanol: dimethyl sulfoxide (DMSO): H_2O_2; and (C): Methanol dehydration with free-thaw cycles**.** (D): Side view of samples treated with methanol dehydration and free-thaw cycles. The images show insulin (red), collagen IV (green) and CD31+ endothelial cells (blue). Scale bar = 20µm.

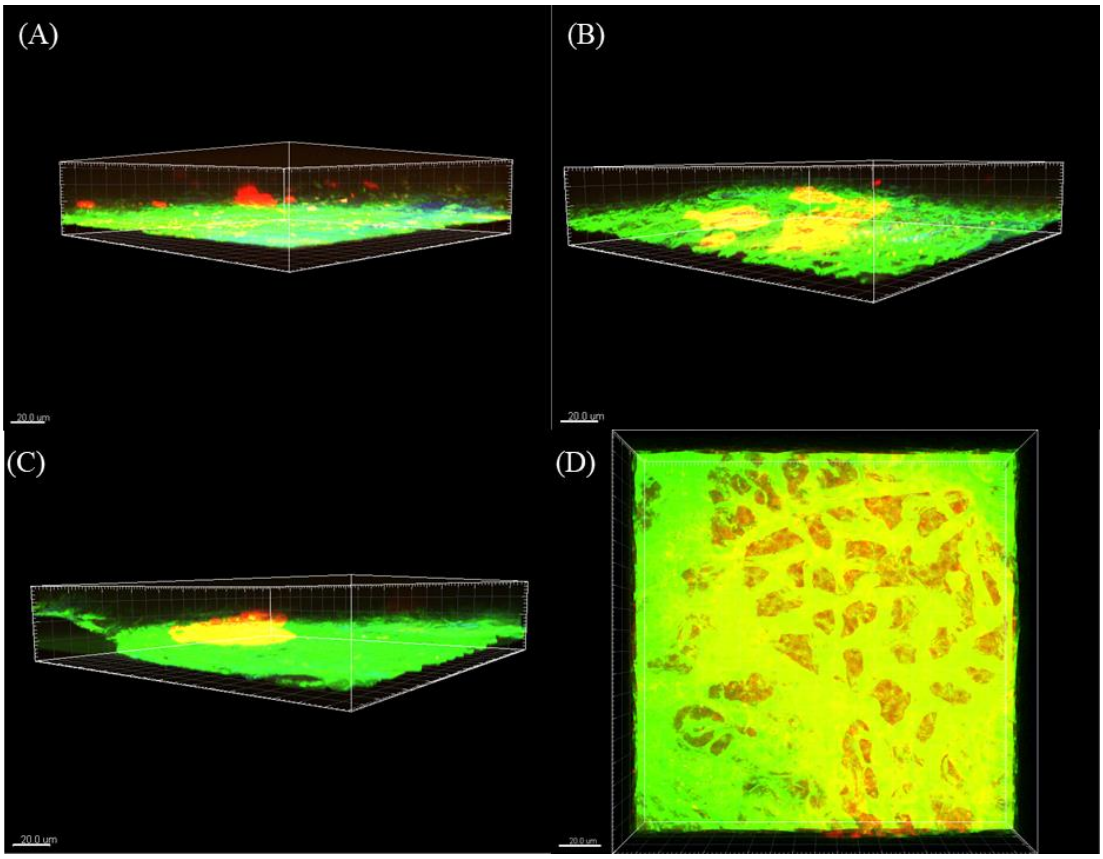

Figure 3.8 Impacts of increasing antibody concentration to (A): 1x; (B): 2x; and (C): 3x. (D): Top view of the obtained image with 3x antibody concentration. The images show insulin (red), collagen IV (green) and CD31+ endothelial cells (blue). Scale bar = 20µm.

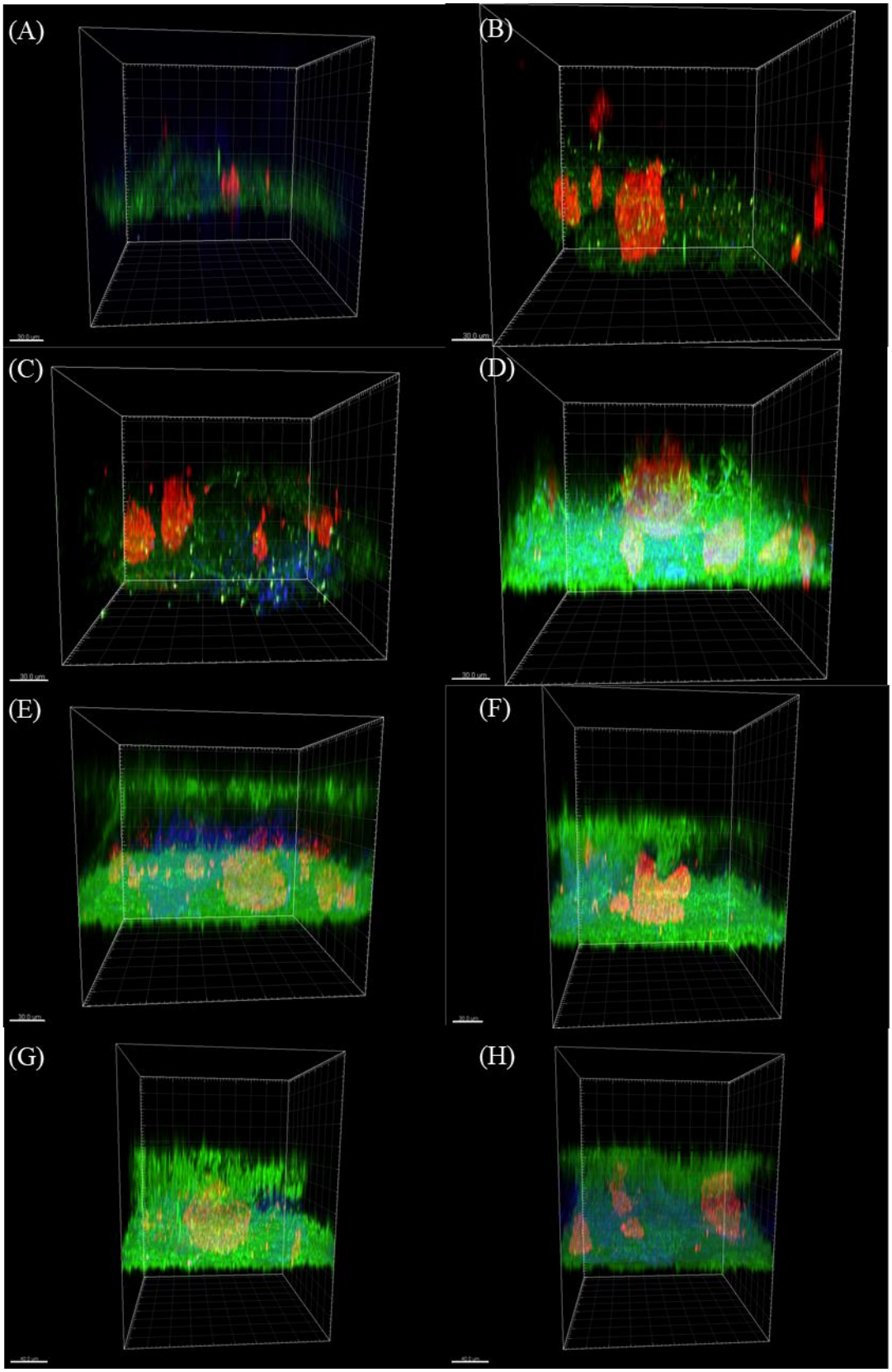

Figure 3.9 Impacts of increasing antibody incubation time to (A): 0.5h; (B): 1h; (C): 2h; (D): 8h; (E): 16h; (F): 26h; (G): 33h; (H): 48h. The images show insulin (red), collagen IV (green) and CD31+ endothelial cells (blue). Scale bar = 30µm for (A) – (F) and 40µm for (G) – (H)

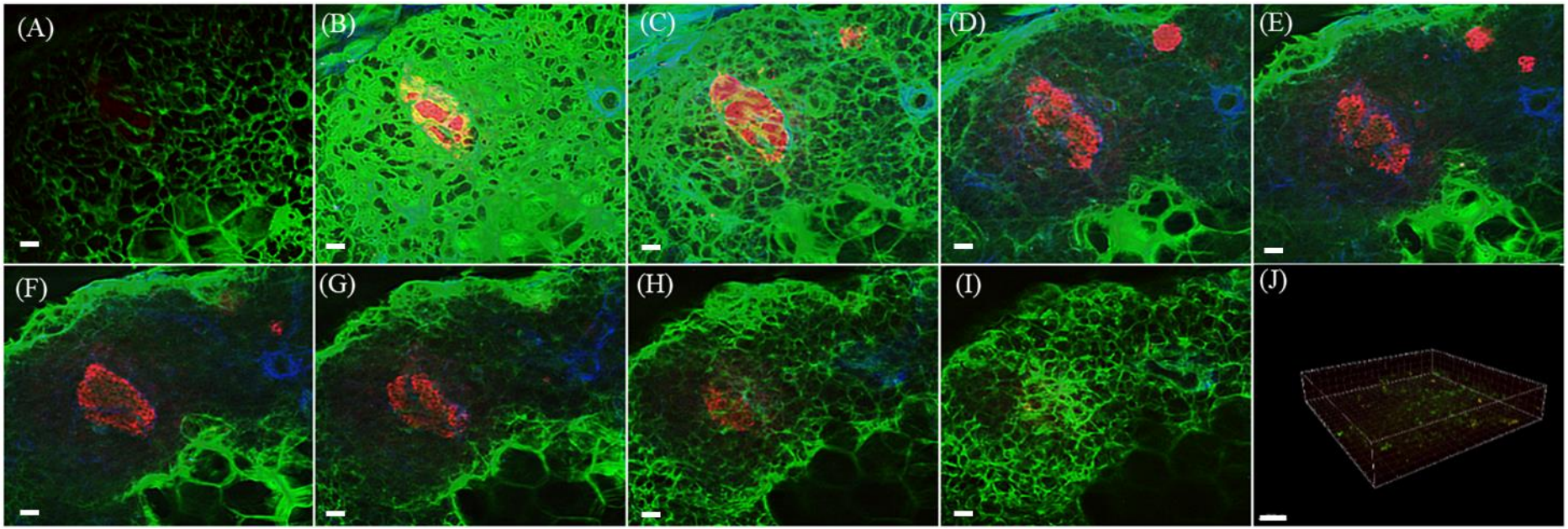

Figure 3.10 Layer-by-layer display of collagen IV, vessels and islet from a donor aged 50 with a BMI of 27 (Isolation ID = 1506). The images show insulin (red), collagen IV (green) and CD31+ endothelial cells (blue). Z-stack interval = 25µm; (J): Results from negative control, where samples were incubated with only secondary antibodies for background check. Scale bar = 20µm.

3.3.2 Thin section staining: impact of donor age & BMI

Thin pancreas sections (10-15µm thick) from 30 donors (**Table 3.1**) with varying age and BMI were double immunostained and analysed. Peri-islet content of collagen I, collagen III, collagen IV, collagen VI, perlecan and laminin were assessed where islets were identified by insulin labelling of the β-cells. Examples of 3D structure of islet-ECM relationship for all proteins are shown in **Figure 3.11**. The ECM proteins of interest form a network structure as a sheet-like structure circumscribing the islet. These proteins also protruded into islet centre possibly to provide necessary structure supporting and aid cell communication. SHG signals from endogenous and extracellular molecules were observed. However, their intensity was considerably weak and were corrected in background calculations.

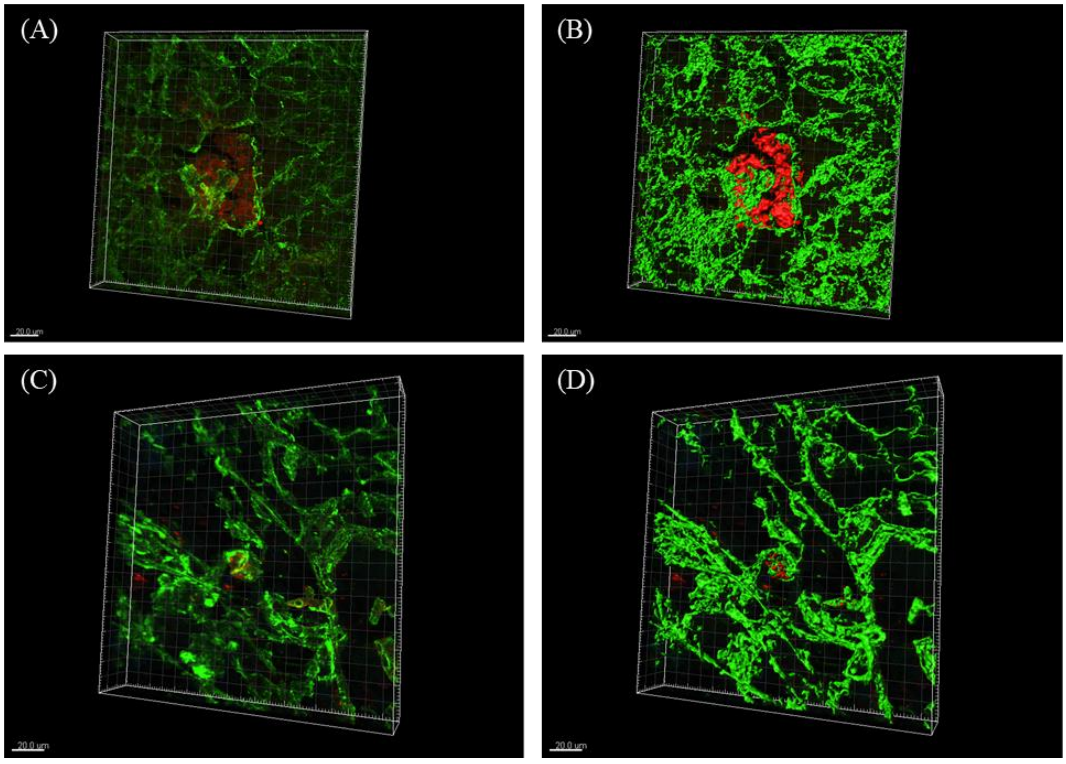

(Image to be continued in the next page)

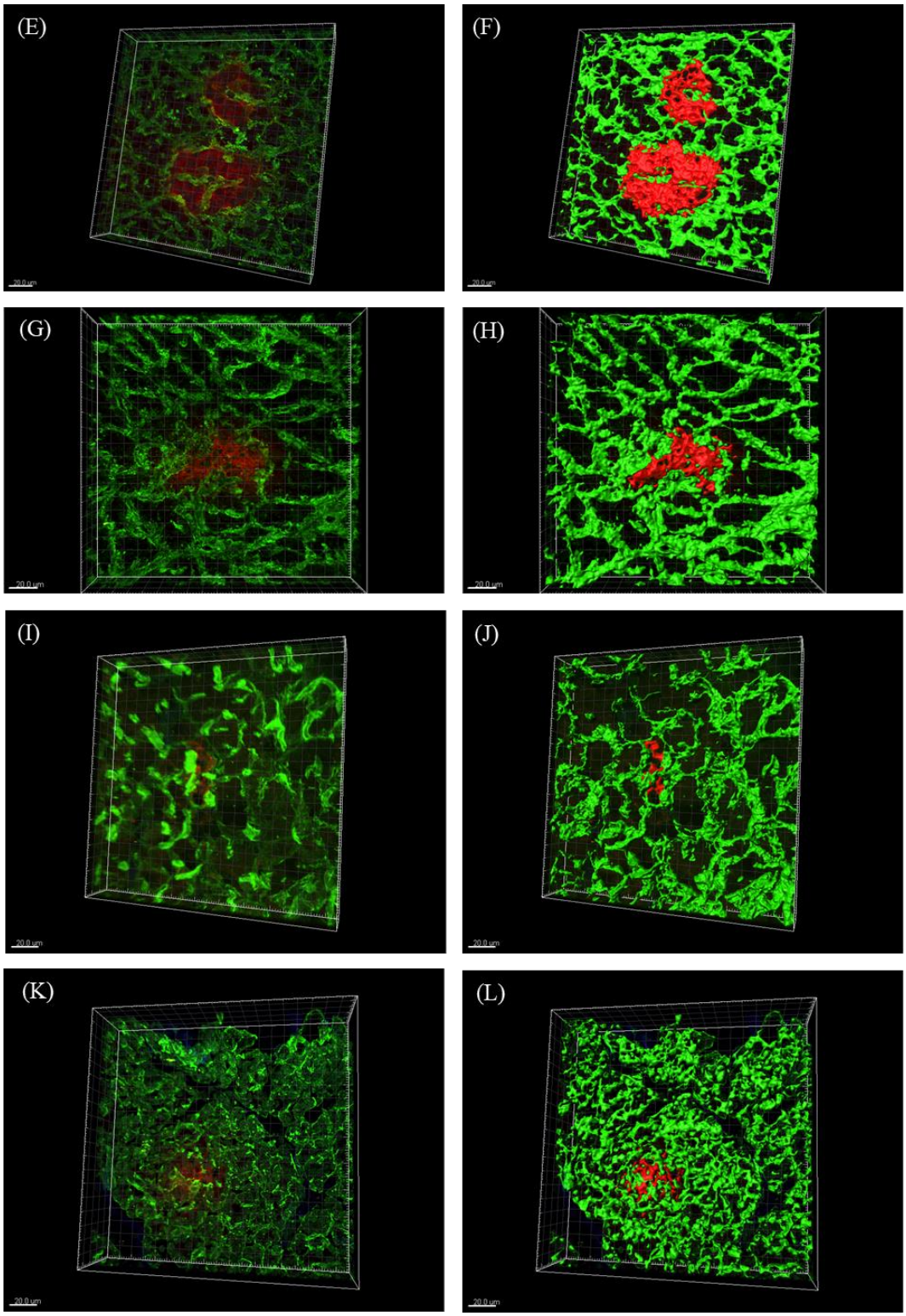

Figure 3.11 Representative 3D images (left) and isosurfaces (right) of ECM proteins (green) and insulin-positive cells (red) from a donor aged 44 with a BMI of 23 (Isolation ID = 23). Immunostained insulin (red) indicated islets. Green indicated immunostained proteins of interest: (A) & (B): collagen I; (C) & (D): collagen III; (E) & (F): collagen IV; (G) & (H): collagen VI; (I) & (J): perlecan; (K) & (L): laminin. Scale bar = 20µm.

The effects of donor age and BMI on the content of ECM proteins at islet-ECM interface were assessed. The results for collagen I, collagen III, collagen IV, collagen VI, perlecan and laminin with respect to donor age and BMI are shown in **Figures 3.12** and **3.13** respectively. As shown, age and BMI resulted in significant variations in specific peri-islet proteins, which were independent of donor co-variance. Peri-islet collagen I and laminin declined slightly, but significantly, with increasing age (both $p<0.001$) and BMI ($p<0.001$ and $p=0.003$, respectively). In contrast, peri-islet perlecan increased marginally, though significantly, with age and BMI (both $p< 0.001$). There was no significant effect of age or BMI on peri-islet collagen III, collagen IV or collagen VI.

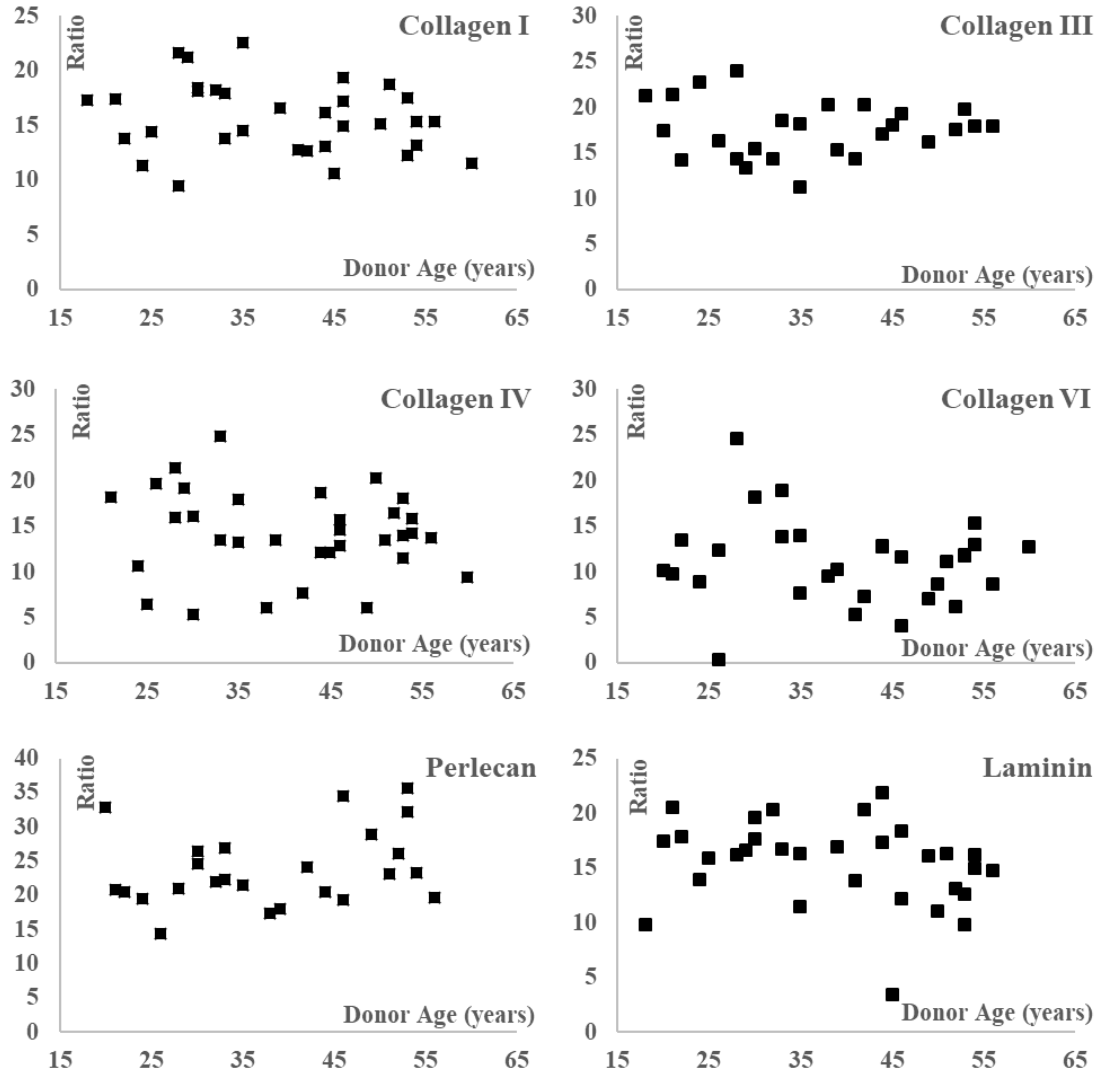

Figure 3.12 Impact of donor age on protein content. The y-axis shows the ratio of protein area*protein concentration to islet area. This ratio is used to represent the amount of protein at peri-islet surface while eliminating the impacts of islet size. Large variations were observed for samples from different donors. No significant results were found for collagen III, collagen IV and collagen VI. The amount of collagen I and laminin decreased with the increase of donor age ($p<0.001$) while the amount of perlecan increased with increasing donor age ($p<0.001$).

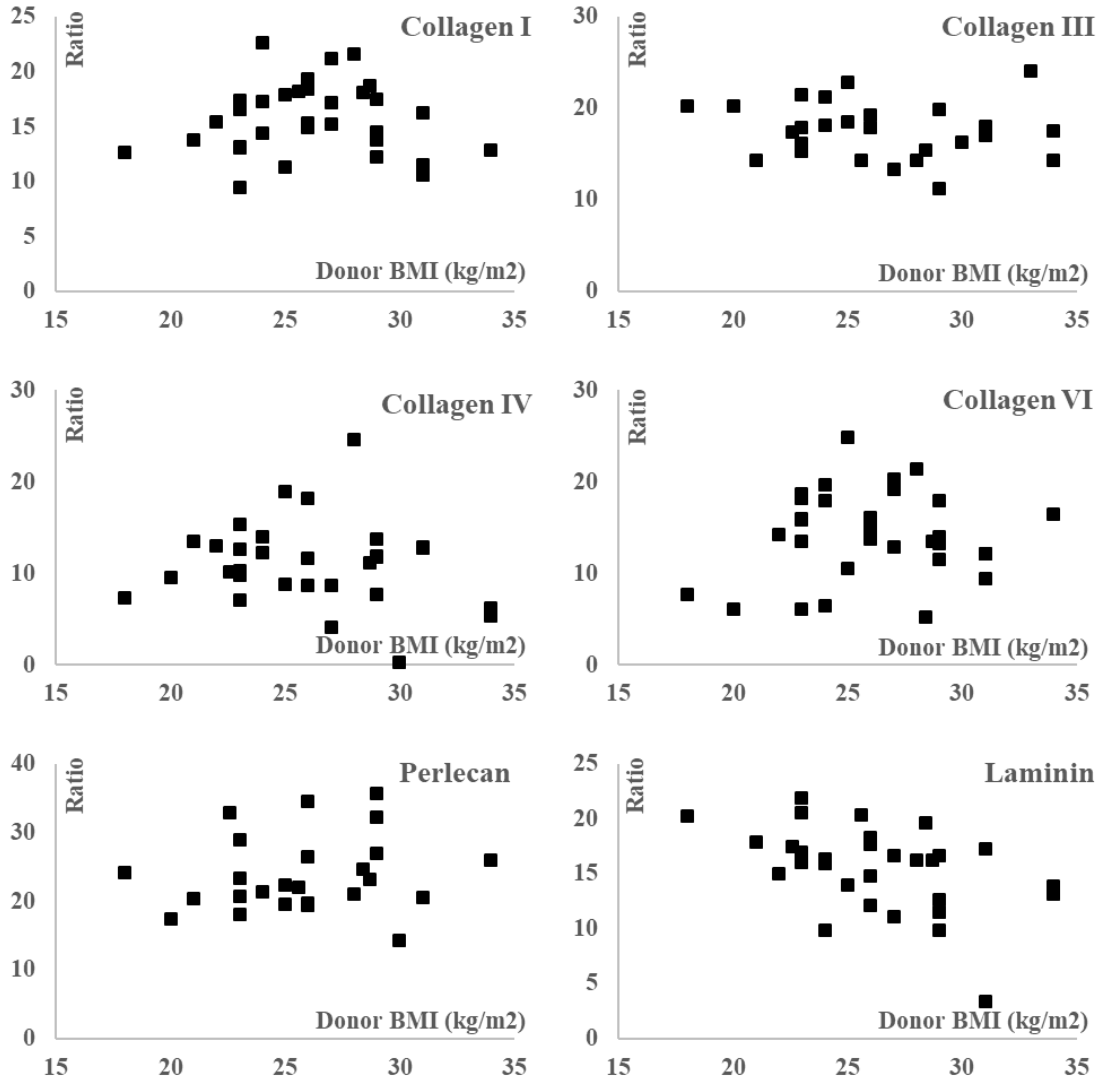

Figure 3.13 Impact of donor BMI on protein content. The y-axis shows the ratio of protein area*protein concentration to islet area. This ratio is used to represent the amount of protein at peri-islet surface while eliminating the impacts of islet size. Large variations were observed for samples from different donors. No significant results were found for collagen III, collagen IV and collagen VI. The amount of collagen I and laminin decreased with the increase of donor age ($p<0.001$ and $p=0.003$, respectively) while the amount of perlecan increased with increasing donor BMI ($p<0.001$).

3.4 Discussion

Although decades have passed since the first islet was isolated, little research has been conducted on characterization of the extracellular matrix. Previous studies have shown that, compared to mouse islets, human islets are surrounded by two layers of basement

membrane, providing the necessary structure support and bridges for cell communication [96]. Some of the main components, such as collagen, laminin, elastin and fibronectin, have been identified in humans [201], [202]. Their composition, structure and quantity have been studied in normal pancreases [81], [203]. Nevertheless, with the increasing demand in islet transplantation, there is an urgent requirement to obtain a thorough understanding and characterization of islet basement membrane as well as how it varies with normal physiological changes such as age and BMI. This would not only help improve clinical isolation results but would also provide information for *in vitro* 3D cell culture. To the best of our knowledge, this is the first experiment in 3D characterization of ECM proteins within islets, as well as the study of their relationship associated with physiological parameters using high resolution MPM imaging.

With MPM, SHG signals from endogenous and extracellular molecules were observed. For thin sections, as antibodies could easily penetrate and attached to tissue sections, the intensity for SHG signals was relatively weak and could be easily excluded in background corrections. However, for 150-200μm sections, the diffusion of antibodies into the centre of tissue sections became difficult and autofluorence was relatively prominent. To avoid confounding of labelled proteins, methods for reducing autofluorence and increasing antibody penetration depths were applied. Detailed tested parameters are listed in **Table 3.2**. Freeze-thaw cycles, doubling antibody concentration and prolonging incubation time proved to be efficient. Nevertheless, an increase of TBST washing was required to remove excessive antibodies at the surface of tissue

sections. Moreover, to facilitate optimal antibody penetration, long incubation periods were introduced. The final protocol was a balance between time and image quality.

Here, insulin positive β-cells were chosen to represent islets. Due to the structure of human islets, where β-cells are more likely to be observed in the centre and surrounded by α-cells [72], there might be a slight underestimation for the actual size of islet, and hence affect the incorporation of basement membrane. Nevertheless, reconstructive 3D images of human islets have shown that although β-cells generally occupy central positions, cytoplasmic extension is widely seen to reach the surface of islets [72]. Therefore, they could be considered as a reasonable representation of the whole native islet.

In our study, we find collagens and laminin are widely distributed, forming a perforated structure surrounding islets as well as extending to the exocrine part of pancreas. 3D images from thick samples reveal that they are organized into a constant pattern, where the large protein sheet is formed and encapsulate the entire islet. This complete-wrapping structure not only helps to separate the endocrine part from exocrine tissue, but also provides the required structural support for islets. In medium or large islets, these proteins were found co-localized with endothelial cells, providing necessary mechanical support, biological separation as well as cues for cell communication and normal function.

Here we successfully developed a protocol for imaging an intact islet and surrounding ECM in their native state. With high resolution MPM images, the detailed islet-exocrine interface could be studied. 3D models could also be built to investigate

the spatial arrangement and porosity of these proteins. This could provide valuable information for 3D islet culture as well as scaffold construction.

The amounts of different collagens and laminin vary with many factors. Upon maturation, collagens have a high resistance to enzyme digestion and a relatively long biological half-life [204]. As a result, their content is expected to increase within old donors. A previous study of collagen VI shows that age has little impact on its content [80]. However, the method employed was an immunohistochemistry (IHC) method, where only the presence of collagen rather than the concentration of collagens at the site of observation was measured. In our experiment, both the area of observation and the amount or concentration of protein on site, as represented by its fluorescence intensity, were included. With this method, decreases in collagen I and laminin were found with increasing donor age. Similar results were also obtained in a recent study using hydroxyproline measurement, where a reduction trend of total collagen content towards ageing was observed [205]. As laminin and collagen are important in stabilizing the ECM network, its reduction may result in an increase in the susceptibility to enzyme digestion. Perlecan, on the contrary, is less abundant in young donors, and its content increased with donor age.

We have further analysed the impact of donor body mass index and found that the content for collagen I and laminin decreased slightly, but significantly, with increased donor BMI. This slight reduction might be caused by fat accumulation within islets, as observed in heavier donors [162]. Fat infiltration may also destabilize the whole ECM network and thus increase the susceptibility to enzyme digestion. Nevertheless it needs

to be mentioned that high BMI donors tend to have hypertrophic islets [20], thus the overall amount of these proteins might be increased, as the content shown here have been normalized to islets size.

It needs to be mentioned large variations were observed during the analyses, leading to difficulties in reaching statistically significant results. Part of the reason was attributed to the intrinsic variations among and within humans. Factors such as hospitalisation, smoking, drinking history could all affect the results and a co-variant was therefore introduced in the analyses to determine the effects of these confounders. The variations were also considered in the interpretation of the results.

A successful islet isolation, which is generally defined as the production of a sufficient number of islets, has been found to correlate with many factors, including donor age and BMI [157], [160]. With the same dosage of enzymes, success isolations are more easily obtained with older and heavier donors, while young and lean donors tend to result in poor isolation with low purity [101], [156]. A close look at islets from young donors shows that they are surrounded by layers of basement membrane [168], suggesting insufficient digestion. Although the isolation efficiency is low, islets from young and lean donors may be preferred as they function better in terms of viability and post-transplantation function [156], [167].

Our results indicated relationships between donor age, BMI and pancreas ECM protein content, thus helping to answer the question of variation in isolation success with respect to these donor characters. Compared to BMI, age was more significantly correlated with protein quantity, where higher collagen I and laminin but lower perlecan

content was found in young donors. Nevertheless, the amount of collagen III, collagen IV and collagen VI were not significantly influenced. This suggests that an increase in enzyme concentration or a prolonged digestion may be required to achieve complete isolation for such a donor group. In fact, centres with elevated protease dosage for young donors have proved their ability in production of sufficient amount of islets with desired purity [187]. A recent study using increased protease combination also showed an elevation of post-purification islet recovery compared to increased collagenase combination [205].

Similar changes might also be applied to lean donors, as their collagen I and laminin content was also higher than overweight donors. However, this correlation is relatively weak and no impact of BMI on other collagen subtypes is observed. The high isolation yield from high BMI donors might be a combined result of hypertrophic islets, fat infiltration and destabilization of ECM network, as suggested by a reduction of laminin content.

Together with donor variations and regional variations among different centres, the optimum enzyme dosage might only be achieved in an empirical way. On the other hand, prolonging digestion time provides flexibility and better controllability. However, this needs to be implemented with extreme care to avoid over-digestion and islet fragmentation.

3.5 Conclusion

In conclusion, our experiment reveals the first 3D image of pancreas islet ECM

with a multi-photon microscope. It was found that collagen and laminin are prevalent in islet ECM, forming a network-like structure in exocrine part and a sheet-like membrane wrapping the entire islet. Quantification analyses show the content of collagen I and laminin decrease with donor age and BMI, while perlecan increases with both donor age and BMI. In terms of clinical significance, our results suggest a specific enzyme blend in islet isolation for different donor groups rather than an "all-in-one" solution, for the improvement in isolation efficiency. However, the exact composition might vary among centres with regional impacts taken into consideration. Also, this analysis could not determine how these proteins interact with each other. Consequently, studies on detailed digestion process with respect to donor age were conducted to help answer above questions in the next chapter.

Chapter 4

Creation and development of a novel perfusion chamber for *in vitro* studying real-time digestion of the pancreatic matrix

4.1 Introduction

With an understanding of the ECM distribution at peri-islet interface, the focus of this study moves to the digestion process. Although almost 20 years have passed since Edmonton protocol [116], there has been little investigation of the digestion process itself. Most research has focused on the development of new enzyme blends [177], [185], [206] while little attention has been paid to digestion process parameters or chamber design [15], [207]. As the digestion process involves enzyme-protein binding [172], the composition of enzyme and process parameters, such as retention time and perfusion flowrate, may have a significant impact on the digestion results.

Currently, the understanding of these variables in islet isolation is relatively limited, partly due to a lack of tools for studying the digestion process in detail at the molecular level. In 2012, the Oxford Islet Transplant Group [208] described a method to investigate the distribution of enzymes in isolated islets. Briefly, samples were taken at various stages during clinical isolations and stained for insulin and collagenase. It was found that following intraductal collagenase administration, the enzyme was detected in the exocrine pancreas and at the periphery of islets. Penetration into the islets was also observed in samples after intraductal administration but not in post-digestion or post-purification samples.

Focusing on the islet-ECM interface, a simple slide-based method was proposed by the same group [209]. Briefly, slide-loaded pancreatic samples were digested statically with enzymes at clinically relevant concentration for 2 and 5 minutes while samples incubated with HBSS were used as control. A semiautomated quantitative

measurement similar to the method employed in **Chapter 3**, **Section 3.2.5** was introduced. The reproducibility of using different samples from the same pancreas was confirmed [13].

With the aid of an in-house macro in ImageJ, the group then investigated the digestion of some key matrix proteins during human islet isolation [102]. Significant but differential loss of collagen IV, pan-laminin, perlecan and laminin-α5 was demonstrated. The group also studied ECM proteins in isolated islets and suggested the disruption of intact basement membrane may have major translational significance. The application of this method to study the impact of various enzyme dosage patterns was also demonstrated. As shown in **Figure 4.1**, significant loss of collagen IV and laminin-α5 was observed under different enzyme combinations [13].

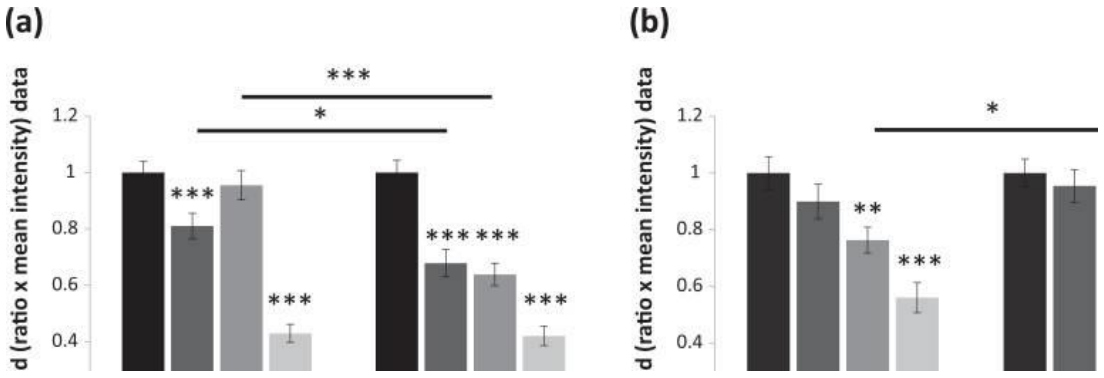

Figure 4.1 Quantitative analysis of collagen IV (A) **and laminin-α5** (B) digestion. Colour-coded for: control group, collagenase only, neutral protease only and combined enzymes (from dark black to light grey), all at clinically relevant concentration. Asterisks represent $p<0.05$ (*), $p<0.01$ (**) and $p<0.001$ (***) respectively. Adopted from Spiers [13].

Despite improvements discussed above, currently all the studies were conducted using static digestion. Clinical islet isolation, however, is a continuous perfusion process with varying enzyme concentrations in different centres [187], [205]. A better

understanding of these parameters and their impact in digestion is therefore required. Not only could this help to reveal the mechanism of the isolation process and improve the isolation yield, but also to establish a firm foundation for enzyme development and process optimization.

With the aim of improving the current understanding of islet isolation for further yield improvement, this study focused on the developing a tool to observe real-time digestion of the islet-exocrine interface. To investigate the digestion mechanism, a perfusion device was developed, allowing real-time observation with a fluorescent microscope. The time-course changes caused by enzyme digestion were also recorded. Process parameters, such as flow rate and temperature were adjusted to optimize the system. To our knowledge, this is the first time that the digestion profile for peri-islet ECM has been reported.

4.2 Methodology

4.2.1 Donor pancreas characteristics

Eight human adult pancreases were retrieved from DBD (donated after brain death) donors in Oxford, the United Kingdom, with appropriate consent and ethical approval obtained. All donors, as shown in **Table 4.1**, fell within an age range of 24 to 60 years and a BMI range of 23 to 26, with cold ischemia times of <18 hours. All pancreatic samples were taken from the head region of donor organs before being snap frozen in liquid nitrogen. Three 10μm samples were cryosectioned onto Superfrost Plus slides (Thermo Fisher, UK) at -20°C.

The proteins were identified by double immunolabeling similar to the protocol described in **Chapter 3, Section 3.2.2**. Details of the antibodies are listed in **Appendix 7.1**. However, after secondary antibody incubation the samples were washed three times with TBS but not mounted.

TABLE 4.1 Summary of donor characteristics and experimental arrangements.

Isolation ID	Age (years)	BMI	Digestion involved
1029	24	25	Static/perfused digestion; Prolonged digestion;
1511	30	26	Static/perfused digestion; Prolonged digestion; Optimization
1521	32	26	Static/perfused digestion; Prolonged digestion; Optimization
1531	60	25	Static/perfused digestion; Prolonged digestion
1554	59	23	Static/perfused digestion; Prolonged digestion
1564	32	26	Static/perfused digestion; Prolonged digestion
1106	20	23	Optimization; Perfusion digestion
1430	56	26	Optimization; Perfusion digestion

4.2.2 Static digestion of human pancreatic sample

To prove that labelling pancreatic tissue with antibodies would not interfere with enzymatic digestion, static digestion experiments were carried out on 6 donors, as listed in **Table 4.1**. Collagen IV, collagen VI, perlecan and laminin were chosen as being representative of collagenase and neutral protease substrate [80], [173]. Briefly, samples stained as described in **Chapter 4, Section 4.2.1** were incubated with Hank's Balanced Salt solution (HBSS, Lonza, Switzerland), Collagenase NB1 (7.2 PZU/ml in HBSS, Serva, LOT: 140619) and Neutral Protease NB (0.14 DMCU/ml in HBSS, Serva, LOT: 10058) at 37ºC for 5min. The samples were then washed under cold running water for 5min before being mounted (Vectorshield Hard-Setting Mounting Media, UK) and imaged with a fluorescent microscope (Nikon TS100, Japan). The control group was prepared following a similar procedure, where samples were firstly incubated with enzymes, washed and then stained for insulin and desired proteins before mounting and imaging. Samples incubated in HBSS were used for both groups to calculate the percentage of digestion. Schematic diagrams showing differences between the experimental and the control groups are shown in **Figure 4.2**. An average of 10 images were taken and analysed for each specimen. Proteins of which digestion was not significantly influenced by antibody-labelling were selected for further experiments.

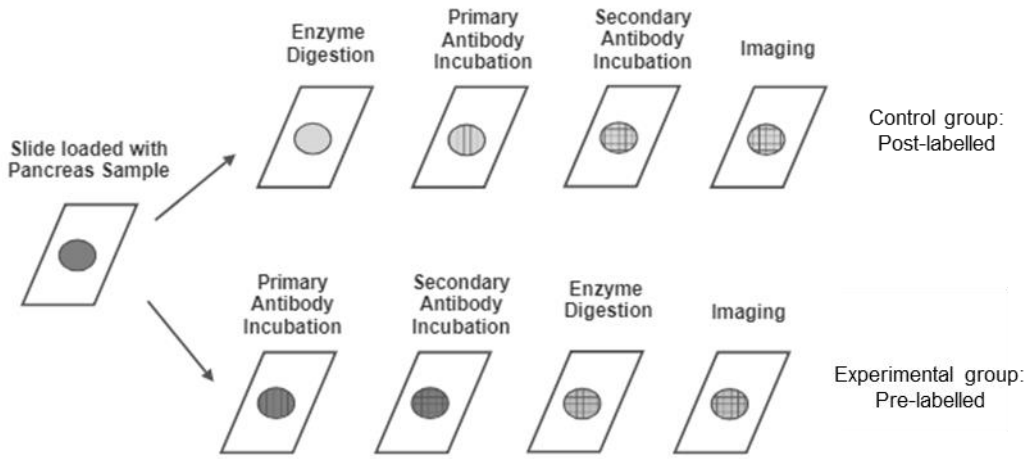

Figure 4.2 Schematic diagram showing the differences between control group and experimental group.

To test the effects of prolonged exposure to enzymes on islet digestion, samples from 6 donors were co-stained with insulin and collagen IV or collagen VI, as their digestions were not significantly affected by antibody-labelling. Details of donor characteristics are listed in **Table 4.1**. Briefly tissue sections were incubated with full enzyme preparation (7.2 PZU/ml for collagenase and 0.14 DMCU/ml for neutral protease in HBSS) at 37ºC for 5, 10, 15 and 20min. The samples were then washed under cold running water for 5min before mounting and imaging. The control group was prepared following a similar procedure, where samples were incubated with only HBSS. 5-10 images were taken and analysed for each specimen at corresponding condition.

4.2.3 Design & build for the perfusion system

In order to achieve real-time observation of pancreatic tissue digestion, a perfusion chamber was designed and built. The perfusion chamber serves for two purposes: to

enable perfusion of enzyme solution; and to enable imaging of the pancreatic tissue in a perfused environment. To this end, polydimethylsiloxane (PDMS) was chosen due to its biocompatibility, transparency and deformability.

For cost-saving purpose, the system was designed to minimize its volume thus the total enzyme requirement could be reduced. As crysosectioned pancreatic tissue-loaded slides were used, a cuboid chamber was preferred. Consequently, the chamber should have an internal shape same as a Superfrost Plus slide (Thermo Fisher).

Another important design criterion was to ensure non-turbulent flow over tissue surface. For this purpose, three designs were proposed, as shown from **Figure 4.3** to **Figure 4.5**.

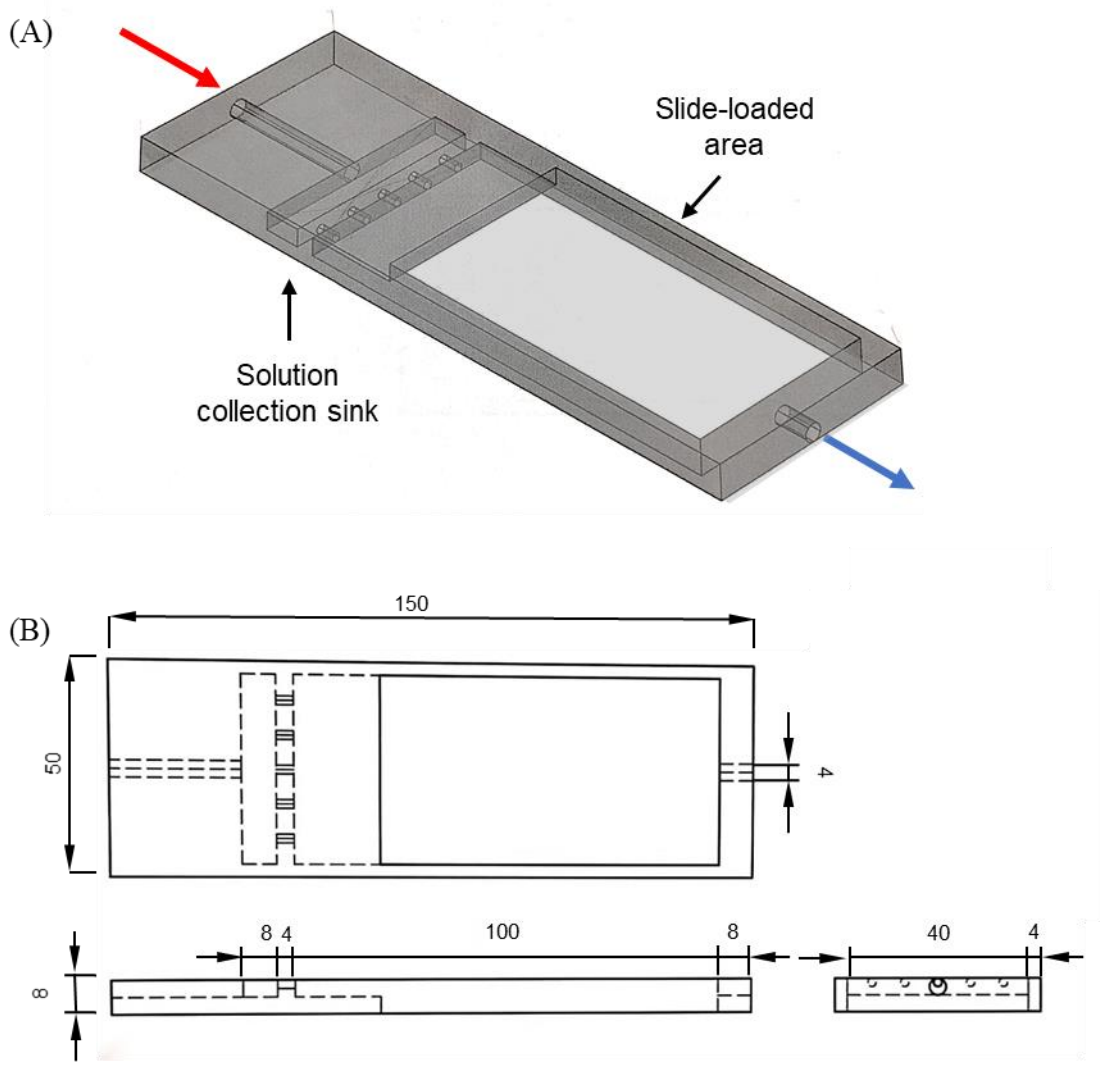

Figure 4.3 Initial design of the perfusion chamber for real-time observation. (A): schematic design of the chamber. Arrows represent flow directions: red: inlet flow; blue: outlet flow; (B): Engineering drawing of the improved design, all measurements were made in mm.

Figure 4.3 shows the initial conceptual design, where a solution collection sink was adopted. Once infused, solution could be pre-mixed in the sink before it was split into five sub-streams for laminar flow. Although these internal designs enabled smooth flow over tissue sections, the chamber was difficult to construct as a single unit.

Figure 4.4 illustrates an improved design for the perfusion chamber, which consisted of four different parts for easy assembly: bottom wall, outer wall and two slide fixers. These components were produced separately. Once the outer wall and

bottom wall were bonded using PDMS, microscope slides could be placed inside. Slide fixers were used to hold the slides in place within the chamber as well as to reduce the internal volume. Inlet flow was introduced vertically from the head fixer (green part in **Figure 4.4 B**) to avoid extra mixing space. Although this design provided minimum internal volume, it was difficult to place the slides within the chamber.

Taking the best of the above designs, **Figure 4.5** shows the final version of the perfusion chamber. This design consisted of three components: surrounding wall, bottom wall and a slide fixer. Instead of introducing solution vertically, a solution collection sink was designed to allow uniform flow over the slide. This was formed by a small contraction of the surrounding wall at the inlet. To ensure smooth flow over tissue sections, the inlet diameter was 1mm, the same size as the height of the slide. The outlet was 2mm to avoid clogging. PDMS-made slide fixer was used to reduce internal volume and to fix the slides in the chamber. A 300μm PDMS layer was made as the bottom wall.

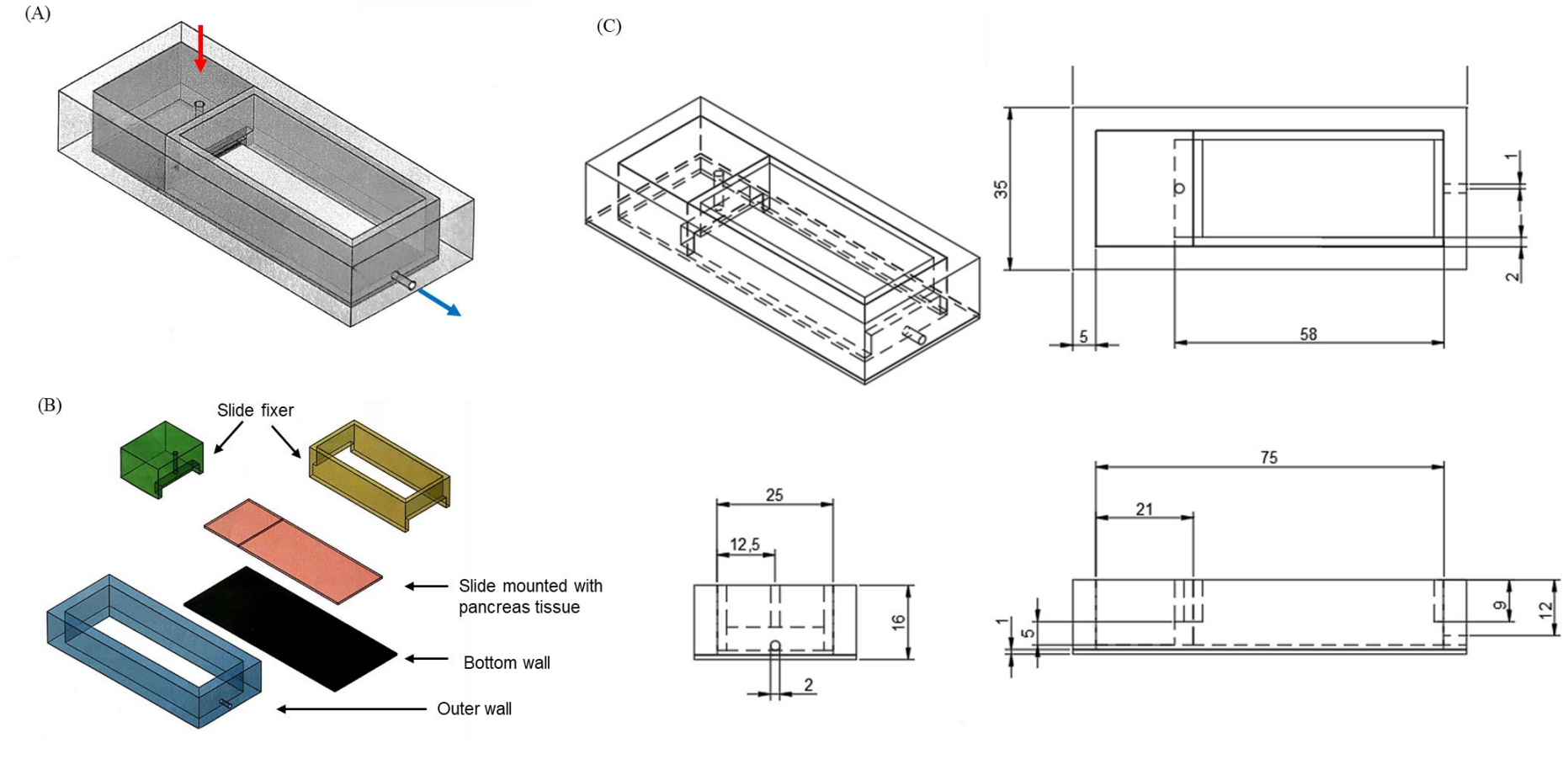

Figure 4.4 Improved design of the perfusion chamber for real-time observation. (A): schematic design of the chamber. Arrows represent flow directions: red: inlet flow; blue: outlet flow; (B): Free components of the perfusion chamber; (C): Engineering drawing of the improved design, all measurements were made in mm.

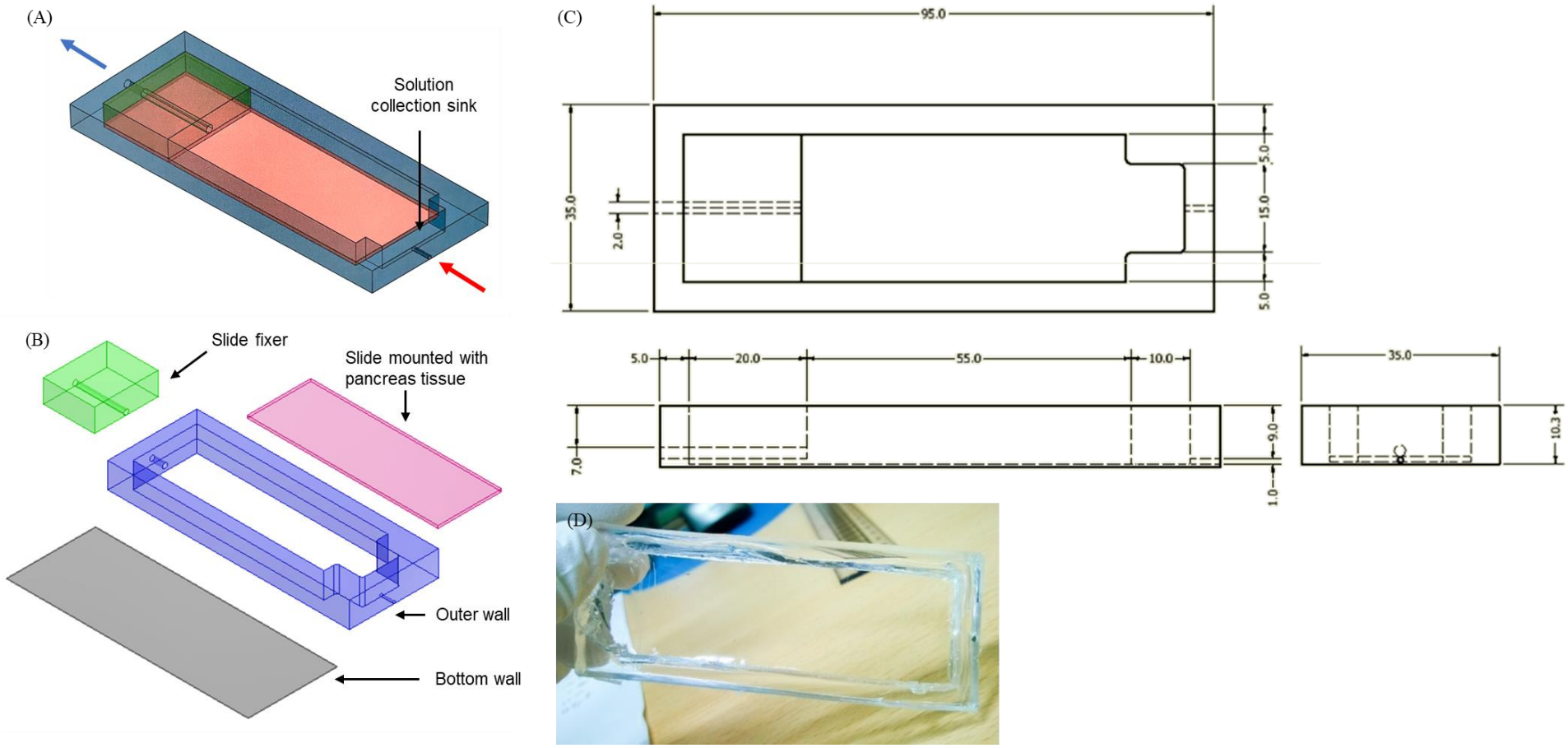

Figure 4.5 Final design of the perfusion chamber for real-time observation. (A): schematic design of the chamber. Arrows represent flow directions: red: inlet flow; blue: outlet flow; (B): Free components of the perfusion chamber; (C): Engineering drawing of the improved design, all measurements were made in mm; (D): Final product of the perfusion chamber, with a thin layer of PDMS as the bottom.

In short, the chamber was prepared by pouring 10:1 wt/wt PDMS (Sylgard® 184 Silicone Elastomer, LOT: 0007466100, Sigma, United Kingdom) and elastomer (Sylgard® 184 Silicone Elastomer Curing Agent, Batch No. H052H8R006, Sigma, United Kingdom) into moulds and then solidified in an oven at 60°C for 2 hours. Microscope slides with cryosectioned pancreatic tissue could be placed in the bottom of the chambers and enzyme solutions could be perfused through this chamber.

For real-time observation, the chamber was placed on an inverted microscope (Nikon TS100, Japan) within a temperature-controlled chamber and connected with a recirculating pump (PPS2, Multichannel Systems, Germany) (**Figure 4.6**). A bubble trap was provided by the pump to minimize disturbance to observation. Sensors were placed in the perfusion chamber and temperature control chamber to ensure that the temperature was maintained around 37ºC. Solutions were placed in a water bath connected to the system to reduce heat loss during perfusion. The total internal volume was 30ml including piping.

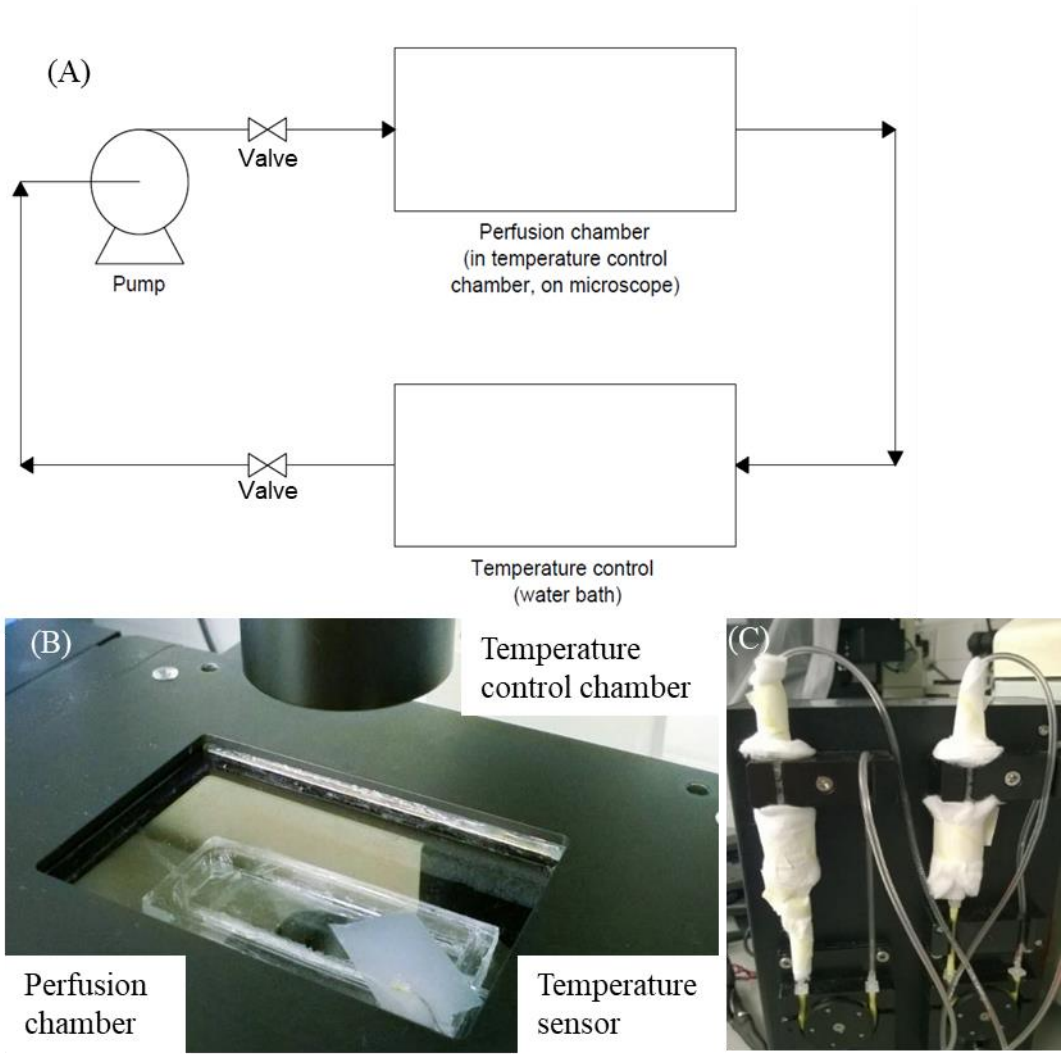

Figure 4.6 Perfusion system designed for real-time digestion. (A): The schematic view of the perfusion system; (B): temperature control chamber with the perfusion chamber placed inside; (C): Cotton-wrapped pump to avoid heat loss.

4.2.4 Optimization of the perfusion system

With the system built, preliminary tests were carried out to optimize the system. Perfusion of deionized water up to 30ml/min was used for to check for leaks. Chambers passed the test were carefully washed with 70% ethanol and perfused with HBSS before further experiments.

For system set-up, slides loaded with antibody-labelled pancreatic tissue sections

were placed inside the perfusion chamber. Details of donor characteristics are listed in **Table 4.1**. Twenty-five ml of HBSS was infused to the chamber to ensure full immersion of the tissue sections.

To determine the effects of mechanical perfusion, samples were perfused with HBSS alone at 37±2ºC (n=3) for 20mins. Images were taken every 15s by the inverted microscope.

To test the influence of temperature control, samples were perfused with full enzyme preparations (7.2 PZU/ml for collagenase and 0.14 DMCU/ml for neutral protease in HBSS) at 30±2ºC and 37±2ºC (n=3) for 25min. Enzymes were added 2min after start of perfusion when temperature and flowrate were stable.

With significant digestion observed at 37±2ºC, one process parameter, flowrate, was manipulated to optimize the system. Perfusion at 20min/min and 10ml/min were tested with full enzyme preparations (n=6). The flowrates were selected to provide smooth flow without significant washing-off of samples or choking of solution.

To ensure non-turbulent flow over the surface of tissue samples, the Reynolds number was calculated as follows:

$$Re = \frac{\rho v d}{\mu} \tag{1}$$

where ρ represents the density of the fluid, v represents the velocity, μ represents the viscosity coefficient and d represents the characteristic length, which can be calculated as:

$$d = \frac{4ab}{2 * (a + b)} \tag{2}$$

where a, b represents the width of the chamber and the depth of the fluid respectively.

4.2.5 Time-course study of pancreatic tissue digestion

According to results obtained in **Section 4.2.2**, collagen IV and collagen VI were chosen as the proteins of interest as their digestions were not significantly affected by antibody-labelling and prolonged digestion time.

Sample preparation and system set-up were same as described in **Section 4.2.4**. Details of donor characteristics are listed in **Table 4.1**. HBSS solution with Collagenase NB1 (Coll, 7.2 PZU/ml in HBSS) and Neutral Protease NB (NP, 0.14 DMCU/ml in HBSS) was perfused in the dark through the chamber for 20min at 37±2°C with a flowrate of 20ml/min. Perfusion with HBSS under the same conditions were taken as the control group. Images were taken every 15s by the inverted microscope for further analyses.

4.2.6 Image and statistical analysis

Qualitative and quantitative analyses were achieved with NIE Elements and *Fiji* software. For quantitative analysis, the final protein quantity was calculated based on a method developed before[13]:

$$Relative\ protain\ quantity = \frac{\sum(Intensity_{protein} * Area_{protein})}{\sum Area_{islet}} \qquad (3)$$

This normalization was applied to exclude the effects of islet size.

For static digestion, data were expressed as mean±SD and statistical analysis was carried out using Student's t-test ($p<0.05$ for statistically significance).

To enable studies of the time-course effects, the average value for the first 2min of perfusion was used to determine the initial protein quantity at time $t0$. The percentage of absolute remaining protein for time $t1$ was then calculated as:

$$Absolute\ remaining\ protein\% = \frac{Relative\ protein\ quantity_{t1}}{Relative\ protein\ quantity_{t0}} * 100\% \quad (4)$$

For real-time observation, data were expressed as mean±SD and statistical analysis was carried out using analysis of variance (ANOVA) or repeated measures ANOVA ($p<0.05$ for statistically significance).

4.3 Results

4.3.1 The impact of antibody labelling on pancreatic ECM digestion

As shown in **Figure 4.7 (A)**, the digestion results of antibody-labelled tissues were similar to those from non-labelled for collagen IV and VI ($p>0.05$). No extra loss of protein signal was observed compared to their non-labelled counterpart suggesting that the digestion of these two proteins would not be interfered by this pre-treatment. Whereas, the results for perlecan and laminin were significantly different from non-treated tissues ($p<0.01$), implying that the enzyme-protein binding sites might be shielded or blocked by previous antibody labelling. As a result, only collagen IV and collagen VI were studied further.

Figure 4.7 (B) shows the impact of extended exposure of pancreatic tissue to enzyme blends. The percentage of collagen IV left experiences a sharp decrease in the

first 5min after the enzyme was introduced; it is then gradually reduced for the next 10min. Further to that the percentage of protein left remained at a similar level ($P<0.05$), proving that the digestion rate became extremely low after a certain amount of time. This trend also holds true for collagen VI, as shown in **Figure 4.7 (C).** Despite the impact of the enzymes on islets' function and viability, these results suggest that extending the digestion time might not help to release islets from surrounding ECM network on a static basis.

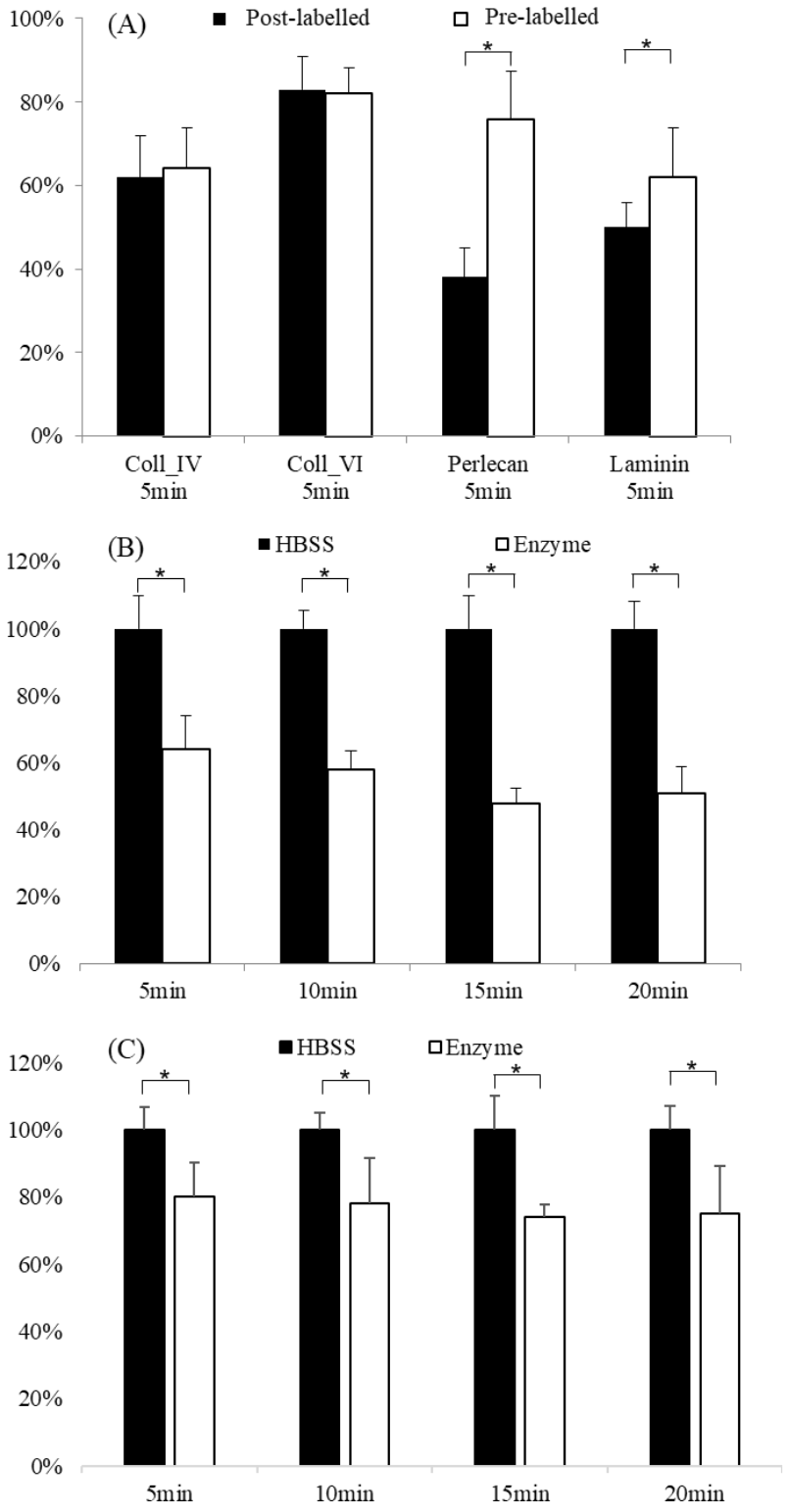

Figure 4.7 Results of static digestion. The y-axis stands for the percentage of protein left after digestion. (A): a comparison of digestion results obtained from antibody-labelled pancreatic tissue with those obtained from native pancreatic tissue; (B) & (C): the impact of prolonged exposure to enzyme on digestion of collagen IV and collagen VI, respectively.

4.3.2 Design & built of the perfusion system

In order to achieve real-time observation of pancreatic tissue digestion, a perfusion chamber was created and built. PDMS was chosen as the main material due to its biocompatibility, transparency and deformability. All three proposed designs fulfilled requirements of uniform flow over tissue sections as well as to reduce operational cost.

The initial design, as shown in **Figure 4.3**, provides pre-mixing and uniform flow by a solution collection sink with split inlets. Practical problems, however, were encountered in manufacturing the mould for this PDMS chamber. The complicated internal designs were difficult to be manufactured as a whole unit. To solve this problem, an improved design with several components was proposed, as shown in **Figure 4.4**. The surrounding wall and bottom layer could be easily assembled. A vertical inlet was adopted to further minimize the internal volume. However, as the chamber had exactly the same shape of the slide, sample-loaded slides could only be pushed into the chamber. Gas could be easily trapped between the slide and the bottom wall, resulting in poor image quality.

The final design, as shown in **Figure 4.5**, overcame above problems by adding a contraction part at the inlet of the chamber. With this extra space, the slide could be slid in. The inlet had a same diameter as the slide height thus once the slide was placed in, a small sink could be formed. Solution infused into the chamber would be accumulated in this small sink before it flowed uniformly across the slides. A PDMS block was used to fix the slide as well as reduce the amount of solution required.

To enable perfusion of the system, the chamber was placed in a temperature control chamber and attached to a recirculating pump. A bubble trap was provided by the pump to minimize disturbance to observation. Water bath and heat-insulating layers were used to reduce heat-loss of the system. The set-up of the system is shown in **Figure 4.6**.

4.3.3 Optimization of the perfusion system

Preliminary tests were carried out for the perfusion system, with results shown in **Figure 4.8**. Perfusion with HBSS was conducted to observe the mechanical effects of perfusion, where after 20min not much disturbance was observed (**Figure 4.8 A & B**). The influence of temperature control is shown in **Figure 4.8 (C)**, where little digestion was observed when the chamber temperature was at 30°C. Nevertheless, digestion with clinical relevant enzyme concentration at 37°C resulted in significant loss of proteins (**Figure 4.8 D**) and was used for further tests.

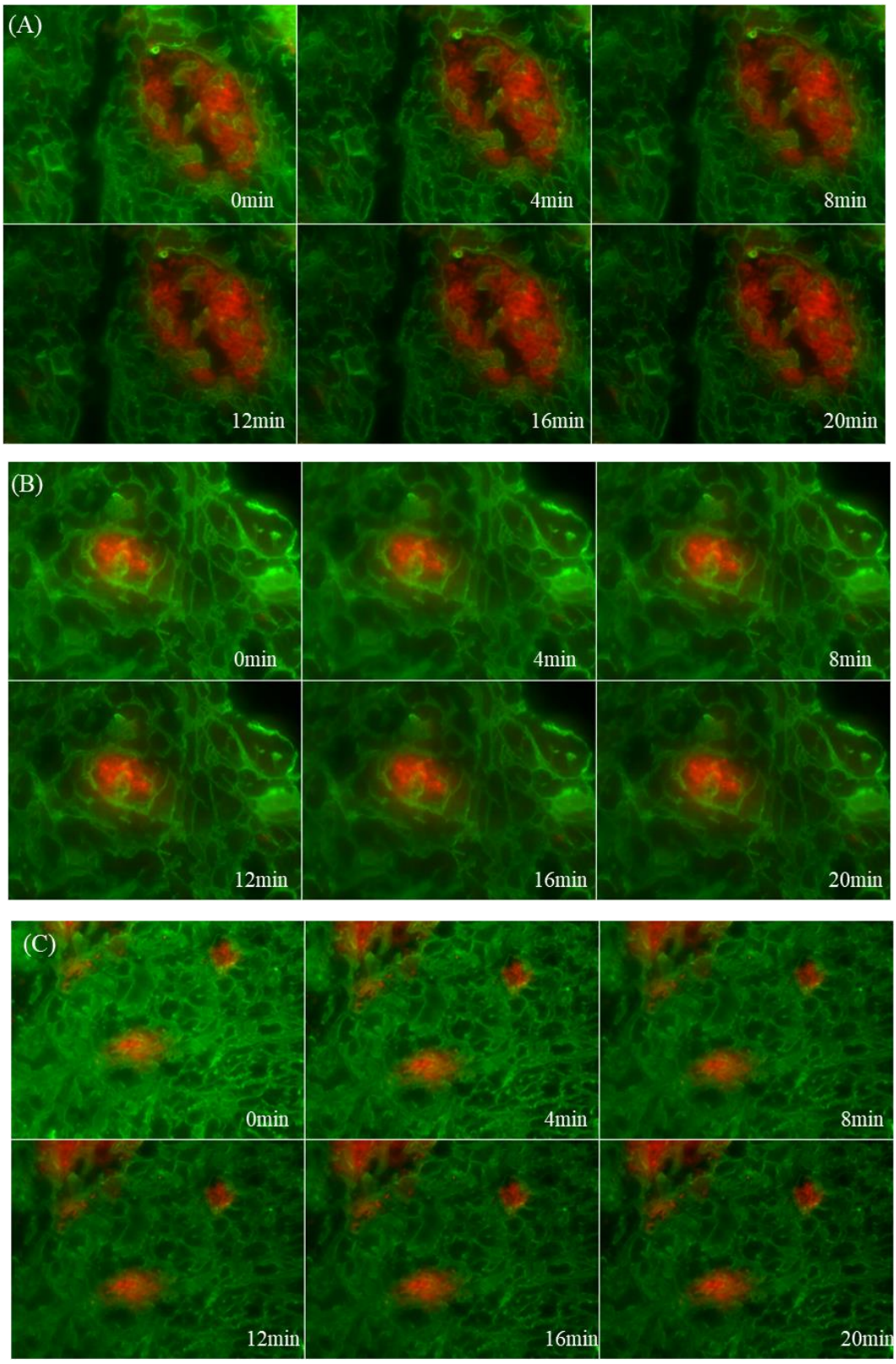

(Image to be continued in the next page)

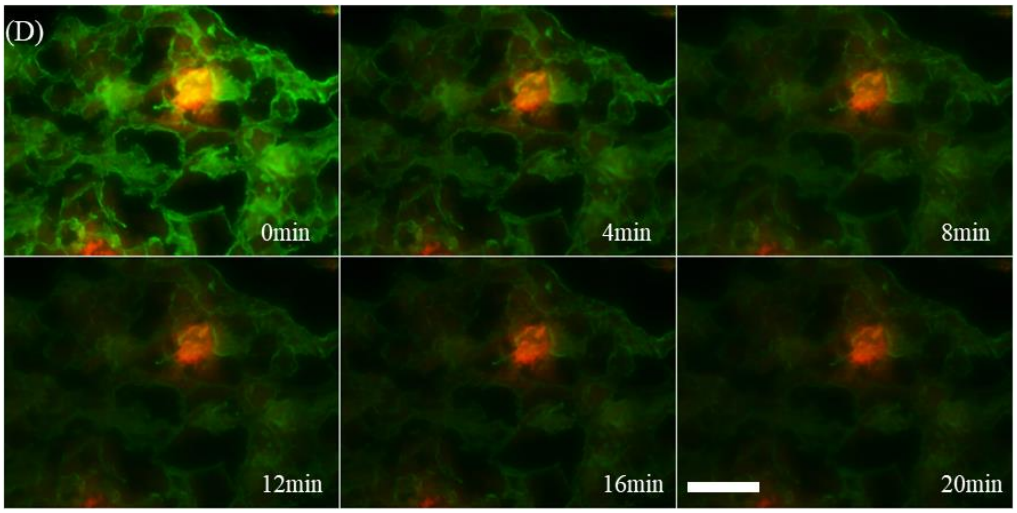

Figure 4.8 Images obtained during preliminary tests. (A): HBSS perfusion for collagen IV; (B): HBSS perfusion for collagen VI; (C): digestion of collagen IV with full enzyme preparation at T<30°C; (D): digestion of collagen IV with 7.2 PZU/ml Collagenase NB1 and 0.14 DMCU/ml Neutral Protease NB. As the loss of proteins was significant at T=37°C with clinical relevant enzyme concentration, further experiments were carried out at the same condition. ECM protein (green) disappears from around islets (insulin in red).ECM protein (green) disappears from around islets (insulin in red). Scale bar = 50μm.

With successful real-time observation of pancreatic tissue digestion, the impact of one process parameter, flowrate, was tested. **Figure 4.9** shows the impact of perfusion speed on the digestion of both protein with full enzyme preparation, where the percentage of relative remaining protein was used for comparison. Although the results at the endpoint were statistically insignificant for collagen VI ($p>0.05$), it was found that lowering the speed of perfusion resulted in less protein loss when perfused with HBSS only, while a slight improvement in protein digestion was observed in the enzyme perfused group (**Figure 4.9 A & B**). Nevertheless, blockage of the system by washed-off tissue was more likely to happen when perfused at a lower speed, which resulted in bubbles and blurred images (**Figure 4.9 C**). Consequently, large fluctuations were observed among different donors. As a result, to achieve easy comparison, further

experiments were carried out with the higher flowrate (20ml/min). Further increases of perfusion speed resulted in turbulent flow over tissue samples. Not only did this result in bubbles blurring the images but also increased tissue sections being washed off from the slides. Consequently, no experiments were conducted at flowrate over 20ml/min.

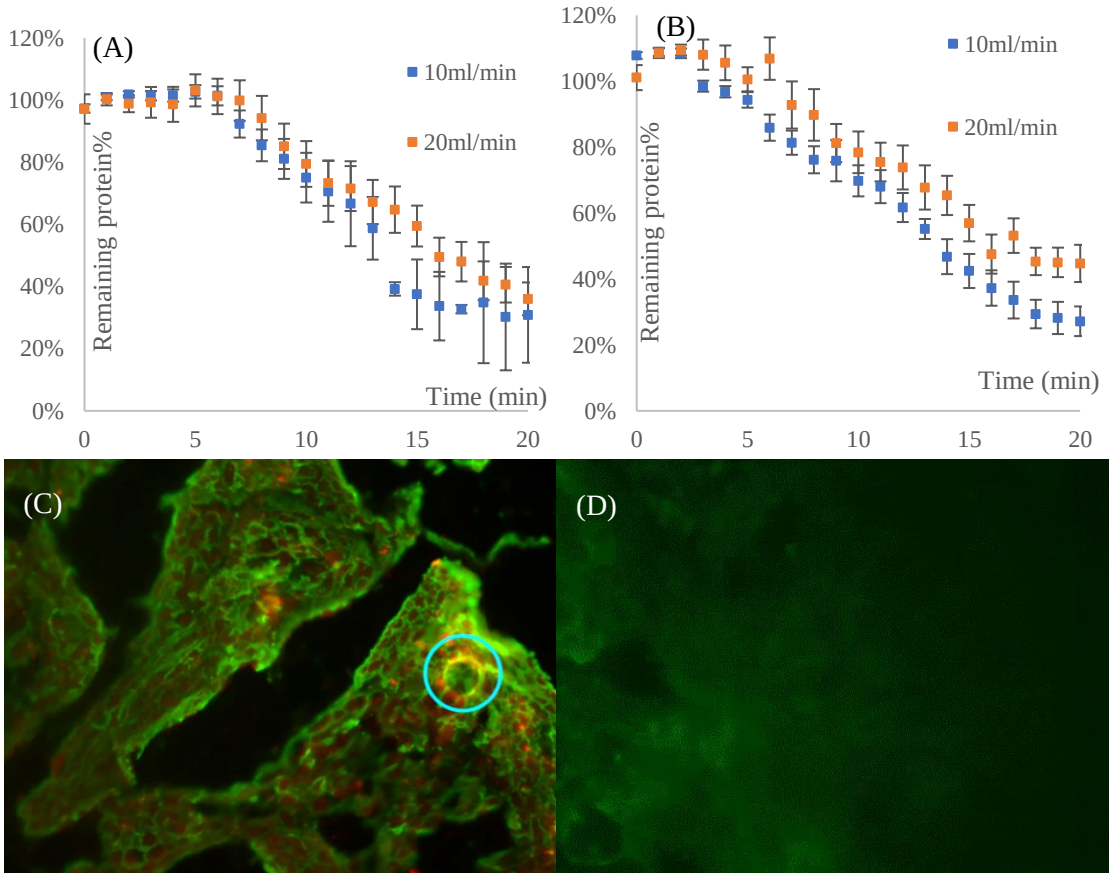

Figure 4.9 The impact of perfusion speed on percentage of remaining protein with combined enzyme dosage for (A): collagen IV; (B): collagen VI. Results shown were expressed as mean+/-SD. (C) & (D): Bubbled & blocked image obtained during 10ml/min perfusion. Insulin staining in red, collagen staining in green.

Taking the fluid depth inside the chamber as 7mm, the characteristic length and Reynolds number was calculated as:

$$d = \frac{4ab}{2 * (a + b)} = \frac{4 * 0.05 * 0.25}{2 * (0.05 + 0.25)} = 0.1094m$$

$$Re = \frac{\rho v d}{\mu} = \frac{10^3 * (20 * 10^{-3}/0.07/0.25/60) * 0.1094}{0.7 * 10^{-3}} = 2976 < 4000$$

Therefore the flow inside the chamber is in the transient state. With the increase of fluid depth, there is a tendency to form laminar flow.

4.3.4 Time-course study of the pancreatic tissue digestion

Figure 4.10 shows the typical image stacks obtained during a real-time perfusion experiment. For enzyme perfused groups, the protein area was gradually reduced and for some regions it was totally removed. Furthermore, qualitative analyses show that the intensity of the signals was markedly reduced, which was also observed in the HBSS perfused experiments.

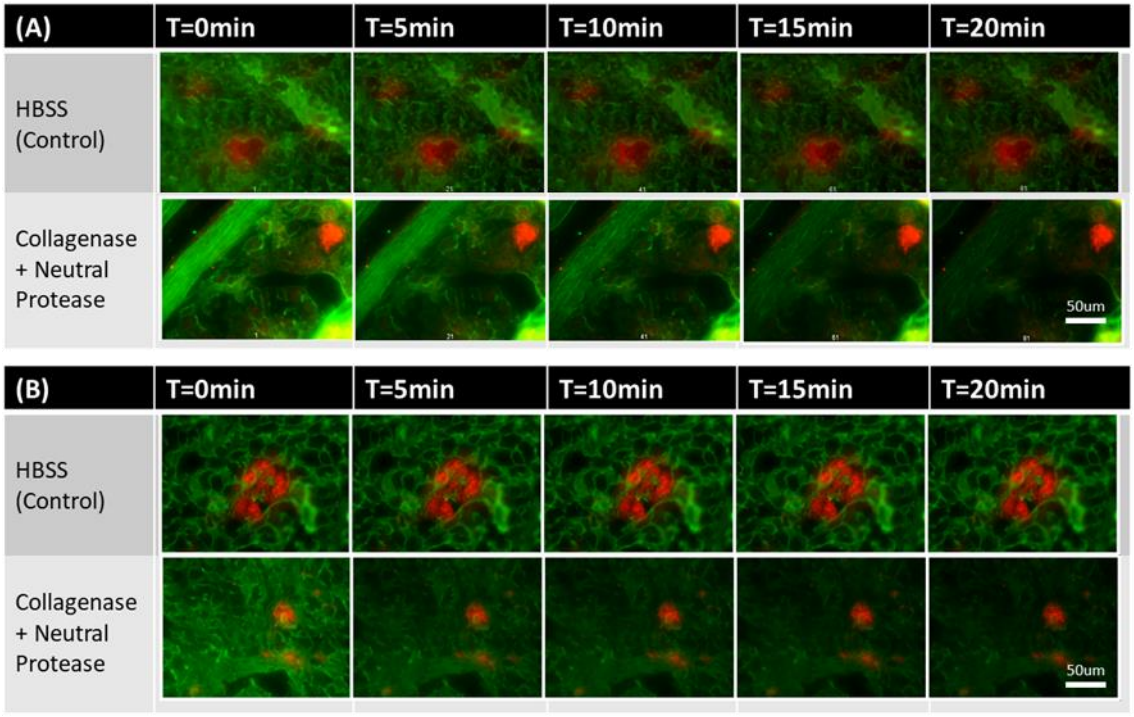

Figure 4.10 Images obtained during a real-time digestion experiment. (A): Collagen IV; (B): Collagen VI. ECM protein (green) disappears from around islets (insulin in red).

Figure 4.11 (A) shows the typical digestion curve after quantitative analysis for a

sample stained with collagen IV and perfused with combined enzymes at 20ml/min. Fluctuations were observed, which might be caused by tissue sections being washed off either by digestion or by perfusion. As the reduction of protein quantity might be affected by antibodies washing off and the mechanical impacts of solution, control groups with HBSS perfusions were also carried out for further comparison. When perfused with only HBSS, a reduction in the protein intensity was observed, but both the extent and the rate were limited compared to the enzymatic digestion groups (**Figure 4.11 C**). Moreover, the protein area remained almost the same.

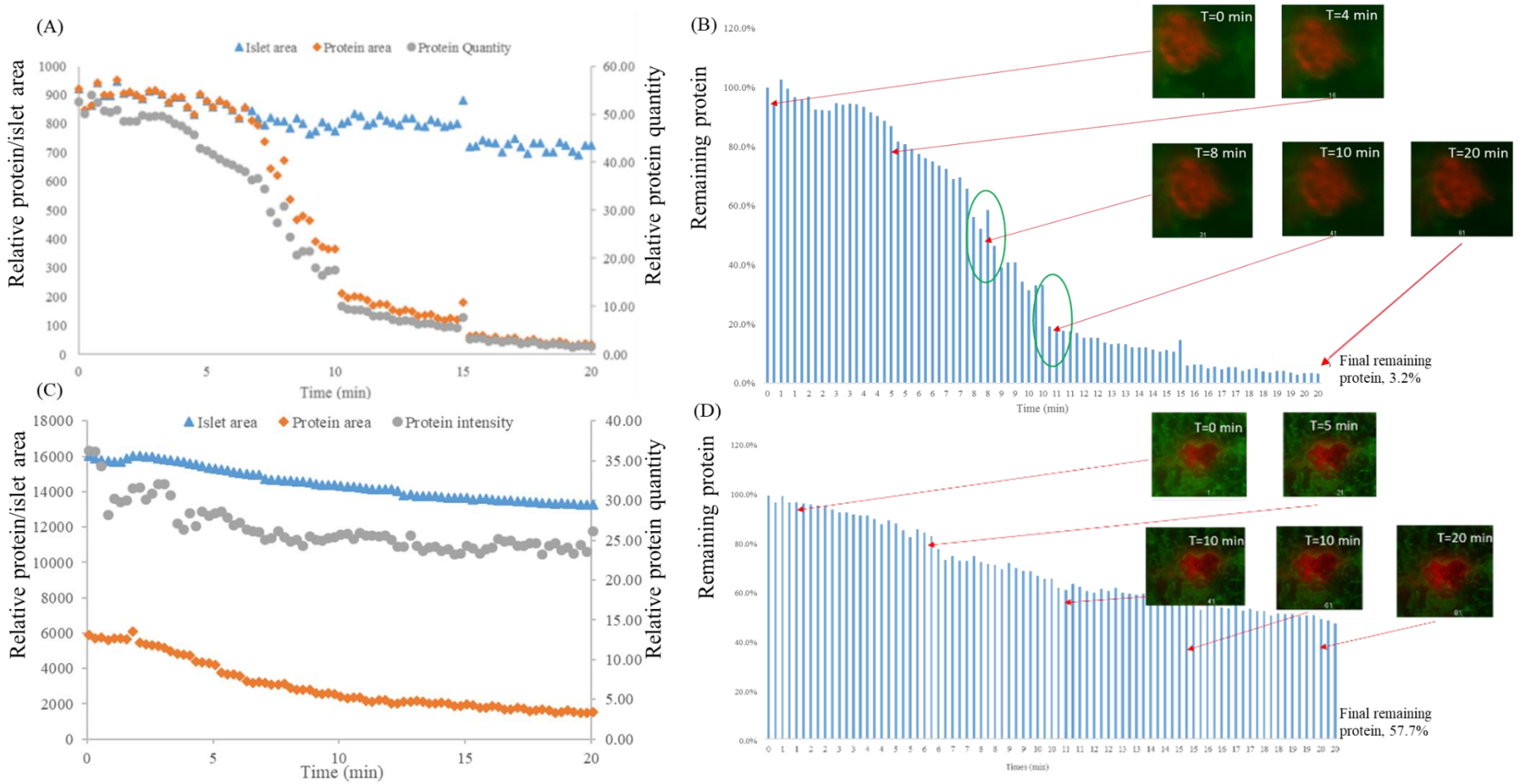

Figure 4.11 Collagen IV quantification of one donor sample and perfused with HBSS and full enzyme concentration (A & B) or HBSS control (C & D). (A) & (C): digestion/perfusion curves, with blue representing islet area, orange representing protein area and grey representing protein intensity; (B) & (D) percentage of protein left around an islet with respect to original obtained image stacks.

When perfused with the full enzyme preparation, digestion started immediately after enzyme infusion and the overall protein quantity reached almost zero after 15min (**Figure 4.11 A & B**). Based on the digestion rate, the curve could be divided into three different phases: an initial stage, an accelerated stage and an end stage.

The initial stage of digestion was characterized by an immediate reduction of the signal intensity of specific peri-islet ECM proteins and a delayed loss of the protein area after enzyme introduction. Compared to the control group, the overall protein quantity was significantly different 2 minutes after collagenase and neutral protease infusion ($p<0.05$), while the protein area was significantly different after 8 minutes ($p<0.01$). This suggests that at an early stage it was protein thickness or density was lost instead of protein area. After 8min, 54% of collagen IV remained for enzyme perfused group while 70% remained in the HBSS control group.

As shown in **Figure 4.11**, both the signal intensity and the area of peri-islet ECM protein were significantly lost in the accelerated stage. This resulted in a total loss of 41% collagen IV from 8min to 11min while only 10% collagen IV was lost in the control group.

Further than 11min, the digestion proceeded to the end stage, where the rate of digestion reduced significantly ($p<0.05$). The reduction of protein area and protein intensity were in a similar pattern to those for the control group.

4.4 Discussion

The digestion phase is one of the key areas for improving islet isolation success rates.

With the increasing demand in islet transplantation, there is an urgent requirement to obtain a thorough understanding of this process. To the best of our knowledge, this is the first observation of real-time enzymatic digestion of the peri-islet ECM of pancreatic tissue.

As discussed in the previous three chapters, ECM proteins like collagen IV, collagen VI, perlecan and laminin could be found in the ECM surrounding human islets. Other subtypes of collagens were also found in human pancreas, but here we examined the digestion of collagen IV and VI, due to their abundance [16], [80], [201], [202] and representation of basement membrane and stromal ECM, respectively. Compared to results obtained in static digestion [13], difficulties were found in observing the loss of perlecan and laminin with antibody labelling prior to digestion. These differences might be caused by the competition of binding sites between antibodies and the enzymes. However, no such difficulties were observed with the digestion of collagen IV and collagen VI.

For real-time observation of the digestion process, a chamber was designed and connected to a perfusion system with adequate temperature control. Three designs were proposed for the perfusion chamber and practical problems were encountered in the manufacturing and system assembly process. With complicated internal designs, the initial proposed chamber was difficult to be manufactured as a single unit. Improvements were made in the second design by introducing several free components, which could be assembled afterwards. However, once assembled, it was difficult to place slides inside the chamber. Nevertheless, this was optimized in the final design and

the system was successful for observing real-time digestion process.

Preliminary tests showed that although signal was lost with HBSS perfusion, not much disturbance was caused by this mechanical impact. Quantitative analyses showed that the signal reduced gradually against perfusion time. This was thought to be caused by fluorophores washed-off by the solution and needed to be considered in further experiments. To compensate this effect, perfusion with HBSS was used as controls and all the digestion results were corrected with corresponding controlled condition.

With the immunofluorescent labelling technique, the time-course digestion processes for some ECM proteins in pancreatic tissue was shown for the first time. Our study showed that the protein signal intensity decreased once enzyme was introduced, but a time lag existed between the start of digestion and the loss of protein area, which was not observed in the control group. These results suggested that the initial enzyme-binding stage was relatively fast and the protein was thinned or its density was lost before the actual disappearance of protein area.

As discussed in **Chapter 2**, **Section 2.3.2**, clinical islet isolation relies heavily on dissociation enzymes. The enzyme blend could either be self-made [186] or pursed from various commercially available manufactures [12], [133], [136], [185]. A complete characterization of all available enzymes and their potency in human islet isolation seems to be impossible. Even with commercially available purified enzyme blends, the batch-to-batch variations in efficiency are inevitable. Our perfusion system, however, provides easy comparison for enzymes from different lots and could be used in quality control improvement for clinical isolations.

However, all the results obtained in this study were based on tissue sections and no mechanical agitation was introduced during the digestion. The flowrate used was also much lower compared to the 55ml/min used during clinical isolations. Nevertheless, this system provides a simplified perfusion model to mimic clinical isolations. It enables direct perfusion of enzymes over tissue sections thus allowing samples from arbitrary regions of pancreas to be assessed. Moreover, this system enables dynamic studies of enzymatic digestions, allowing detailed investigations on proteins digestions and end-point determination for various donor groups.

4.5 Summary

In conclusion, this chapter has presented a method to enable studies of the time-dependent characteristics of the digestion phase of islet isolation. A post-labelling technique was developed and its application in enzyme digestion for specific pancreatic ECM proteins was proved. Three designs for the perfusion chamber were proposed and their application was discussed. With the built perfusion system, operating parameters such as temperature and flowrate were optimized. Focusing on collagen IV, enzymatic digestion at clinically relevant concentrations were studied. The results showed a three-phase digestion profile, which provided valuable information for enzyme designs. With successful real-time observation of the dynamic digestion process, further proof-of-principle tests will be conducted in the next chapter for donors of different ages with different enzyme combinations.

Chapter 5

An *in vitro* study for the time-course effects on pancreatic matrix digestion: age related variations of the normal human pancreas

5.1 Introduction

During routine clinical isolation it has been reported that higher isolation yields are generally obtained from older donors but the isolated islets are of inferior function [101], [156], [166], [167]. Many studies have attempted to characterize donor variables and link these variables with isolation results but few reports are consistent [154], [157], [158]. Following our detailed histological study for the presence of ECM proteins around an islet in **Chapter 3**, it was found that age and BMI have a significant impact on specific peri-islet proteins. This suggested that the higher yields found with old and obese donors may be the consequence of improved digestion of these proteins [168]. Detailed investigations are thus required to determine the impact of these donor characteristics on the islet-exocrine interface during pancreas digestion, to help development of new specific enzymes and to improve clinical isolation yields.

As discussed in **Chapter 2**, **Section 2.3.2**, both collagenase and neutral protease are required for an efficient and successful isolation. Various concentrations of these two enzymes used during clinical isolations have been reported [187], [205]. Nevertheless, many report incomplete digestion from juvenile donors as their islets are often mantled by layers of exocrine tissues [101], [166]. According to Meier [170], the difficulty in isolating islets from these donors is not related to body weight or BMI. Balamurugan [101] reports part of the reason arises from anatomical features of juvenile donors and changing the enzyme delivery method helped in obtaining mantle-free islets. Nevertheless, considerable efforts have been directed to manipulating enzyme dosage combinations, including modifying digestion protocol and optimizing

enzyme concentration [210], [211]. A detailed study on the digestion phase at molecular level is thus required, not only to improve current understanding but also aid in new enzyme formulation.

Compared to static digestion on a slide [13], [102], [208], the perfusion system developed in **Chapter 4** provides a simplified model mimicking clinical isolations. Coupling with the pre-labelling technique, this allows a direct observation of the digestion phase and samples from arbitrary regions of pancreas can be assessed. Enzyme-containing solutions could be perfused directly over the pancreatic tissue sections so that a real-time observation of the digestion phase could be achieved.

With the aim of improving current understanding of islet isolation for further yield improvement, this chapter focuses on exploiting the newly developed chamber in the investigation of pancreatic tissue dissociation in relation with donor age and enzyme combinations. Using the system developed in **Chapter 4**, the digestion kinetics for collagen IV and VI under three enzyme dosage combinations were investigated. Moreover, the impact of donor age on islet isolation were investigated, which may aid new enzyme formulation in the future.

5.2 Methodology

5.2.1 Donor pancreas characteristics

Seventeen human adult pancreases were retrieved from DBD (donated after brain death) donors (11 male, 6 female) in Oxford, the United Kingdom, with appropriate

consent and ethical approval obtained. All donors, as shown in **Table 5.1**, fell within an age range of 24 to 60 years and a BMI range of 22 to 26, with cold ischemia times of <18 hours. All pancreatic samples were taken from the head region of donor organs before being snap frozen in liquid nitrogen. Three 10μm samples were cryosectioned onto Superfrost Plus slides (Thermo Fisher, UK) at -20ºC. The proteins were identified by double immunolabeling technique developed in **Chapter 4**.

TABLE 5.1 Summary of donor characteristics for real-time observation. (Table to be continued in the next page)

Age (years)	Sex	BMI	Isolation ID	Digestion involved
20	F	23	1106	Perfusion test with collagen IV, VI
24	M	25	1029	Perfusion test with collagen VI
26	M	23	1439	Perfusion test with collagen VI
27	F	23	1622	Perfusion test with collagen IV, VI
30	M	26	1511	Perfusion test with collagen IV, VI
32	M	26	1521	Perfusion test with collagen IV, VI
32	M	26	1564	Perfusion test with collagen IV
35	M	24	1530	Perfusion test with collagen IV
46	F	26	1222	Perfusion test with collagen IV, VI
46	M	26	1431	Perfusion test with collagen IV, VI
49	F	24	1610	Perfusion test with collagen IV
51	F	22	1552	Perfusion test with collagen VI

(Table to be continued in the next page)

Age (years)	Sex	BMI	Isolation ID	Digestion involved
56	M	22	1534	Perfusion test with collagen IV
56	F	26	1430	Perfusion test with collagen IV, VI
57	M	26	1555	Perfusion test with collagen VI
59	M	23	1554	Perfusion test with collagen IV
60	M	25	1531	Perfusion test with collagen VI

5.2.2 Perfused digestion of human pancreatic tissue from young and older subject with different enzyme combinations

To study the effects of donor age and enzyme combinations on pancreatic ECM digestion, real-time observation experiments were carried out for collagen IV and collagen VI.

Sample preparation and system set-up were the same as described in **Chapter 4**, **Section 4.2.4**. In order to study the impact of donor age, donors were divided into young (≤ 35) and old (≥ 45) age groups (n=6 for each group). Details of donor characteristics are listed in **Table 5.1**. For enzymatic digestion, Collagenase NB1 alone (Coll, 7.2 PZU/ml in HBSS), Neutral Protease NB alone (NP, 0.14 DMCU/ml in HBSS) or both enzymes together (7.2 PZU/ml for collagenase and 0.14 DMCU/ml in HBSS) were perfused in the dark through the chamber for 20min at 37±2ºC. The enzymes were added 2min after start of perfusion when temperature was stable and steady state was fully achieved. Images were taken every 15s and for each condition and the digestion

was repeated three times. Perfusion with HBSS under the same conditions were taken as the control group.

Practical problems such as losses of focus, clogging of the system and tissue sections being washed off were encountered. Manual adjustment was therefore applied. Nevertheless, repeated experiments were conducted to compensate for these fluctuations.

5.2.3 Image and statistical analysis

Qualitative and quantitative analyses were achieved with NIE Elements and *Fiji* software. For quantitative analysis, the final protein quantity was calculated based on a method developed before[13]:

$$Relative\ protain\ quantity = \frac{\sum(Intensity_{protein} * Area_{protein})}{\sum Area_{islet}} \qquad (1)$$

This normalization was applied to exclude the effects of islet size.

To enable studies of the time-course effects, the average value for the first 2min of perfusion was used to determine the initial protein quantity at time t_0. The percentage of absolute remaining protein for time t_1 was then calculated as:

$$Absolute\ remaining\ protein\% = \frac{Relative\ protein\ quantity_{t1}}{Relative\ protein\ quantity_{t0}} * 100\% \qquad (2)$$

To enable comparison of protein digestion among various donors or different enzyme combinations, the percentage of remaining protein was introduced. This value was used to represent protein remained sorely due to enzymatic digestion, with mechanical impacts from perfusion excluded:

$$Remaining\ protein\% = 1 - \frac{Absolute\ remaining\ protein\ \%_{control,\,t1} - Absolute\ remaining\ protein\ \%_{digestion,\,t1}}{Absolute\ remaining\ protein\ \%_{control,\,t1}} * 100\% \quad (3)$$

To determine the digestion kinetics, the rate of digestion was calculated as:

$$Digested\ protein\% = 1 - Remaining\ protein\% \quad (4)$$

$$Rate\ of\ digestion = \frac{Remianing\ proteint\%_{t0} - Remianing\ proteint\%_{t1}}{t_1 - t_0} \quad (5)$$

It needs to be mentioned that with continuous perfusion and above-mentioned practical problems, large variations were observed. This resulted in negative rate of digestion for certain time points, which were considered as '0' in further analyses

Data were expressed as mean±SD and statistical analysis was carried out using analysis of variance (ANOVA) or repeated measures ANOVA ($p<0.05$ for statistically significance) with IBM SPSS version 22 (Chicago, USA).

5.3 Results

5.3.1 Time-course study of digestion of pancreas from one donor (ID: HP1511)

Figure 5.1 shows the typical image stacks obtained during a real-time perfusion experiment. For enzyme perfused groups, the protein area was gradually reduced and for some regions before it was totally removed. Furthermore, qualitative analyses show that the intensity of the images was markedly reduced, which was also observed in the HBSS perfused experiments.

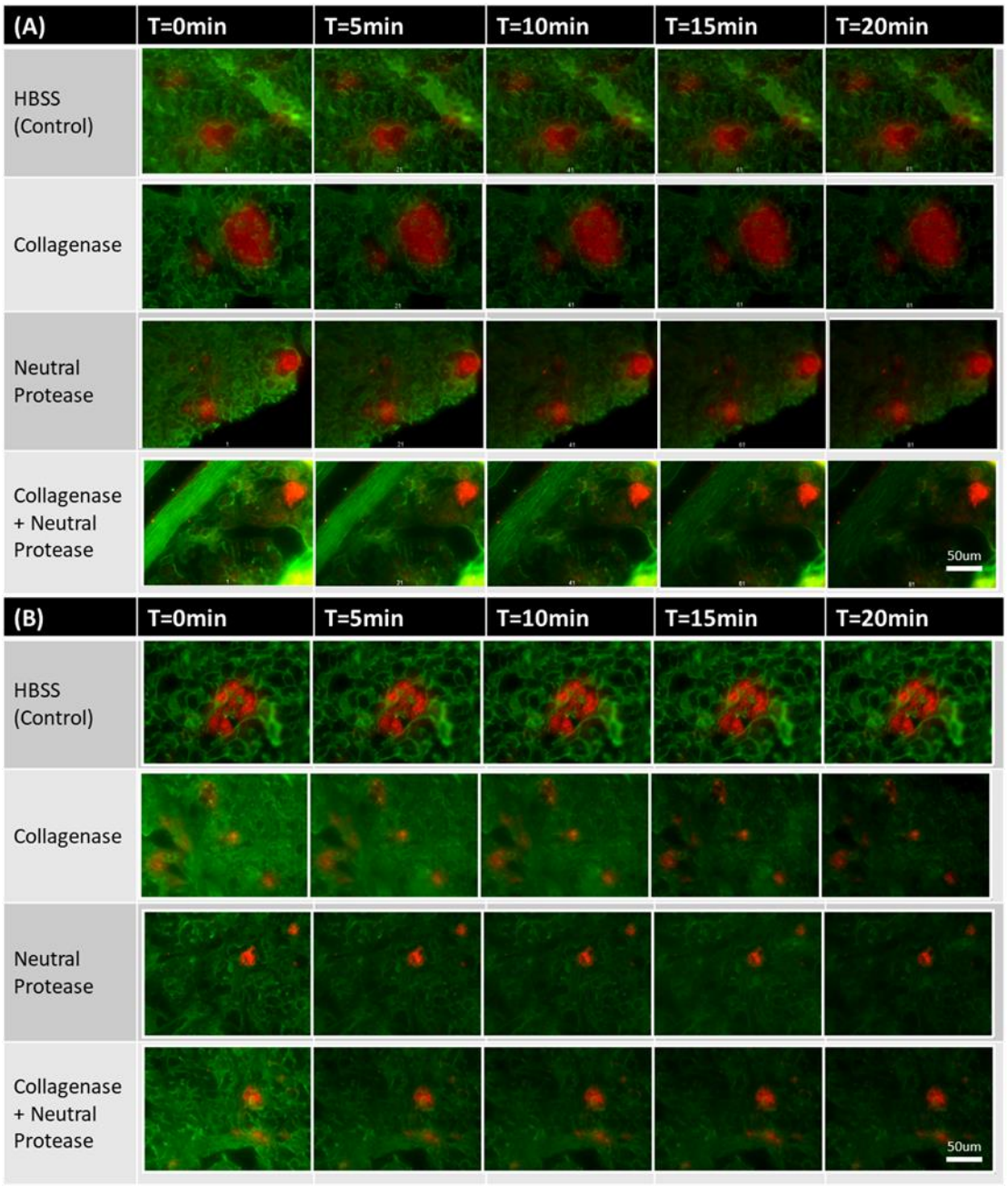

Figure 5.1 Images obtained during a real-time digestion experiment. (A): Collagen IV; (B): Collagen VI. ECM protein (green) disappears from around islets (insulin in red).

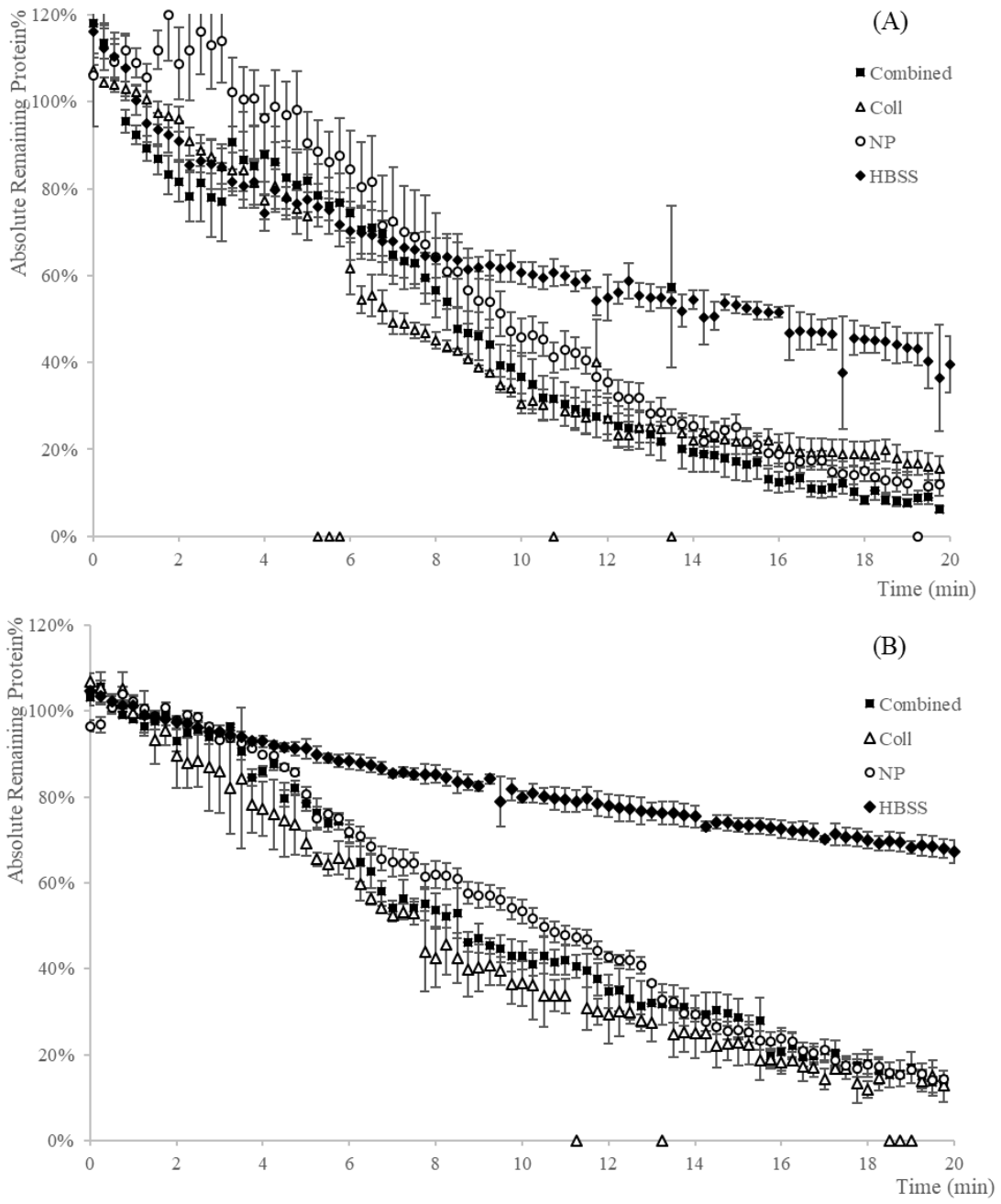

Figure 5.2 Digestion profiles obtained for one donor sample stained with collagen IV (A) and collagen VI (B) under different enzyme dosage combinations. Y-axis represents the amount of protein remaining at peri-islet interface. Results shown were expressed as mean+/-SD. As shown, the amount of protein in the control group reduced steadily while the amount of protein reduced more significantly in the enzymatic digestion groups. Large variations were observed during the experiments.

Figure 5.2 shows the typical digestion profiles obtained during a real-time perfusion experiment. As shown, perfusion with HBSS resulted in gradual reduction of the protein signal. Nevertheless, this reduction was more significant when enzymes

were added. To compensate mechanical impacts caused by HBSS perfusion, results for further experiments were corrected with HBSS control group, as demonstrated in **Equation (3)**. Digestion with collagenase alone was found to be the fastest when compared with digestion using neutral protease or combined, although the differences were statistically insignificant ($p>0.05$). Previous studies and our static digestion experiment in **Chapter 4**, **Section 4.3.1** showed that it was difficult to digest collagen VI [212]. However, in our system, up to 80% of collagen VI was found to be lost, even with collagenase alone.

5.3.2 Impact of enzyme combinations and donor age group on the digestion of collagen IV

To further investigate the impact of enzyme combinations and age group on the digestion of collagen IV, enzymatic perfusion experiments were conducted for 12 donors, as characterized in **Table 5.1**.

Figure 5.3 shows the digestion profiles of collagen IV for two age groups (young, age≤35 vs old, age ≥45) under three enzyme dosage combinations. When perfused with collagenase alone (**Figure 5.3 A**), significant loss of protein was observed after 2min for young donors and 1min for old donors. Nevertheless, the digestion ended at 13.75min for both donor groups. Differences between the digestion of the two donor groups became significant after 13min ($p=0.01$), with only 38.41%±3.18% collagen IV remaining in the young old group and 22.93%±3.37% collagen IV remaining in the old donor group ($p=0.001$).

When perfused with neutral protease alone (**Figure 5.3 B**), significant loss of protein was observed after 1.75min for young donors and 3.25min for old donors. Insignificant loss of protein was observed after 15.75min for young donors and 16min for old donors. The digestion was found to be similar between the two groups ($p>0.05$), with 34.96%±3.97% collagen IV remained for younger donors and 38.16%±3.76% remained for older donors ($p>0.05$).

When perfused with combined enzymes (**Figure 5.3 C**), the loss of protein starts at 2.75min for young donors and 3.5min for old donors, and ends at 14.25min and 16.75min for young and old donor group, respectively. Insignificant differences were observed between the two groups ($p>0.05$). However at the end of digestion, 37.68%± 3.515 of collagen IV remained in the young donor group while 27.11% ± 2.78% remained in the old donor group ($p=0.02$).

Focusing on the same data but with respect to enzymes used on samples from young donors (**Figure 5.4 A**), digestion using collagenase alone was found to be the fastest, although a significant difference was only found between collagenase and neutral protease group (1.5 to 18.5min, $p=0.05$). The amount of remaining protein was similar among all three groups ($p>0.05$).

Focusing on old donors (**Figure 5.4 B**), a similar observation was made. However, differences were found among all three enzyme combination groups ($p<0.05$ for all comparations). The amount of remaining protein was significantly higher in the neutral protease alone group than compared with collagenase alone group ($p=0.004$) or combined enzyme group ($p=0.02$).

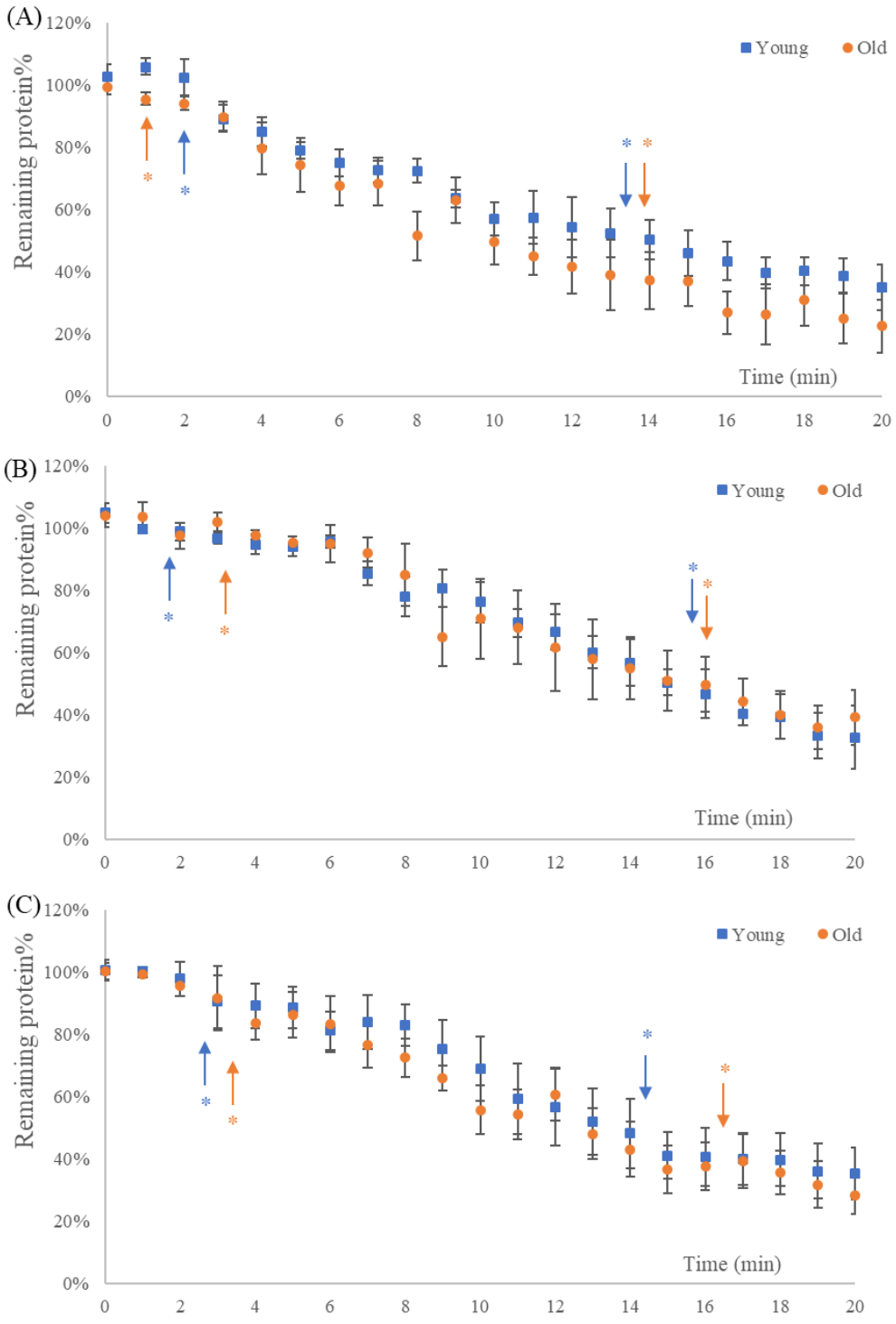

Figure 5.3 The impact of donor age (n=6 for ≤35 years vs n=6 for ≥45years) on percentage of remaining protein for collagen IV, with different enzyme combinations. (A): collagenase only; (B): neutral protease only; (C): both collagenase and neutral protease. Results shown were expressed as mean+/-SD. Upward arrows with a star represents time points when significant losses of protein were observed while downward arrows with star represents time points when insignificant losses of protein were observed ($p<0.05$).

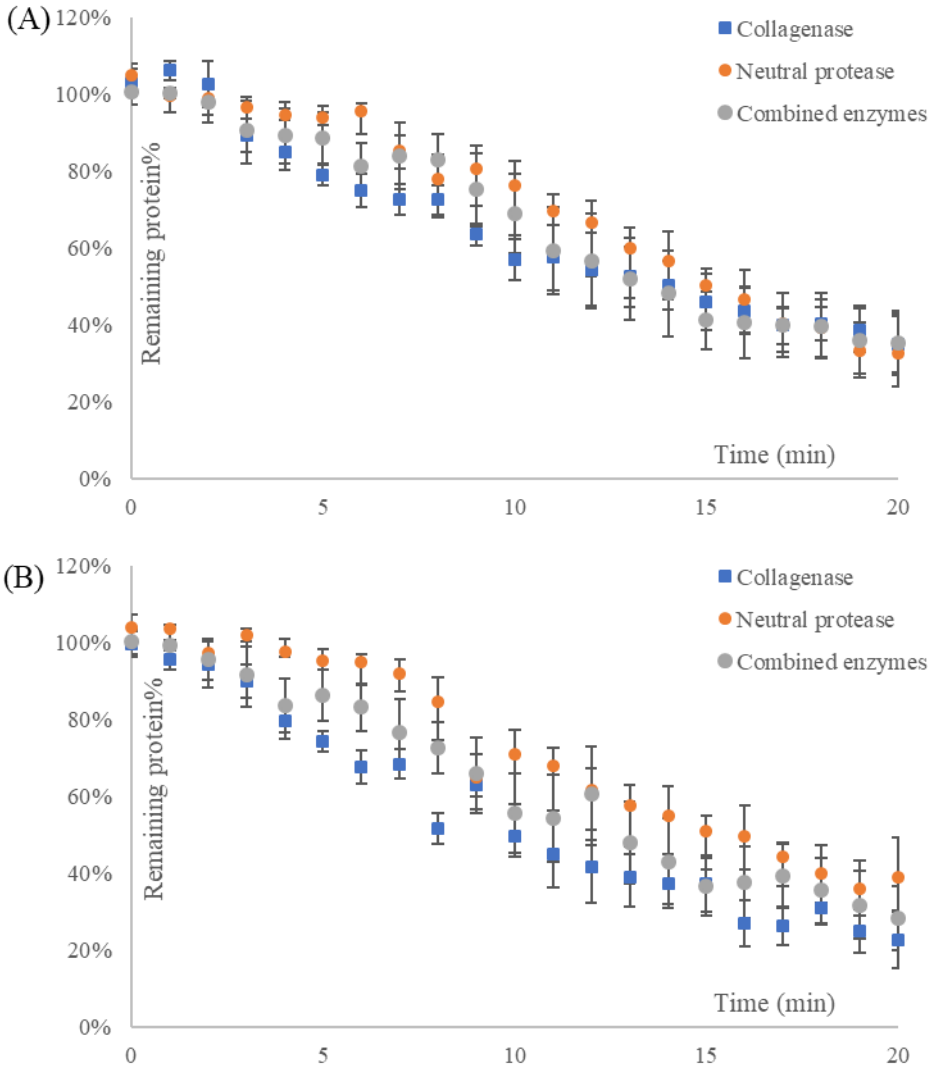

Figure 5.4 The impact of enzyme combinations (n=6 for each test group) on percentage of remaining protein for collagen IV for (A): young donors (≤35 years); (B):old donors (≥45years). Results shown were expressed as mean+/-SD. Data were regrouped and plotted from **Figure 5.3**.

Figure 5.5 shows the rate of digestion against the percentage of remaining protein. At the beginning of digestion, binding between enzyme and collagen IV may limit the rate of digestion. Over time, the overall digestion speed increased. The digestion may have been limited by insufficient amount of substrate and the rate of digestion decreased.

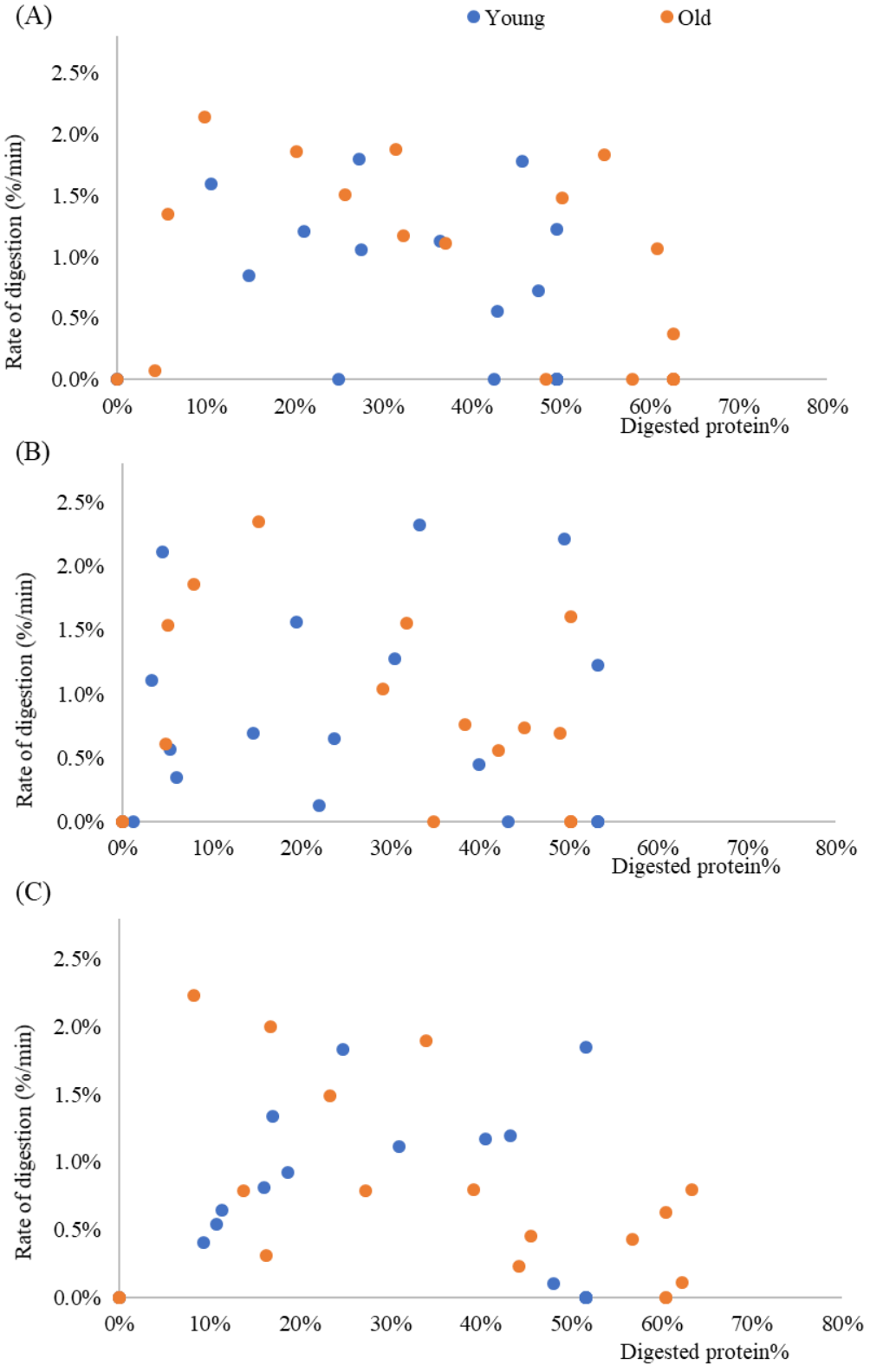

Figure 5.5 The impact of donor age (n=6 for ≤35 years vs n=6 for ≥45years) on rate of digestion for collagen IV, with different enzyme combinations. (A): collagenase only; (B): neutral protease only; (C): both collagenase and neutral protease. Results shown were expressed as mean values.

Due to large variations observed in the experiments, none of the comparisons on rate of digestion was of statistical significance. However, it was found that when perfused with collagenase alone, the rate and extent of digestion were both higher in the old donor group. Introducing neutral protease resulted in a reduction in the digestion speed in the old donor group while the opposite trend was observed in the young donor group. Nevertheless, perfusion with combined enzymes resulted in a similar pattern between the donor groups to perfusion with collagenase alone group. Furthermore, time to reach the maximum digestion rate was the shortest when perfused with collagenase alone.

5.3.3 Impact of enzyme combinations and donor age group on the digestion of collagen VI

To further investigate the impact of enzyme combinations and age group on the digestion of collagen VI, enzymatic perfusion experiments were conducted for 12 donors, as characterized in **Table 5.1**.

Figure 5.6 shows the digestion profiles of collagen VI for the two donor age groups under three enzyme dosage combinations. When perfused with collagenase alone (**Figure 5.6 A**), significant loss of protein was observed immediately after 0.5min while the digestion ended at 15.75min for young donors. Similar observation was observed from 1.75min to 17.25min for old donors. Differences between the digestion of the two donor groups were insignificant, with only 31.91%±3.59% collagen VI remained in the young old group and 25.97%±1.25% collagen VI remained in the old

donor group ($p>0.05$).

When perfused with neutral protease alone (**Figure 5.6 B**), significant loss of protein was observed after 4.5min for young donors and 3.75min for old donors. Insignificant loss of protein was observed after 14.25min for young donors and 15.5min for old donors. The digestion was found to be similar between the two groups ($p>0.05$), with 37.38%±3.16% collagen VI remained for younger donors and 33.13%±4.12% remained for older donors ($p>0.05$).

When perfused with combined enzymes (**Figure 5.6 C**), the loss of protein started at 4.5min for young donors and 3.5min for old donors, and ended at 15min and 12.75min for young and old donor group, respectively. Insignificant differences were observed between the two groups during the digestion ($p>0.05$). However at the end of digestion, 43.50%±4.35% of collagen VI remained in the young donor group while 34.50%±5.85% remained in the old donor group ($p=0.02$).

Focusing on young donors (**Figure 5.7 A**), digestion using collagenase alone was found to be the fastest, although only insignificant differences were observed ($p>0.05$). At the end of digestion, the amount of remaining protein was lower in the collagenase alone group when compared with combined enzyme group ($p=0.05$).

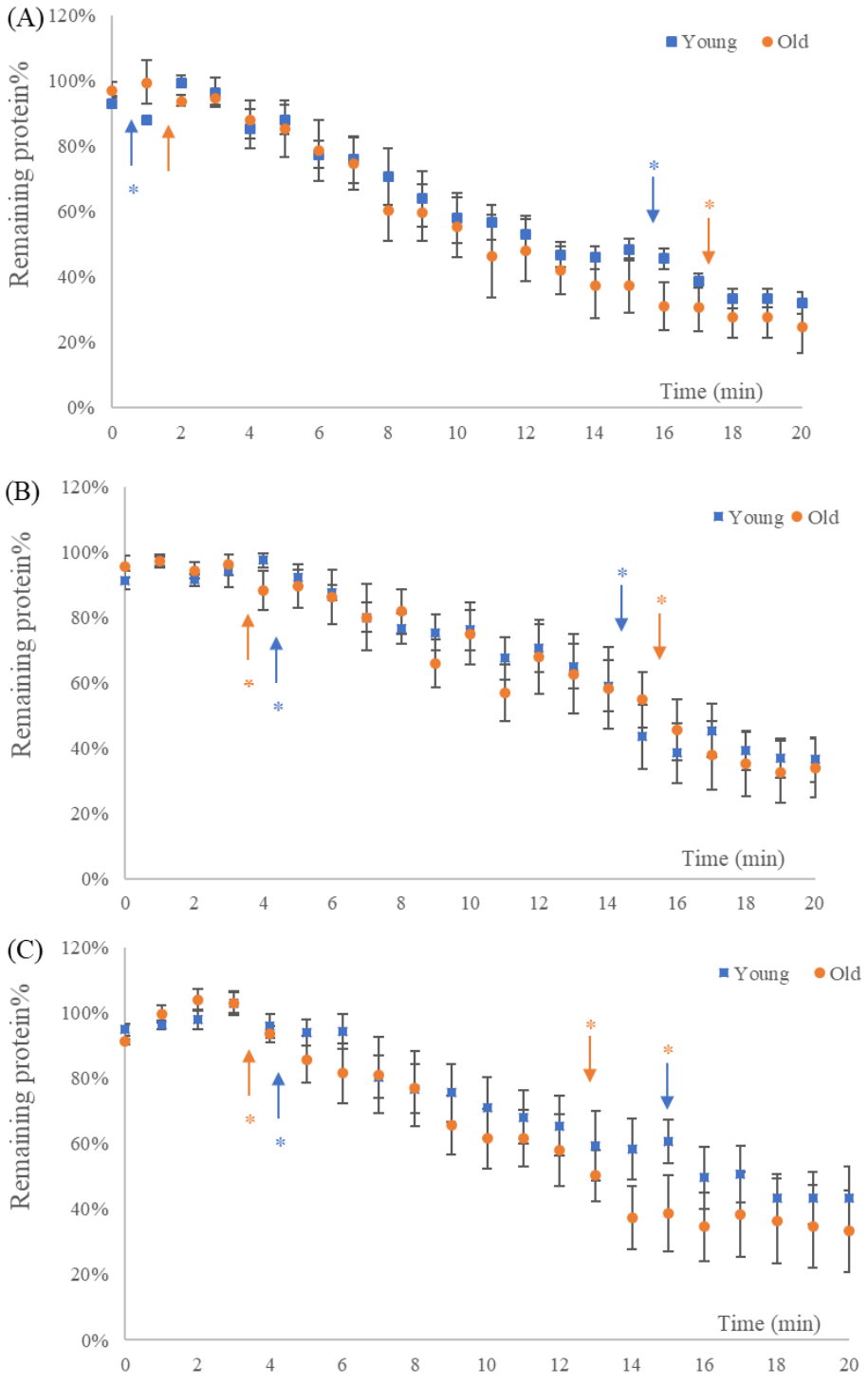

Figure 5.6 The impact of donor age (n=6 for <35 years vs n=6 for >45years) on percentage of remaining protein for and collagen VI, with different enzyme combinations. A): collagenase only; (B): neutral protease only; (C): both collagenase and neutral protease. Results shown were expressed as mean+/-SD. Upward arrows with star represents time points when significant losses of protein were observed while downward arrows with star represents time points when insignificant losses of protein were observed ($p<0.05$).

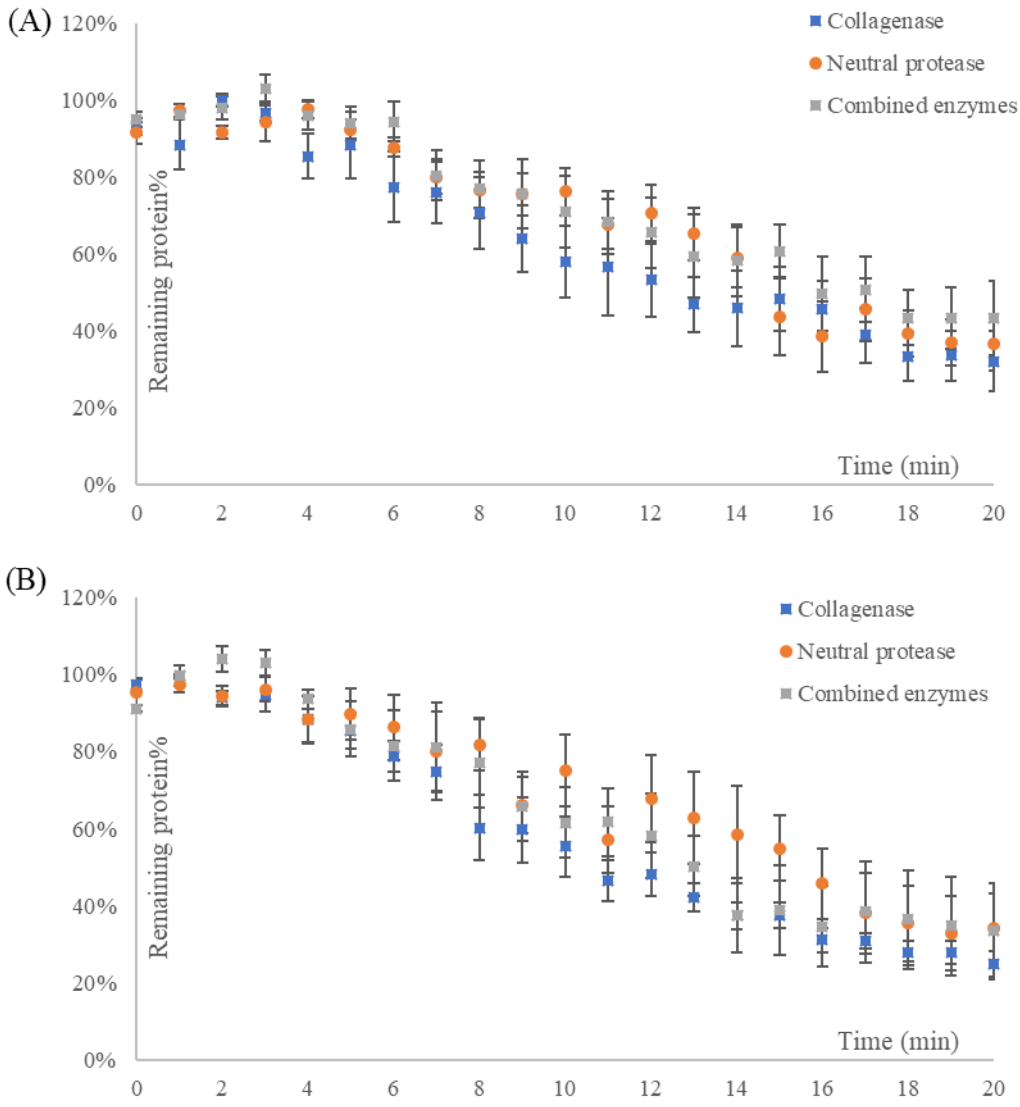

Figure 5.7 The impact of enzyme combinations (n=6 for each test group) on percentage of remaining protein for collagen VI for (A): young donors (≤35 years); (B):old donors (≥45years). Results shown were expressed as mean+/-SD. Data were regrouped and plotted from **Figure 5.6**.

Focusing on old donors (**Figure 5.7 B**), similar observation was obtained, where the digestion seemed to be faster with collagenase alone group. However, differences caused by the three enzyme combinations were found to be of statistically insignificance ($p>0.05$). At the end of digestion, the amount of remaining proteins was also similar in all three groups ($p>0.05$).

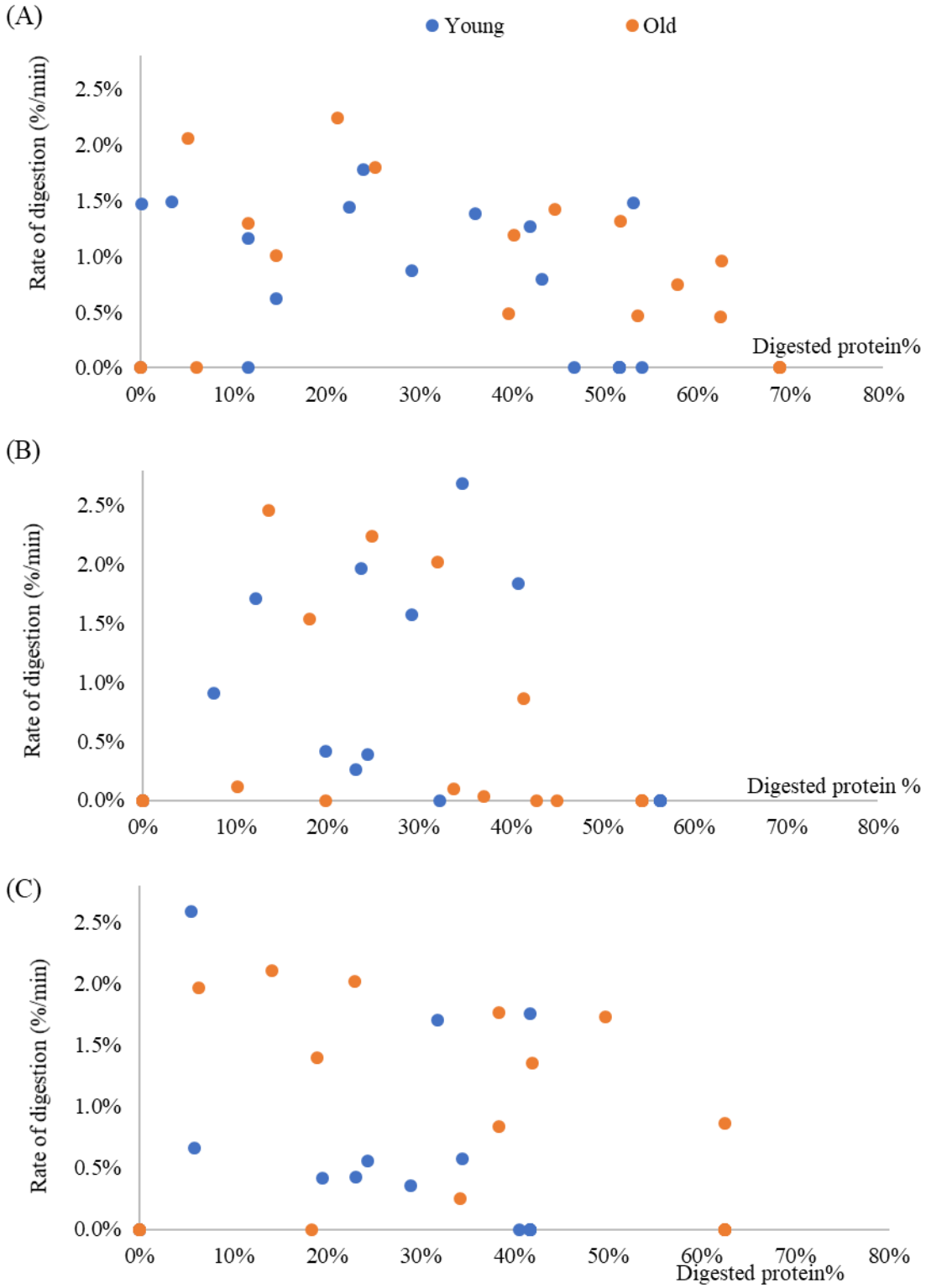

Figure 5.8 The impact of donor age (n=6 for ≤35 years vs n=6 for ≥45years) on rate of digestion for collagen VI, with different enzyme combinations. (A): collagenase only; (B): neutral protease only; (C): both collagenase and neutral protease. Results shown were expressed as mean values.

Figure 5.8 shows the rate of digestion against the percentage of remaining

collagen VI, fitted to polynomial equations. Due to large variations observed in the experiments, none of the comparisons on rate of digestion was of statistical significance. Nevertheless, similar observations to the digestion of collagen IV were obtained. The rate and extent of digestion were both higher in the old donor group when perfused with collagenase alone. However, the opposite trend was observed when perfused with neutral protease. Perfusion with combined enzymes resulted in a similar pattern between the donor groups to perfusion with collagenase alone group.

5.4 Discussion

The digestion phase is one of the key areas for improving islet isolation success rates. With the increasing demand in islet transplantation, there is an urgent requirement to obtain a thorough understanding of this process. In **Chapter 4**, we developed a method for real-time observation of enzymatic digestion process. To further explore this and to answer clinically relevant questions on donor-related variations, this chapter continued the study of the time-course effects of enzymatic digestions. To the best of our knowledge, this is the first study of the dynamic enzymatic digestion process of pancreatic tissue at molecular level with relation to physiological variables.

Following our experiments in **Chapter 4**, collagen IV and collagen VI, two ECM proteins representing basement membrane and stromal ECM proteins, were chosen as their digestion was not interfered with by the pre-labelling technique. Collagen IV is a network collagen and has been reported as the main composition of basement membrane [90]. Collagen VI has been identified as one of the major stromal ECM

proteins at islet-exocrine interface [80] and is resistant to collagenase digestions [213].

With this technique we observed the digestion of collagen VI with collagenase alone. Part of the reason was attributed to the continuous perfusion of the system. In **Chapter 4**, we found the proteins was firstly thinned before the reduction of protein area was observed. With continuous mechanical impacts of perfusion, these thinned proteins might be easier to be torn apart. This applies not only to collagen VI but also to other peri-islet proteins. As a consequent, although only collagen VI was labelled, its loss was affected by other proteins surrounding the islets as well. In fact, the digestion of collagen IV and collagen VI was not significantly different from each among all tested groups.

The real-time perfusion system also enabled studies on the rate of digestion during the process. As shown in **Figure 5.5** and **5.8**, upon binding to the substrate (100% remaining protein and 0% digested protein), enzymatic digestion started at a relatively low rate. With increased exposure of substrate to the enzymatic environment, the rate of digestion continued to rise until maximum rate of digestion was achieved. The progress of digestion resulted in a reduction of available protein. The rate of digestion was therefore limited by this reduced substrate concentration, as suggested by Michaelis-Menten model. Although reaction constant could not be calculated due to large variations, comparisons using fitted models provide a potential method for enzyme evaluation.

Similar to previous chapters, large variations were also observed during the analyses. As suggested in **Chapter 3**, the intrinsic variations among and within humans

lead to difficulties in reaching statistically significant results. Moreover, although manual adjustment of focus and careful operations were conducted, digested tissue samples were easily washed off, which may affect the ECM structure in the area of interest. Further to this, to achieve comparison among different experimental conditions, the digestion results were normalised to the control group, which resulted in propagation of error. All these variations were considered in the interpretation of the results.

Previous studies have shown the introduction of collagenase and neutral protease could accelerate the digestion process [12], [206]. A very recent study focusing on young donors by Balamurugan group shows a positive correlation between mantle-free islets and increased enzyme dosage [205]. Within a "trisected" pancreas model, a threefold increase of collagenase concentration from 20 units/gram pancreas to 60 units/gram pancreas resulted in a 5% decrease of mantled islets. Interestingly, a fivefold increase of neutral protease led to a more significant reduction of mantled islets from 60% to 17%. The results were confirmed in 13 whole pancreas islet isolations and the ability of isolated islets in reversing diabetes was demonstrated. Nevertheless, the group didn't propose any potential causes for the differences between the two enzyme groups.

Here, it suggests that collagenase alone resulted in an early start of uncontrolled digestion compared with a combination of collagenase and neutral protease, suggesting a controlling effect of Neutral Protease. It suggested that when only collagenase is present, digestion of pancreatic tissue starts directly from the breakdown of collagens, but when neutral protease is introduced, a competition between the two enzymes may

take place thus lowering the efficiency. For collagen IV, introducing neutral protease also resulted in prolonged digestions. However, this was not observed in the digestion of collagen VI.

The impact of donor age was found to depend heavily on enzyme blends. When only collagenase was perfused, greater extent of digestion was found in older donors, although significant differences were observed only for collagen IV. Analysis on the rate of digestions revealed that digestion in pancreatic tissue from old donors were usually faster than that from young donors. The difference could potentially be caused by a change in the composition and quality of ECM proteins in relation with donor age. In **Chapter 3**, we reported a decreasing trend in collagen IV and collagen VI in older donors. Consequently, although the digestion in older donors were more thorough, the total amount of protein digested might be less or equal to that for younger donors. Furthermore, glycation of collagens, which results in deteriorated proteins and is expected to more prevalent in old people [214], might also contribute to the difference in rate of digestion.

When neutral protease was introduced, the above-mentioned trends were distorted, suggesting the competition between the two enzymes might dominant in digestion thus reducing the impact caused by donor age. For combined enzyme preparations, greater extent of digestion was always observed in older donors, which complies with clinical observations, where old donors tend to result in higher rate of successful isolations.

With the same dosage of enzymes, successful isolations are more easily obtained with old and overweight donors, while young and lean donors tend to result in poor

isolation with low purity [101], [156], [166]–[168]. Considering the competing nature of enzymes involved, this proves that clinical isolations could benefit from perfusion of collagenase ahead of the introduction of neutral protease, as suggested by Edmonton group [180], [215]. For further improvements of isolation yield for this donor group, a change or tailored enzyme dosage pattern for specific donor groups might be required. However, with large variations of donor characteristics, it is impractical to find an optimal enzyme dosage combination for each individual donor. Prolonging the digestion sounds more feasible, but this requires prompt removal of early-released islets to avoid further fragmentation.

5.5 Conclusion

In conclusion, we have successfully developed a method to enable detailed studies of 'real-time' pancreas digestion. With a focus of collagen IV and collagen VI, it is found that digestion is the fastest when only collagenase is involved. With the introduction of neutral protease, a competing effect is observed. Donor age leads to differences in digestions when perfused with collagenase, potentially caused by glycation of collagens. The results suggest that a change in enzyme dosage combination or prolonging the digestion time should be conducted in younger donors for optimized human islet isolation and consistently better islet yields. Considering the time and effort required to find optimal enzyme dosage pattern for each individual donor, prolonging the digestion is more feasible and practical. This calls for prompt removal of early-released islets,

which is currently absent in clinical isolation. For this purpose, a new bioreactor with an early-separation system was built and tested in the next chapter

Chapter 6

Development of a novel bioreactor with an early separation system to protect isolated islets against fragmentation in prolonged isolations

6.1 Introduction

As mentioned in **Chapter 2.4.2.3**, research focusing on the improvements of digestion process and device design is relatively limited. For pancreas digestion, the fine collagen framework separating the exocrine and endocrine components can be removed by intraductal injection of collagenase. For thick interlobular and ductal framework, further mechanical agitation can be used to accelerate the breakdown process.

A turning point for clinical islet transplantation in its early stage was the introduction of an 'automated' process, as shown in **Chapter 2, Figure 2.8** [216]. In the Ricordi system, this was achieved by introducing glass ball bearings into the chamber to impact on the pancreatic tissue under vigorous shaking. Although this could enhance the dispersion of pancreatic tissue, the method is designed based on grinding [14] or particle size reduction mechanism rather than using any separating technique. Consequently, it is not ideal for breaking down fibrous tissue like pancreatic ECM [15]. Moreover, islets could potentially be damaged due to the battering between ball bearings and the tissue, which may result in necrosis of the tissue, reduced islet size and potentially impaired islets viability and functionality.

In **Chapter 4** and **5** we revealed that a time lag exists between the start of digestion and the release of islets following an initial enzyme-binding stage. This suggests that with the progress of digestion, the number of released islets would increase exponentially, and the early-released islets would face not only mechanical impact but also a toxic enzymatic environment [178]. This calls for a system with improved controllability, where early-released islets could be separated and protected from

fragmentation.

As discussed in **Chapter 2.4.2.3**, two improved designs, the Oxford chamber [15] and the MCT system [189] were proposed. The first design tackled improving mechanical destruction of the tissue while the latter one aimed for early separation of isolated islets. However, for the Oxford chamber no clinical results have yet been reported and the system still faces the problem of a harmful enzymatic environment for released islets. For the MCT system, although early-released islets were separated and protected from toxic enzymatic environment, the process was designed for mice pancreas digestion and worked in batch mode. Another study on the gradual removal of released islet for clinical islet isolations was conducted in 2003 [217]. After observing free intact islets, 75ml solution was manually extracted from the circuit and centrifuged to separate isolated islets. Although the isolation yield was significantly higher with this method, continuous extraction and centrifugation were required during the digestion phase. Furthermore, intervention of the system also increases the risk of contamination. Consequently, an automated system with a large capacity is desired.

Pig pancreases are favoured in diabetes research and islet transplantation. Part of the reason is the high similarity of their insulin structural properties to those from human [137], as well as being readily available from slaughterhouses. Further to this, porcine islets are much more fragile and the dissociation process is relatively rapid [218], making them attractive in studies involving early separations.

With the aim of improving the current islet isolation technique for further yield and greater viability, this study focuses on designing a new bioreactor for the digestion

of the islet-exocrine interface that could be potentially used in clinical isolation centres. To avoid massive mechanical impact, a mastication bag with internal spiky plates was designed. Several prototypes for the early separation system were designed and compared. The final design was settled on, and the prototype was assessed for enzymatic digestion using pig pancreas in proof-of-principle experiments.

6.2 Methodology

6.2.1 Design & build of the digestion system

6.2.1.1 Mastication bag

Clinical isolations use rigid Ricordi chambers, which cannot be altered to fit the shape of pancreatic tissues. As a result, extra enzyme solution is required to fill the entire chamber to ensure the tissue is fully immersed. A better fitting of the digestion chamber to the pancreatic tissue could therefore reduce the total volume of recirculating solution or enzyme required. In addition, replacing the expensive solid chamber with disposable products could also avoid problems in sterilization. For this purpose, a deformable mastication bag to hold pancreatic tissue was designed.

The first design of mastication bag consisted of two pieces of PVC sheet heat welded while the top side could be clipped once the tissue was placed in. A solution circulation port was designed and heat-bonded to the bag so that additional enzymes could be added at any required time point (**Figure 6.1**). This allowed flexible enzyme dosage pattern if prolonged digestion was required. The port was prepared by pouring

10:1 wt/wt PDMS (Sylgard® 184 Silicone Elastomer, LOT: 0007466100, Sigma, United Kingdom) and elastomer (Sylgard® 184 Silicone Elastomer Curing Agent, Batch No. H052H8R006, Sigma, United Kingdom) into a specially made mould and then solidified in an oven at 60°C for 2 hours.

However, difficulties were found in assembling the mastication bag by simple heat-welding. Leakages were found at the connection of the solution circulation port. Consequently, a commercially available hydration bladder water bag was used to hold the tissue. A bespoke cap (**Figure 6.2**) was designed for tube connection and sampling as well as to avoid leakage. The cap was 3D-printed with Formlabs® Clear Resin or Durable Resin using a Formlabs® Form 2 SLA 3D Printer and double washed in ethanol for 10min. The top side of the bag could be clipped once tissue samples were placed in. The outlet tube was surrounded by a Nylon mesh bag.

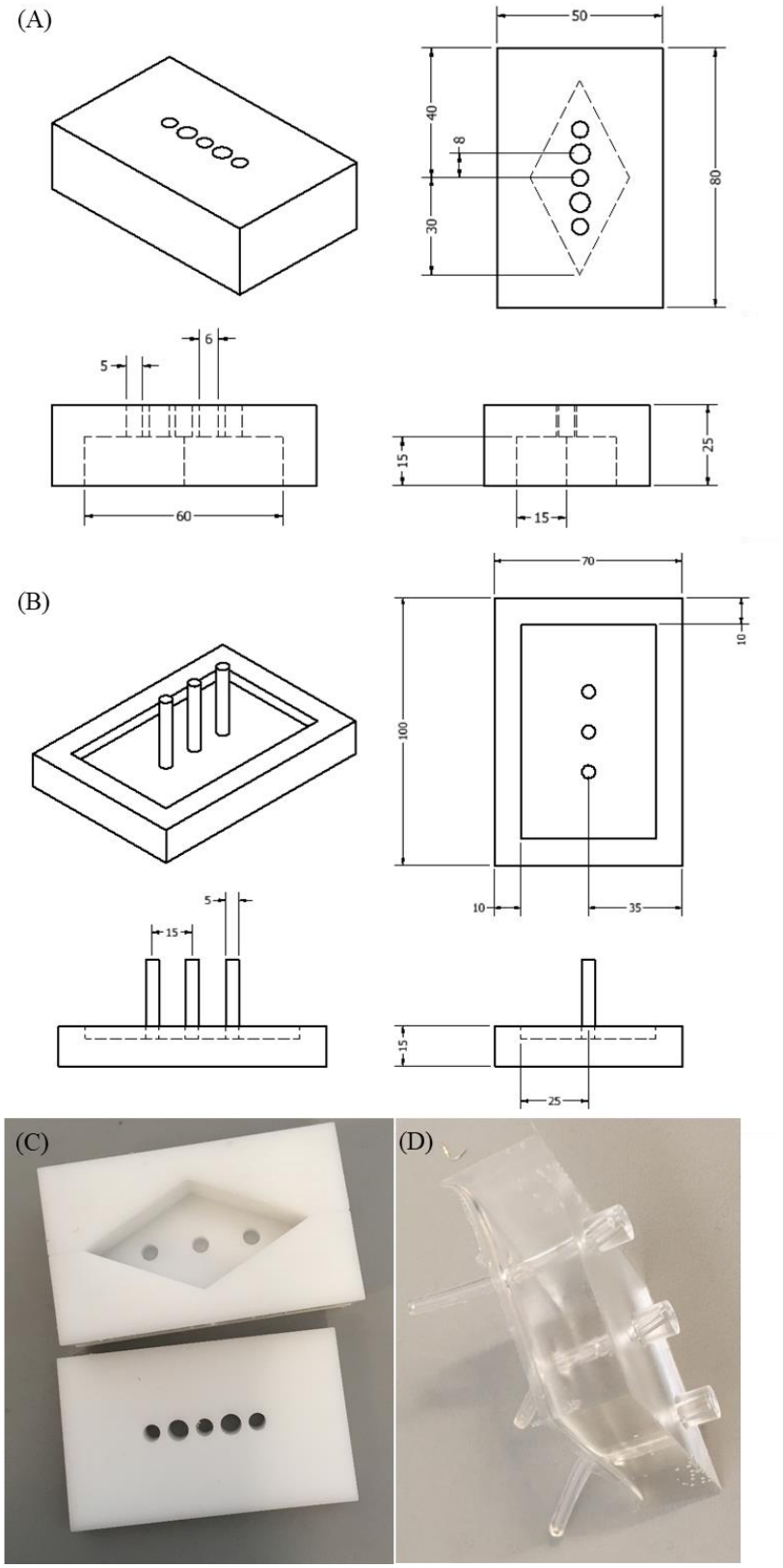

Figure 6.1 Solution circulation port. (A) & (B): schematic design of the PDMS mould; (C): final product of the mould; (D): final product of the solution circulation port, holes are left for solution circulation and sampling ports. All measurements were made in mm.

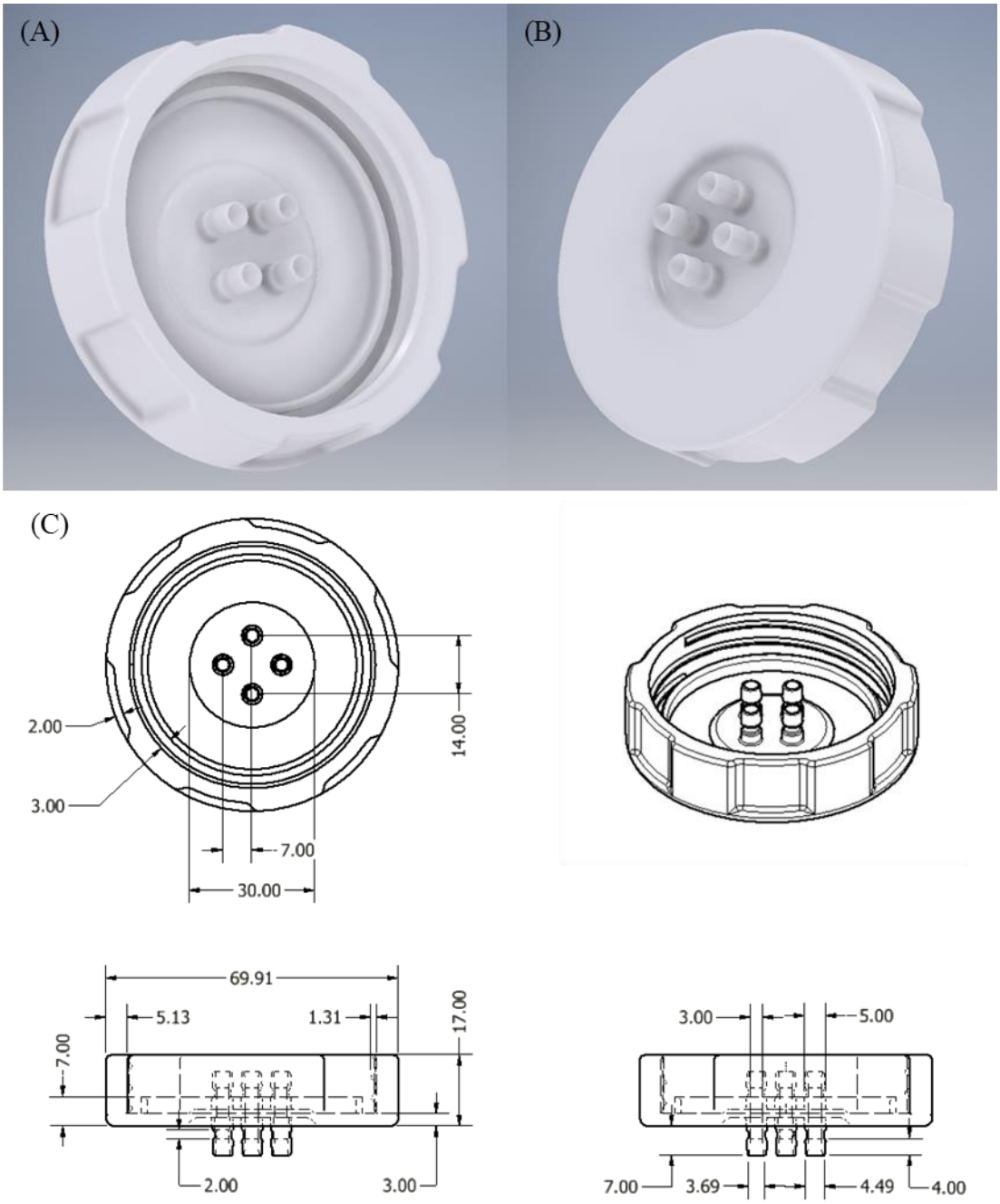

Figure 6.2 Bespoke cap. (A) & (B): schematic design of the cap; (C): Three-view drawing of the Bespoke cap. Rubber band was placed inside the cap for sealing. The four ports were designed for recycling solution in/outlet, sampling and enzyme addition for mastication bag and for recycling solution in/outlet, wash stream in/outlet and sampling point. All measurements were made in mm.

6.2.2.2 Internal designs

In order to accelerate tissue dissociation, two iterations of mastication plates were also

3D printed with Formlabs® Durable Resin, as shown in **Figure 6.3** and **Figure 6.4**. The Christmas-tree-like spikes act as barbed hooks which could help to tease apart the tissue and release isolated islets. This design would also help to avoid massive mechanical impact and the released islets could thus be kept integrate. With pressing, the bag could be squeezed, and the plates could 'bite' together to provide mechanical agitation. The initial design was composed of only 24 10mm-long spikes.

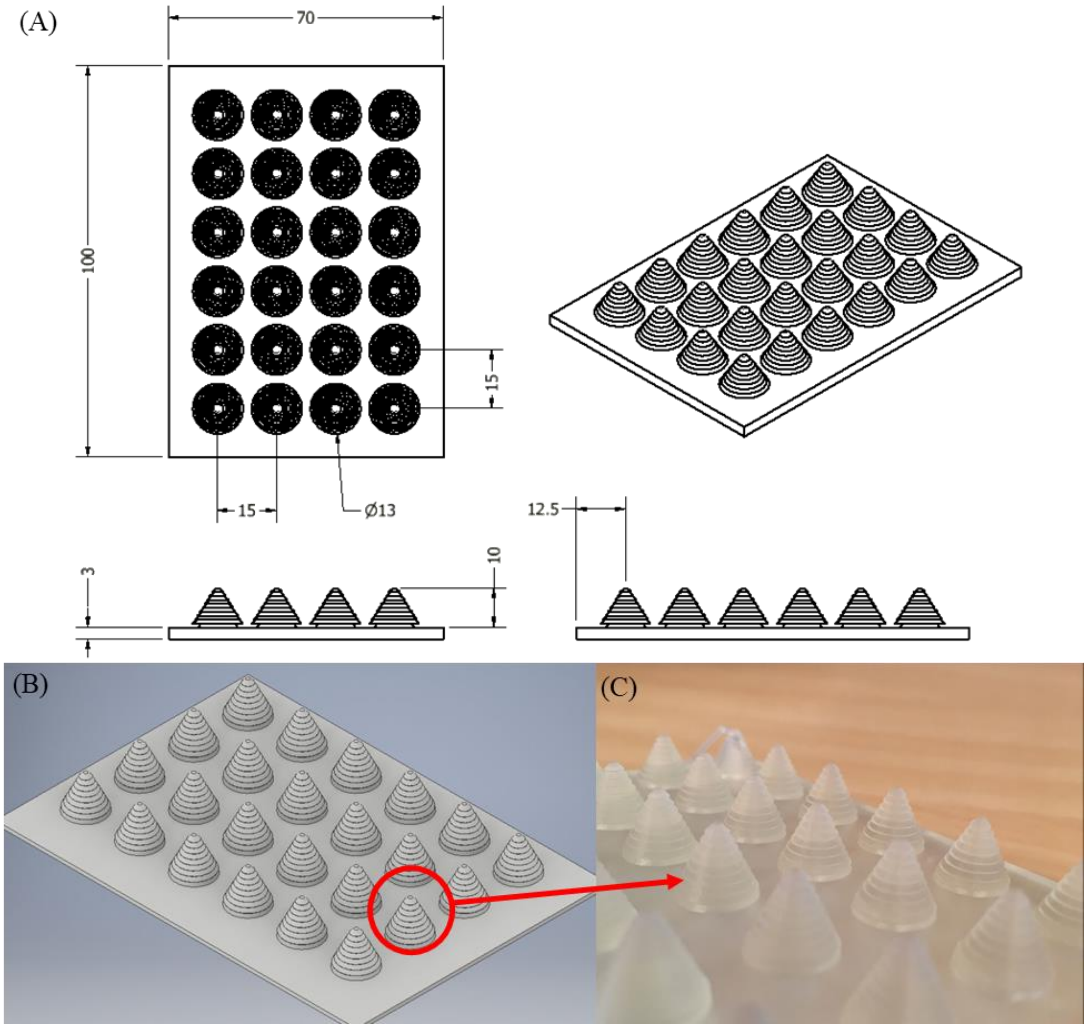

Figure 6.3 Initial design of the mastication plate. (A): Engineering drawing of the initial design of the mastication plate; (B): schematic drawing of the initial design; (C): product of the initial mastication plate with spikes enabling 'biting' of the plates. All measurements were made in mm.

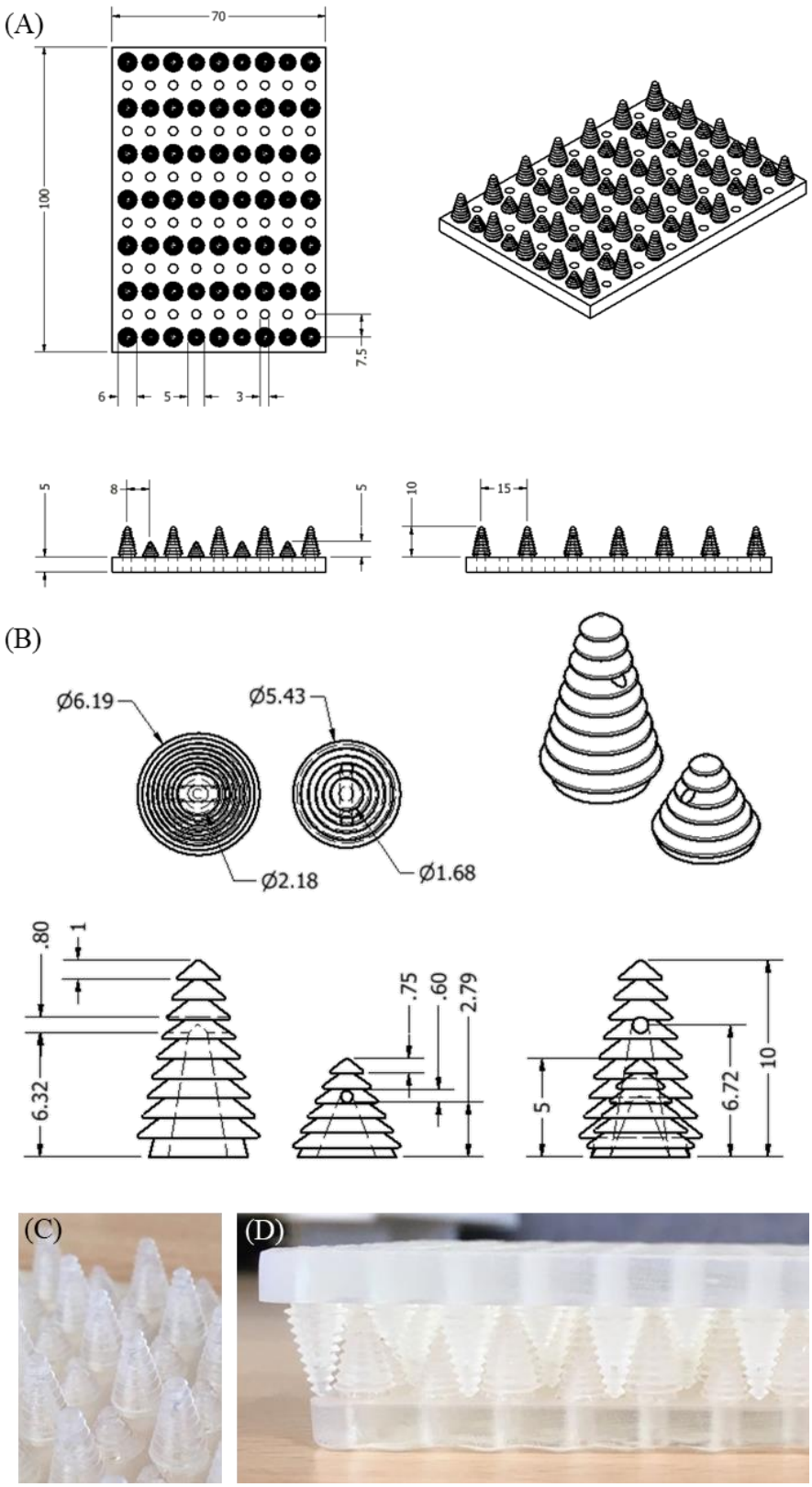

Figure 6.4 Improved second design of mastication plate. (A): Engineering drawing of the improved design of the mastication plate; (B): engineering drawing of the spikes; (C): 3D-pinted mastication plate; (D): 'biting' of the plates. All measurement was made in mm.

As shown in **Figure 6.4**, the improved design provides much denser spikes of varying lengths. Small holes throughout the plates (**Figure 6.4 A**) and spikes (**Figure 6.4 B**) were also incorporated which could help local fluid mixing and circulation. Springs were attached to the plates to avoid excess compression movement and provide the repulsion force pulling the spikes out from the tissue.

A 'leaky' one-way valve was also designed to regulate the flow direction and to provide back-wash solution for the filters **(Figure 6.5**). The valves were printed with Formlabs® Clear Resin and rubbers were placed in the chamber and fixed with the printed screw. The two parts of the valve were held together by screws and sealed by a layer of rubber sheet.

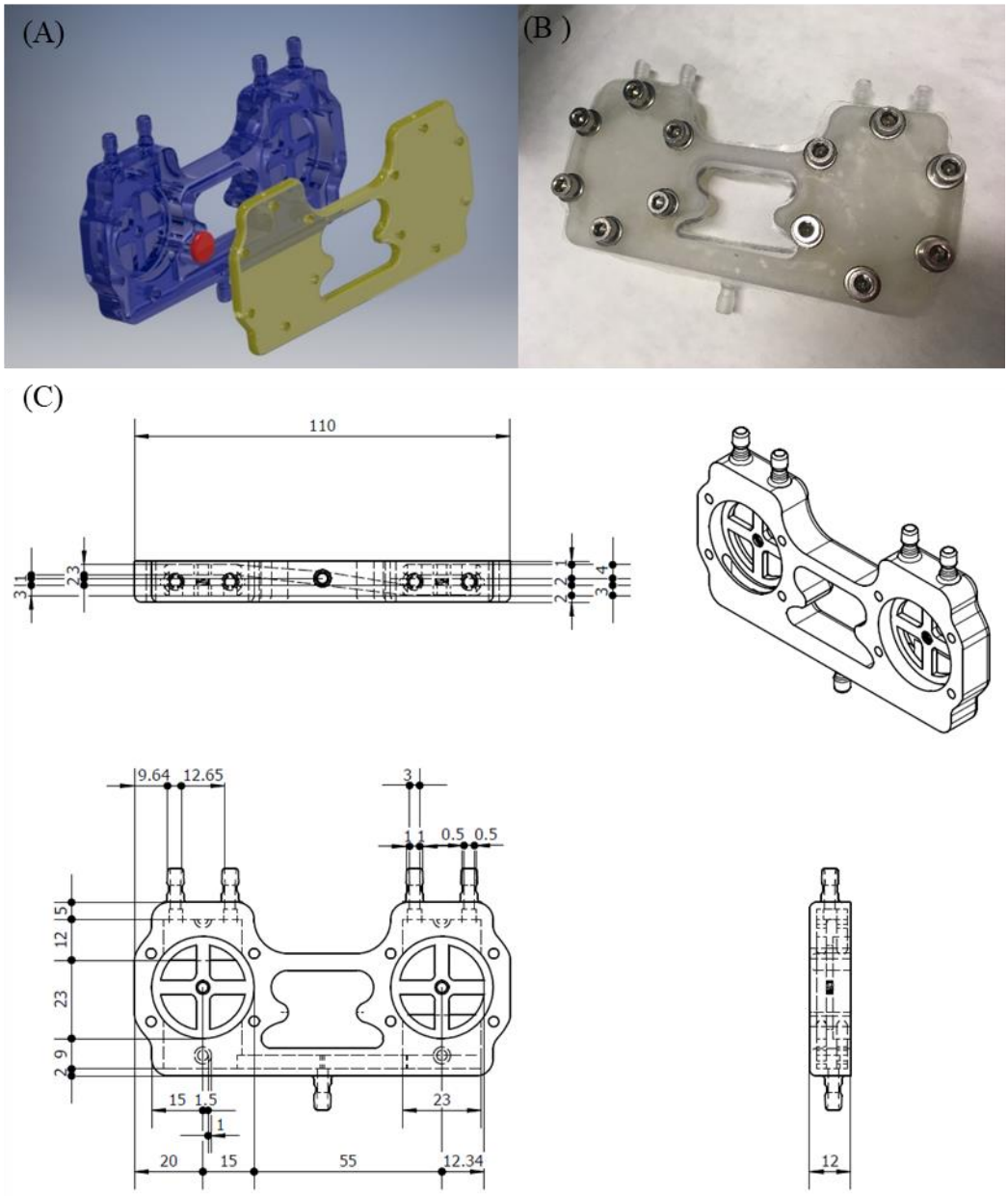

Figure 6.5 'Leaky' valve design. (A): Schematic design of the 'leaky' valve; (B): 3D-printed and assembled product; (C): Three-view drawing and dimensions of the 'leaky' valve. Rubbers were placed in both chambers to allow one-way flow of the fluid. For the outlet chamber, the rubber was not tightly fixed so that small stream of flow could be injected back to the mesh bag for back wash.

6.2.3 Design & build of the early separation system

An early separation system was designed to protect isolated islets from harmful enzymatic solutions to avoid further fragmentation. The size range of early-released

islets was determined based on average islet diameter (150μm) and the smallest counting diameter in standard IEQ calculation (50μm). It is true that cell clusters larger than 150μm might also be islets rather than exocrine tissue and if left in the solution, might be fragmented. To compensate this and to avoid clogging, Nylon meshes with slightly larger mesh size (400μm and 200μm) were used. Three designs were proposed for the early separation system (see below).

6.2.3.1 Hydrocyclone

Figure 6.6 shows the schematic view of the hydrocyclone system designed based on centrifugation. In brief, a 400μm Nylon mesh bag was used to hold pancreatic tissue. Fluid was recirculated through the system using a rotary pump and cell clusters were separated from the main solution by the hydrocyclone. Concentrated solution was then filtered with a 200μm Nylon mesh. Solution passed through the filter could then join with the overflow of hydrocyclone and be recycled back to the mastication bag. The collected cell clusters were accumulated in the ice cooling zone where enzymatic activities were quenched.

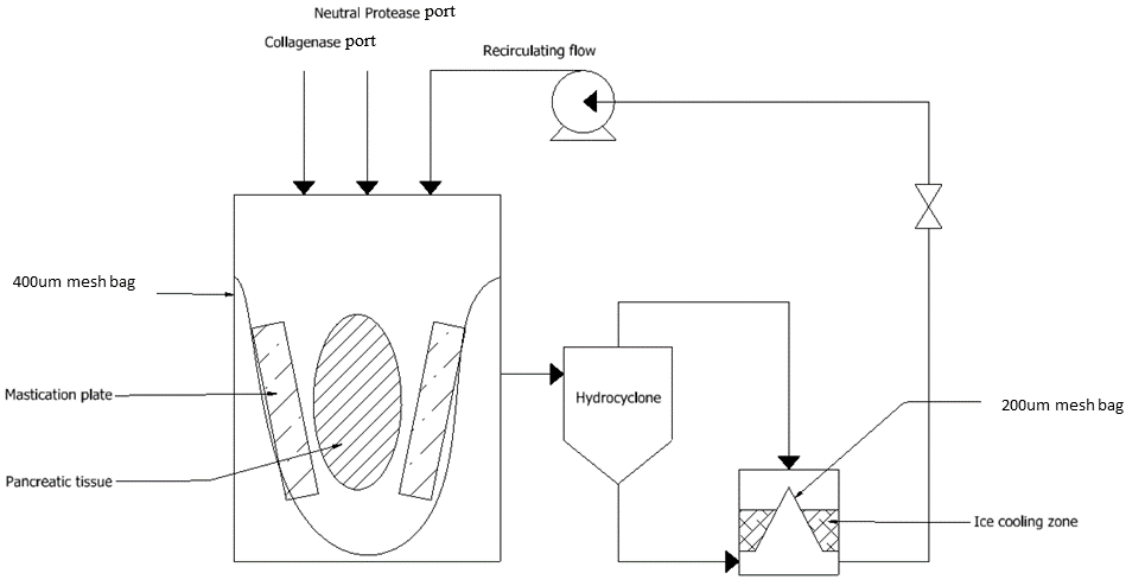

Figure 6.6 Schematic view of the hydrocyclone system.

6.2.3.2 Filtration bag

Figure 6.7 shows the schematic view of the tank system design based on simple filtration. In brief, a 400μm Nylon mesh bag was used to hold pancreatic tissue while. Fluid was recirculated through the system using a rotary pump and cell clusters were separated from the main solution by a 200μm Nylon mesh bag. Cell clusters accumulated were dropped down to the ice cooling zone where enzymatic activities could be stopped. The liquid would pass through and be recycled back to the mastication bag. For further improvement, several filtration bags could be run in cascade, with Nylon mesh bags of different sizes.

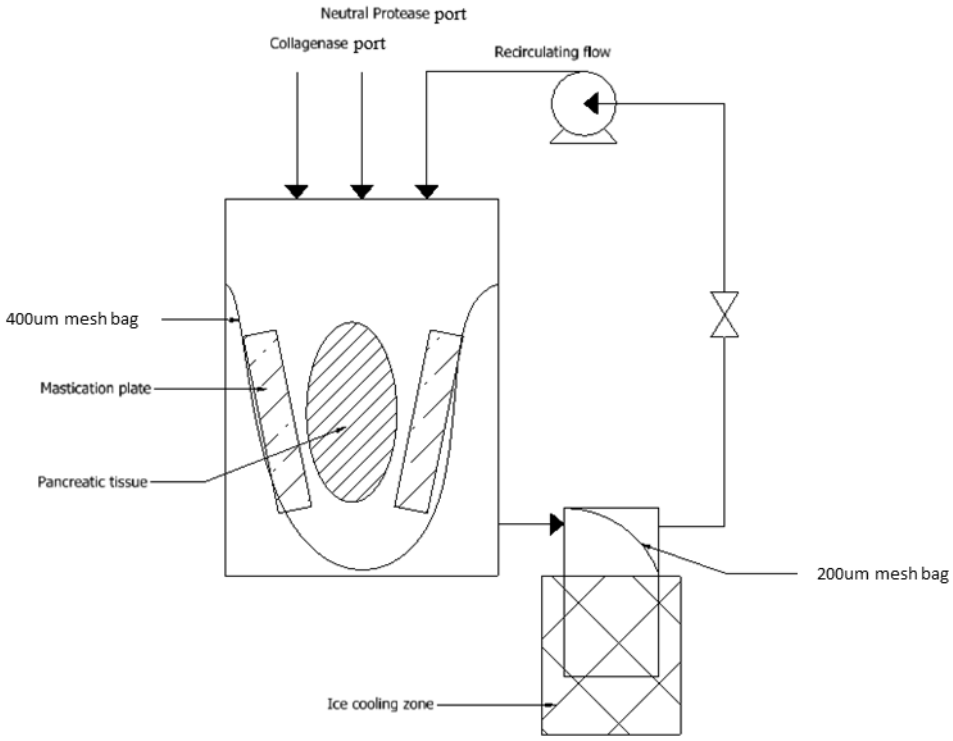

Figure 6.7 Schematic view of the filtration bag system

6.2.3.3 All-in-one system

Figure 6.8 shows the schematic view of the all-in-one system design based on simple filtration. In brief, a 400μm Nylon mesh bag was used to hold pancreatic tissue. A syringe pump was used to recirculate fluid through the system and a 200μm filter would be placed at the outlet of the mastication bag. A sponge placed at the bottom of the bag was used to collect and trap isolated cell clusters from the main solution. Once most of the solution was sucked out of the bag, cell clusters would then be trapped and accumulated in the sponge. Once the fluid was injected back into the bag, the sponge would fall into the ice cooling zone where enzymatic activity could be quenched. A 'leaky' one-way valve was placed at the outlet of the mastication bag thus when fluid is injected back into the bag, a small portion of it could be used as back-wash solution

for the 200μm filter. For further improvement, a small stream of buffer solution could be introduced to the sponge area to reduce the local enzyme concentration.

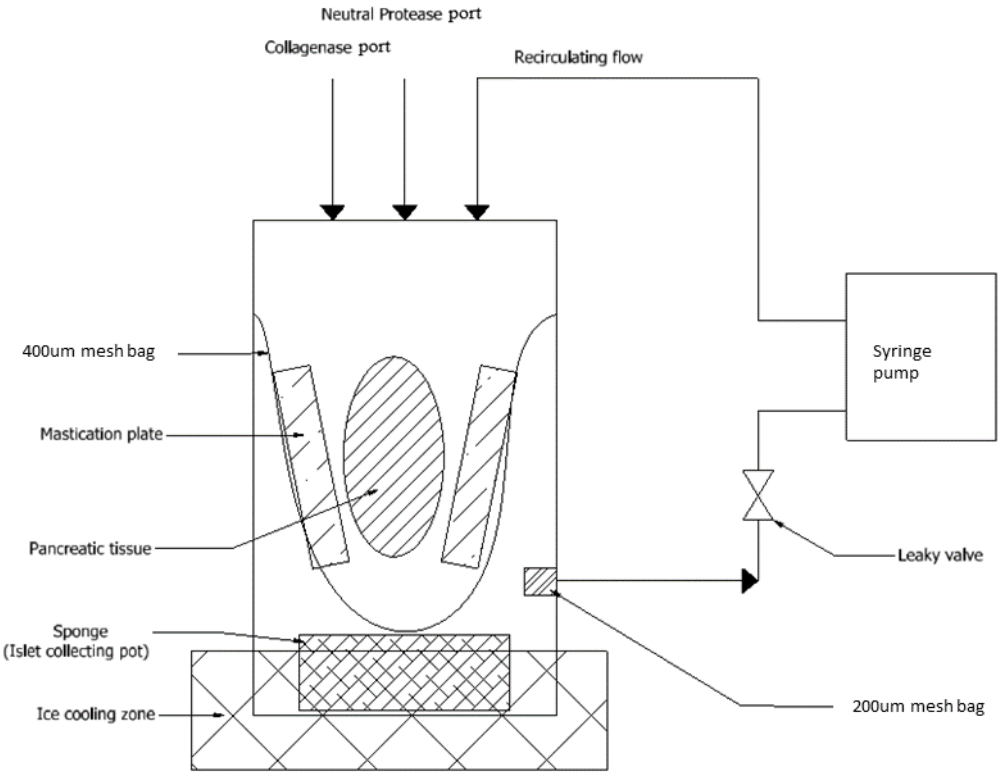

Figure 6.8 Schematic view of the all-in-one system

6.2.4 Set up of the bioreactor

For temperature control, a self-built system with a 3 wire PT100 temperature sensor (RS Components Ltd., United Kingdome) and a silicone heater mat (RS Components Ltd., United Kingdome) was used. An Arduino Uno board (Arduino, Italy) with LCD interface (Cool Components, United Kingdom), was used to achieve precise PID control. The circuit is shown in **Figure 6.9** and the system was attached to the mastication bag.

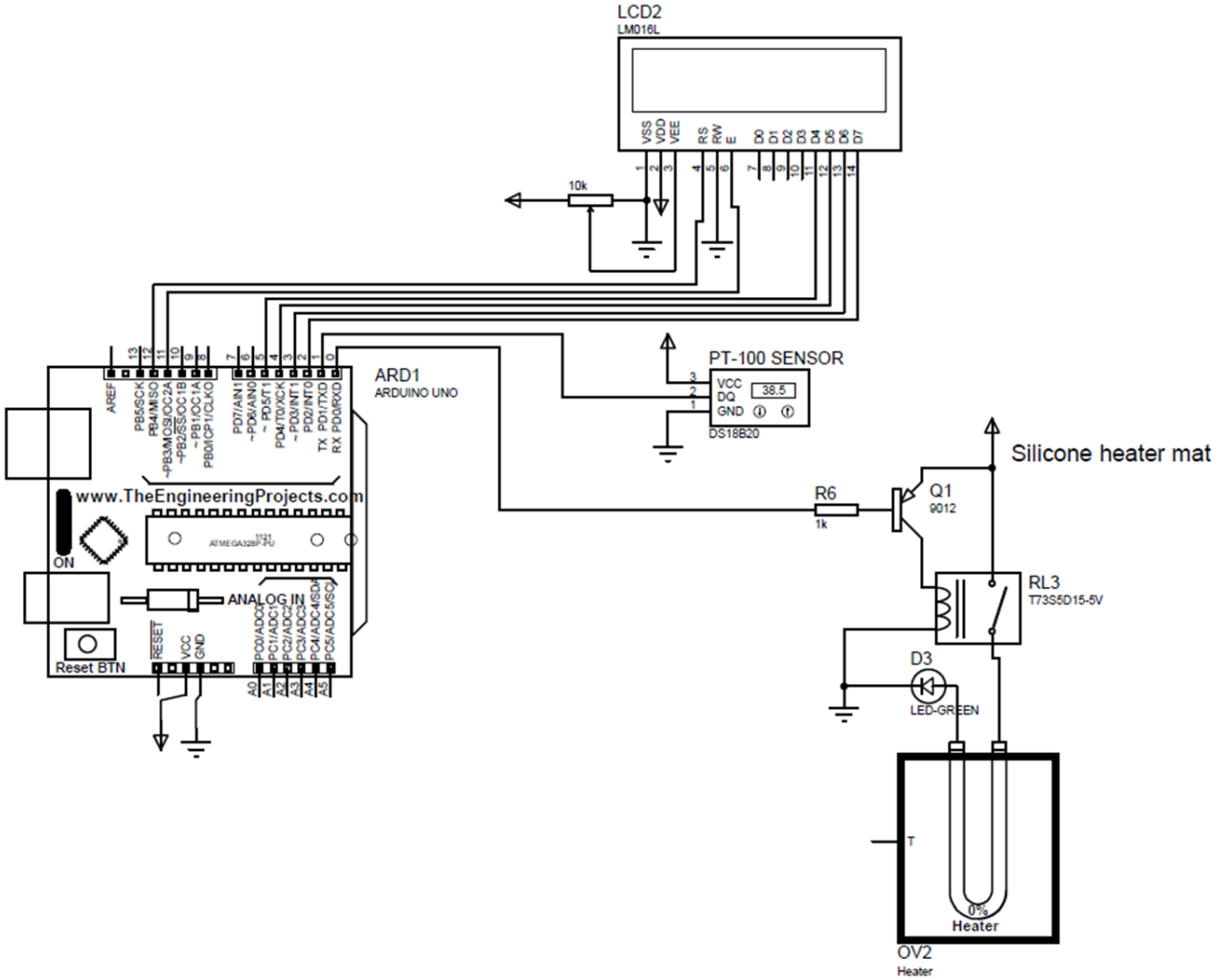

Figure 6.9 Circuit diagram of the PID temperature controller.

Comparison and analyses of the filtration system and 'all-in-one' system were made. Leak testing and temperature control testing (n=3) were conducted for the filtration bag system and the 'all-in-one' system without the pancreatic tissue. Briefly, the two systems were filled with 37°C Gibco Phosphate-buffered saline (PBS, ThermoFisher, United Kingdom) and placed in a 37°C chamber. Two MCP Standard Digital Peristaltic Pumps (Ismatec, Germany) were used to perfuse PBS through the filtration bag system for 30s every 2min while a Aladdin AL300-220 syringe pump (World Precision Instruments, United States) with a 50ml syringe (BD Plastipak, UK) was used to perfuse PBS through the 'all-in-one' system once every 2min. After 20min, temperature in the mastication bag was recorded and compared. Based on the results, it was decided that further experiments would be carried out with a modified filtration bag system. **Figure 6.10** shows the flow arrangement for the designed system.

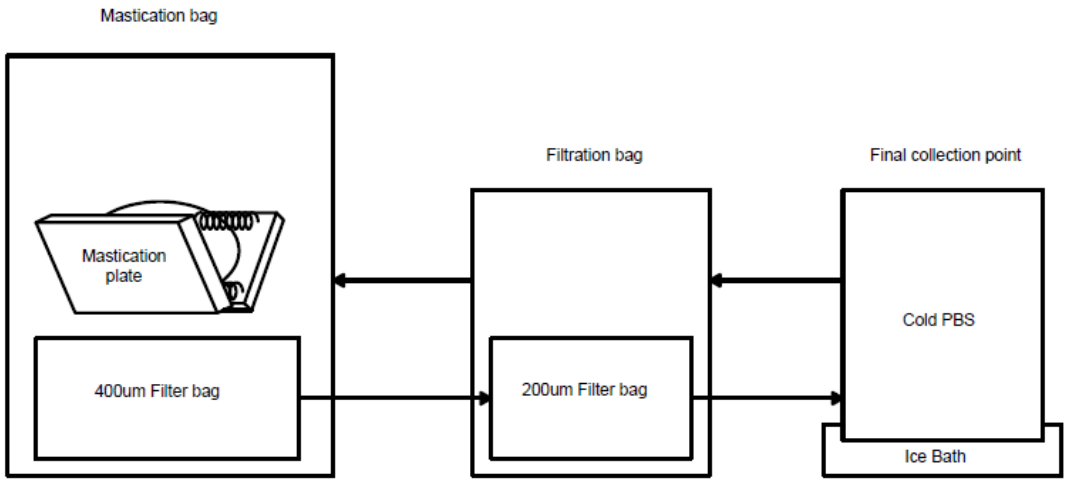

Figure 6.10 Schematic diagram showing the flow arrangement within the bioreactor. Solution flow is controlled by peristaltic pump and leaky way as mentioned above.

Figure 6.11 shows the actual set-up of the bioreactor. Briefly, a 1500ml

thermoplastic urethane bladder bag (Outdoor Local Lion, China) was used to as the mastication bag while a 1000ml thermoplastic urethane bladder bag (Outdoor Local Lion, China) was used as the filtration bag. 200μm and 400μm Nylon monofilament filter bags (Cole-Parmer, United Kingdom) were used to separate isolated cell clusters in the desired range. The mastication bag and filtration bag were connected using Masterflex L/S 16 C-Flex tubing (Cole-Parmer, United Kingdom) and two MCP Standard Digital Peristaltic Pumps (Ismatec, Germany) were used to circulate solution through the system.

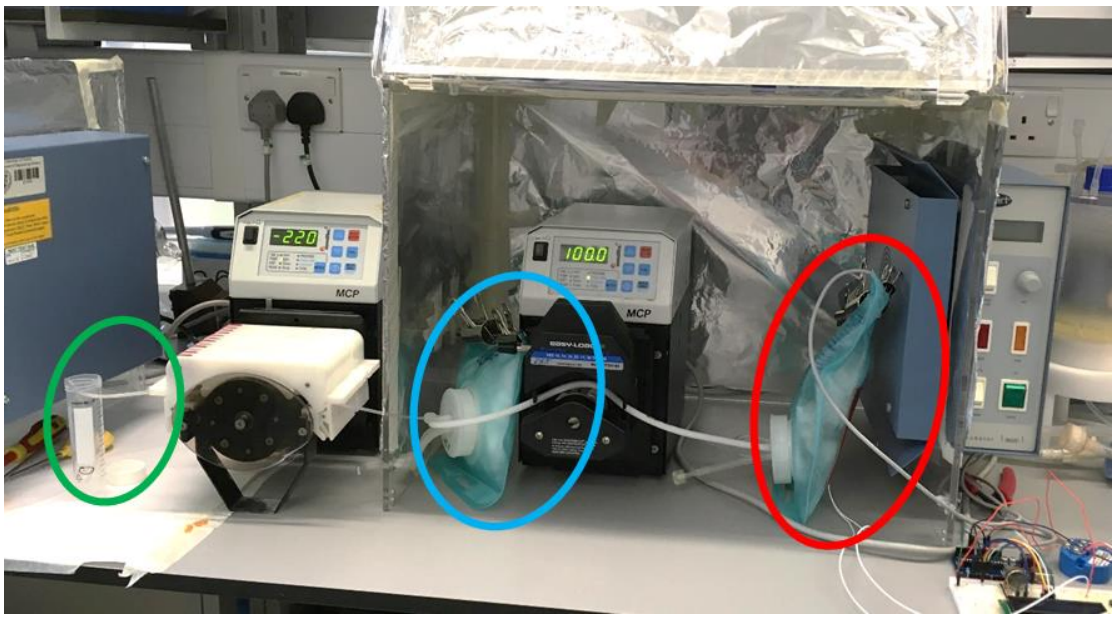

Figure 6.11 Spatial arrangement of the bioreactor. Red: mastication bag with mastication plates and 400μm nylon mesh bag; Blue: filtration bag with 200μm nylon mesh bag; Green: final product collection.

6.2.5 Pig pancreas digestion

Nine pig pancreases were retrieved from Long Compton Abbatoir, Shipston-on-Stour, the United Kingdom, with appropriate consent and ethical approval. All pigs fell within an age range of 50-55months and weight range of 50-60kg. Porcine pancreases were

placed in 4°C PBS solution (ThermoFisher, United Kingdom) and transported in an ice box. The warm ischemia times were kept within one hour and the cold ischemia times were less than 24 hours. Details of all the pigs and experimental arrangement are listed in **Table 6.1**.

As pancreases were not processed and procured in an aseptic environment, contaminations, sometimes even faecal contaminations were observed. Although excessive washing with antibiotic antimycotic solution (Sigma Aldrich, UK) was conducted, the culture of islets proved to be difficult. Almost all islets died 12 hours after culture. Consequently, no further comparison on the purity, viability and recovery of cultured islets could be carried out.

To test the performance of this bioreactor, digestion with pig pancreas was conducted (n=3). Isolating solution was composed of Hank's Balanced Salt solution (HBSS, Sigma Aldrich) with 15mM $CaCl_2$ (Sigma Aldrich). The solution was filter-sterilized through a 0.22μm filter and adjusted to pH 7.2–7.4 prior to storage at 4°C until use.

TABLE 6.1 Pig characteristics for bioreactor performance test. (Table to be continued in next page)

Isolation ID	Breed	Age (months)	Sex	Pig Weight (kg)	Pancreas weight (g)	Digestion chamber involved
1	Lop	4	Female	55	207	Bioreactor
2	Sandy & Black	5	Female	50	62	Bioreactor

(Table to be continued in next page.)

Isolation ID	Breed	Age (months)	Sex	Pig Weight (kg)	Pancreas weight (g)	Digestion chamber involved
3	Sandy & Black	5	Female	50	61	Bioreactor
4	Large White	5	Female	65	177	Bioreactor
5	Large White	5	Female	55	104	Bioreactor
6	Large White	5	Female	60	147	Bioreactor
7	Large White	5	Female	60	121	Ricordi chamber
8	Large White	5	Female	55	108	Ricordi chamber
9	Large White	5	Female	60	139	Ricordi chamber

After removing the extraneous tissue and cannulation of the duct, Collagenase NB1 (6.77U/ml in HBSS, Serva) and Neutral Protease (NB, 0.14U/ml in HBSS, Serva) was injected into the ducts. The pancreatic tissue was then placed between the spiky plates in the mastication bag. After addition of 200ml of HBSS solution, the bag was sealed at the top.

For the first 10min, pancreatic tissue was digested in the mastication bag at 37°C with manual pressing of the bag. 1ml samples were taken from the bulk solution as well

as from the 400μm Nylon mesh bag at 5 and 10min to monitor the digestion process. After 10min of digestion, solution was recirculated through the filtration bag for 90s and stopped before a 30s back wash from the collection point took place.

Samples were taken at the end of PBS wash from bulk solution in the mastication bag, 400μm Nylon mesh bag, residual solution in filtration bag, 200μm Nylon mesh bag and the final collection point. Due to the difficulties in prompt analyses of free islets, the digestion lasted for 35min for each test. The system was then stopped and the collected digest was diluted with approximately 1L of room temperature PBS. The digest was collected in 250ml conical tubes and centrifuged at 1500 rpm for 10 min. All centrifuged pellets were then washed and recombined in PBS solution three times. 1ml of sample was taken for postdigestion islet size, purity and viability comparison

To compare the effects of the bioreactors with traditional Ricordi chamber, digestion with a Ricordi chamber was also conducted (n=3 for each group). Collagenase-perfused pig pancreas was chopped into 4 pieces and digested with collagenase and neutral protease at 37^{o}C. The pancreases used for the two groups were matched for breed, age, sex, pig weight and cold ischemia time. 1ml of sample was taken at 5 and 10min and every 2.5min till 35min. The digest was collected and treated using the same method as above.

6.2.6 Postdigestion analysis

For postdigestion islets, viability was determined using Trypan blue, which stains dead cells blue while viable cells remain unstained. Briefly, 100μl of sample was mixed with

100µl of 0.4% Trypan blue (Thermofisher, United Kingdom) and imaged with a Nikon TS100 microscope (Japan).

The size distribution, yield, purity and morphology of islets was determined with dithizone (Sigma Aldrich, United Kingdom) staining and assessed manually. For islet yield, measurements were made based on the criteria established at the Second Congress of the International Pancreas and Islet Transplantation Association [219]. In short, the diameter of individual islets would be directly measured manually and categorized according to their diameters within 50-µm increments. The number of islets in each category was then multiplied by a related factor that converts the islet number and diameter category to islet equivalent (IEQ) for yield calculation. For islets of irregular shape, the equivalent diameter with same area was used for further analyses.

For statistical analysis, results from both methods were compared. Data were expressed as mean±SD and statistical analysis was carried out using analysis of variance (ANOVA) or *t*-test ($p<0.05$ for statistically significance) with IBM SPSS version 22 (Chicago, USA).

6.3 Results

6.3.1 Bioreactor design

The bioreactor was designed to reduce mechanical battering as well as to achieve controllable enzyme introduction and early separation of released islets. For this purpose, a mastication bag with two spiky plates (**Figure 6.4**) was designed. Compared

to a solid device, bags are more flexible and could easily fit to the shape of internal designs. This could reduce the total volume and minimise enzyme requirement. Further to this, bags could be disposed after usage and avoid the need of complex sterilization.

The use of spiky plates instead of marbles introduces shearing forces aiding the dissociation of lobular fibrous tissue. To hold the pancreas in place, spikes of different lengths were used. Shorter spikes were arranged at the bottom thus once the pancreas tissue is placed in, the plates could form a Y-shape to hold the pancreas while enabling compression of the plates. Long and sharp spikes are preferable as they could easily pierce into the tissue and tear it apart. However, those spikes are more fragile and could be easily broken during digestion process. For this purpose, a flat bottom was adopted for each spike and a Christmas-tree like arrangement was used to increase total spike numbers. Manual compression of the plate results in mechanical agitation and in this way the Christmas-tree-like spikes could tear the tissue apart. Small holes throughout the spikes would also assist local fluid distribution thus help the digestion of pancreatic tissue.

Difficulties were encountered in the design of the separation system. The most straightforward idea was to introduce centrifugation forces, as used in purification process. For this purpose, a hydrocyclone system based on centrifugation was proposed. However, it was believed to be the most complex and least feasible design. Not only does it require delicate pressure control for cell separation, but also a subsequent filtration system to collect separated islets. Pumping fluid was also difficult, since the overflow of hydrocyclone would be of positive pressure while the filtration system may

require excess pressure drop for smooth fluid flow. Introducing another pump between the two systems may result in low separation efficiency or by-passing of the unit. No back wash would be provided for the system thus the filter could be blocked relatively easily. Moreover, multiple units would increase total volume and thus increase operational cost for enzymes. Therefore, this design was abandoned for further experiments.

Compared to the hydrocyclone system, the filtration bag system provided a much easier and simpler approach. The initial idea was to have tubular Nylon mesh bags attached to the inlet tube and cell clusters accumulated could be dropped into a bag placed in the ice cooling zone. However, it was found that with perfusion, mixing and heat transfer within the filtration bag could take place, resulting in poor temperature control. As a result, a modified version was used, as shown in **Figure 6.10**.

The all-in-one system was an improved version compared to the filtration tank system. The idea was to integrate all the units into the mastication bag. This could help to reduce heat loss during recirculation and the total volume of the system. The sponge to trap cell clusters could be a porous scaffold with further coatings of proteins like collagen IV or laminin to protect released islets. Moreover, the ‘leaky’ one-way valve provides backwash of the system thus blocking is believed to be minimised.

Problems like heat loss and clogging are expected during recirculation and cold PBS wash. A PID temperature control system was therefore used to maintain the temperature in the mastication bag at 37^{o}C (**Figure 6.9**). Compared to conventional by-pass heating circuit used in clinical isolations, the PID system provides a moderate but

direct control of the temperature as well as reduce volume required for by-pass heating. As for clogging, backwash provided by the 'leaky' one-way valve was used. Filter bag instead of filter screen was also used to improve surface area and to avoid complete clogging of the system.

Preliminary leakage and temperature tests were conducted for the filtration and 'all-in-one' system where temperature control was found to be a problem in the latter design. As shown in **Figure 6.12**, the temperature for the 'all-in-one' system was always lower than 35°C. Consequently, the filtration tank system was used for the digestion experiments.

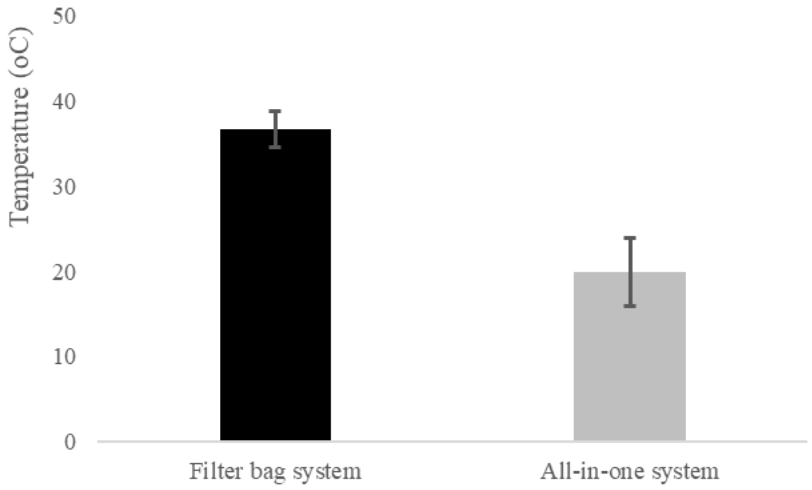

Figure 6.12 Results for temperature control test for the filtration system and 'all-in-one' system. Experiments were conducted by perfusion prewarmed PBS through the system. No pancreatic tissue was placed in the system for temperature control test.

6.3.2 Pig pancreas digestion

To test the performance of the bioreactor, pig pancreases were digested with the new bioreactor (n=3, isolation ID 1-3). With observation of free islets, the performance of this bioreactor was compared with traditional Ricordi chamber (isolation ID 4-9). As

shown in **Table 6.1**, the pancreases used for the two groups were matched for breed, age, sex, pig weight and cold ischemia time. All experiments were conducted at 37^{o}C with 6.77U/ml collagenase and 0.14U/ml neutral protease.

Figure 6.13 shows the pig pancreas after procurement, fat and connective tissue removal and enzymatic digestion. As shown in **Figure 6.13 (A)**, fresh pig pancreases obtained directly from the abattoir were covered with fat and connective tissue. Efforts were put to carefully remove these extraneous tissues, leaving only pancreas for further tests (**Figure 6.13 B**). For enzyme injection, the pig pancreases were generally cut into 2-4 pieces to find the pancreatic duct. Pieces of tissue were then put between the mastication plates in the mastication bag. After introduction of HBSS the bag was sealed from the top. Manual compression of the bag was performed to provide mechanical agitation and to help tearing of the tissue.

After 35min of digestion, the pig pancreases were significantly thinned, as shown in **Figure 6.13 (C)**. Small pieces of tissues torn from the pancreas were found on the mastication plates and the 400μm bag (**Figure 6.14**). Nevertheless, problems like significant clogging were not observed in all the experiments.

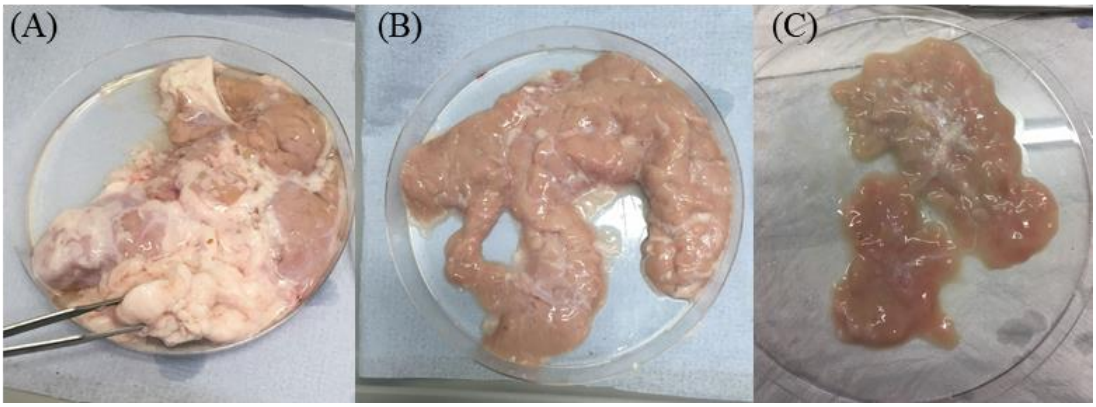

Figure 6.13 Pig pancreas for digestion experiment. (A): fresh pig pancreas obtained from the abattoir, covered with fat and connective tissue; (B): pig pancreas after dissection of fat and connective tissue; (C): pig pancreas residue after digestion.

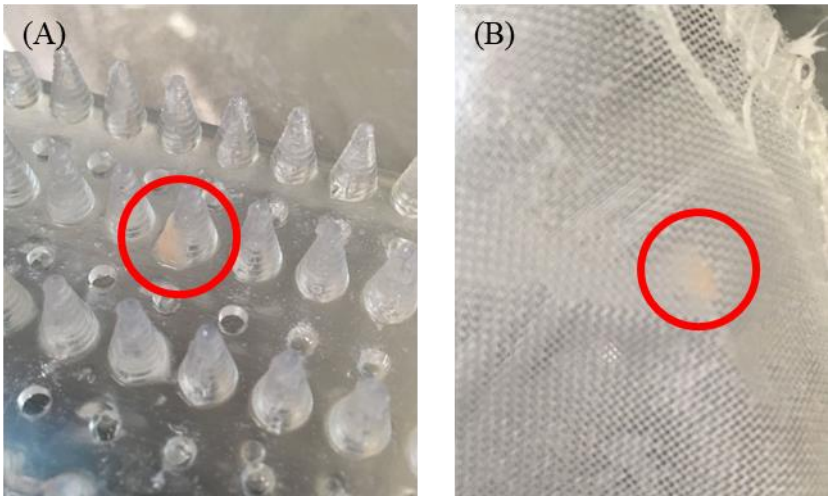

Figure 6.14 Tissue residue left in bioreactor. (A): tissue residue left on the mastication plate. The tissue was teared off from the main body under the shearing forces caused by plate movement; (B): tissue residue left on the 400μm bag.

To observe the isolation outcome, dithizone was used to stain islet for morphology, purity and size distribution analyses. **Figure 6.15** shows free islets in the mastication bag during digestion. Compared to 5min after digestion, more free islets were observed found at 10min. Further to this, as free cell clusters were continuously transported to the collection point, the number of free islets in the mastication bag remained almost constant. On the contrary, at the collection point, a steady increase of free islets was observed, as shown in **Figure 6.16**. Overall, the bioreactor allowed the separation of more than 100,000IEQ islet with >38% purity.

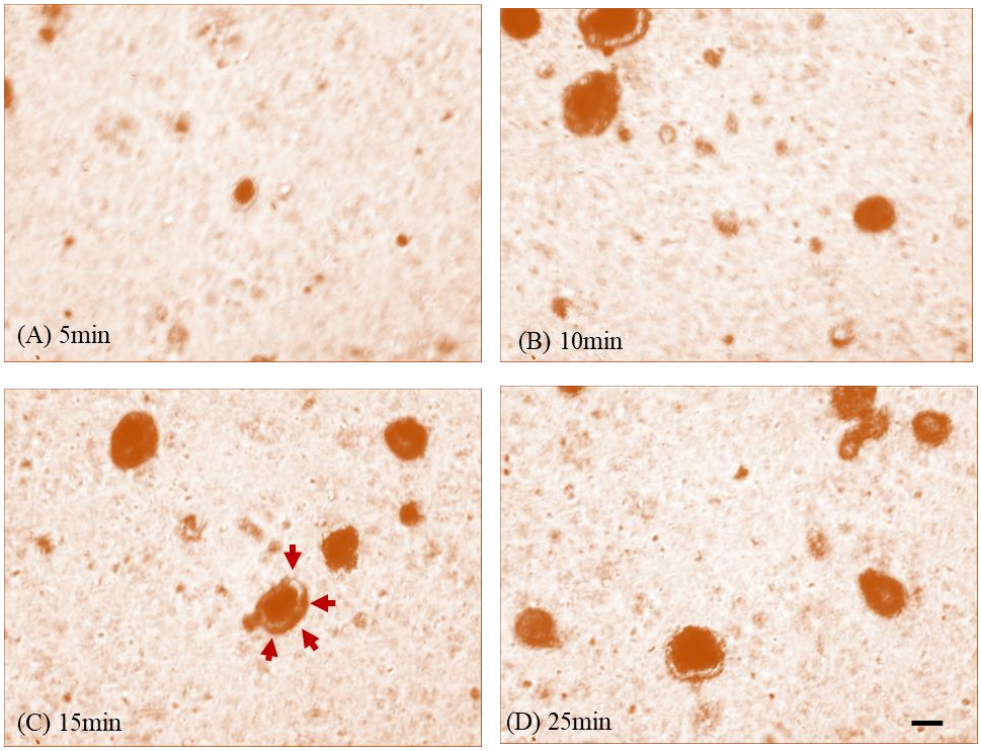

Figure 6.15 Free dithizone-stained islets isolated from mastication bag at (A): 5min; (B): 10min; (C): 15min; (D): 25min. Layers of connective tissue were also observed suggesting incomplete digestion (arrowheaded). Scale bar = 50μm.

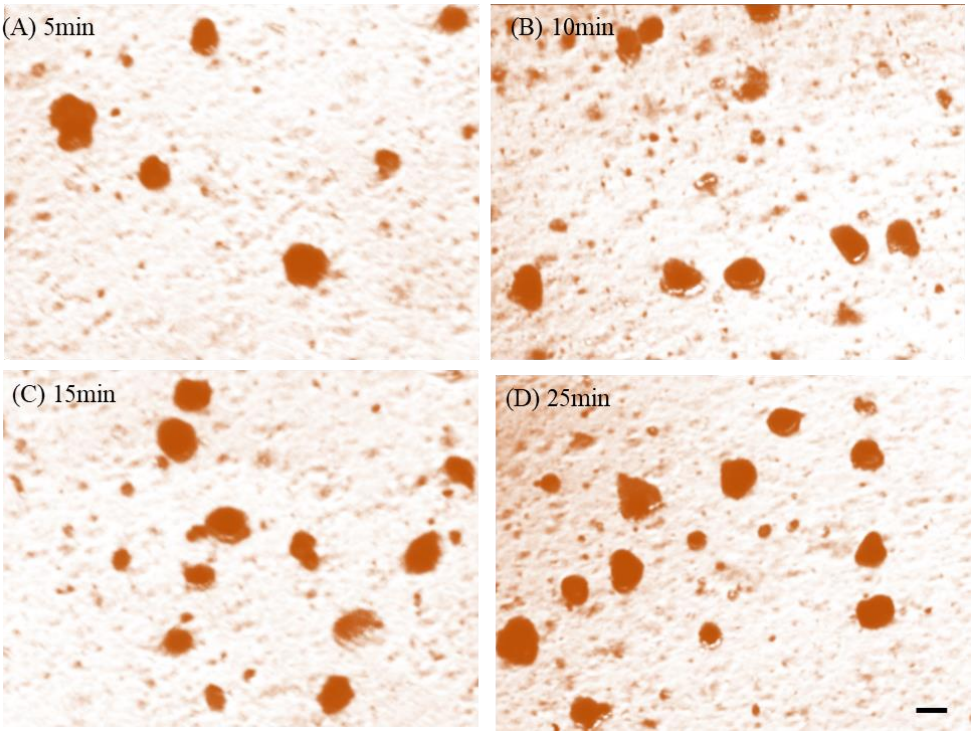

Figure 6.16 Free dithizone-stained islets isolated from collection point from the designed bioreactor at (A): 15min; (B): 20min; (C): 25min; (D): 30min. Layers of connective tissue were also observed suggesting incomplete digestion. Scale bar = 50μm.

With the observation of free islets, the performance of bioreactor was then compared to Ricordi chamber (n=3 for each group, isolation ID 4-9). The weight and cold ischemia time of pancreas allocated to each experiment were managed to be the same ($p>0.05$). Unlike what was observed by Gray *et al.*[15], digestion of pig pancreas was achieved with Ricordi chamber (**Figure 6.17**). The performance of the two methods are shown in **Table 6.2**.

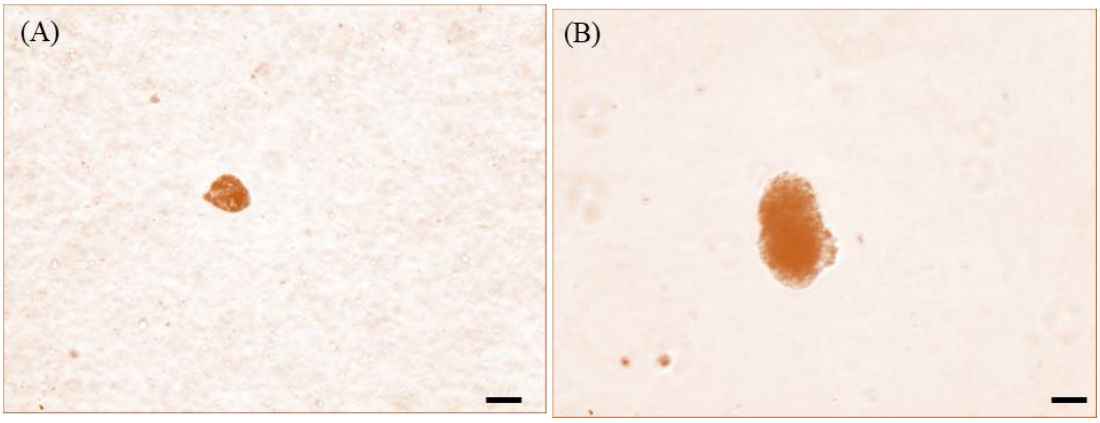

Figure 6.17 Free dithizone-stained islets isolated from both methods. (A): Free islets isolated using Ricordi chamber; (B): Free islets isolated using the bioreactor. Scale bar = 50μm.

As shown in **Table 6.2**, about 50% of the pancreas were digested using the two methods. Insignificant differences were found for purity and viability ($p>0.05$) while IEQ and IEQ/g pancreas were slightly higher using the bioreactor ($p=0.03$ and $p=0.05$ respectively). Nevertheless, a significant increase of islet number was found using the Ricordi chamber ($p<0.01$), suggesting islets obtained in this group were generally smaller. In fact, as shown in **Figure 6.17 (A)**, most islets obtained using this device were <50μm and were discarded for IEQ calculation. **Figure 6.18** shows the islet size distributions from both methods. It is apparent that isolations using the traditional device results in relatively small islets ($p<0.01$). Detailed performance for each

isolation can be found in **Appendix 7.3**.

Table 6.2 Performance of bioreactor and Ricordi chamber. Asterisks represent p<0.05 (*) and p<0.01 (**) respectively.

	Bioreactor	Ricordi chamber	p-value
CIT (h)	7.3±1.5	7.3±2.5	p>0.05
Pancreas weight (g)	143±37	122±16	p>0.05
Digested tissue (%)	50±4	49±3	p>0.05
Yield (*1,000 IEQ)	221±50	162±50	p<0.05 *
Islet number (*1,000)	40±8	78±4	p<0.01 **
IEQ/g Pancreas	1533±70	1332±80	p<0.05 *
Purity (%)	55%	55%	p>0.05
Viability (%)	42%±4%	43%±6%	p>0.05

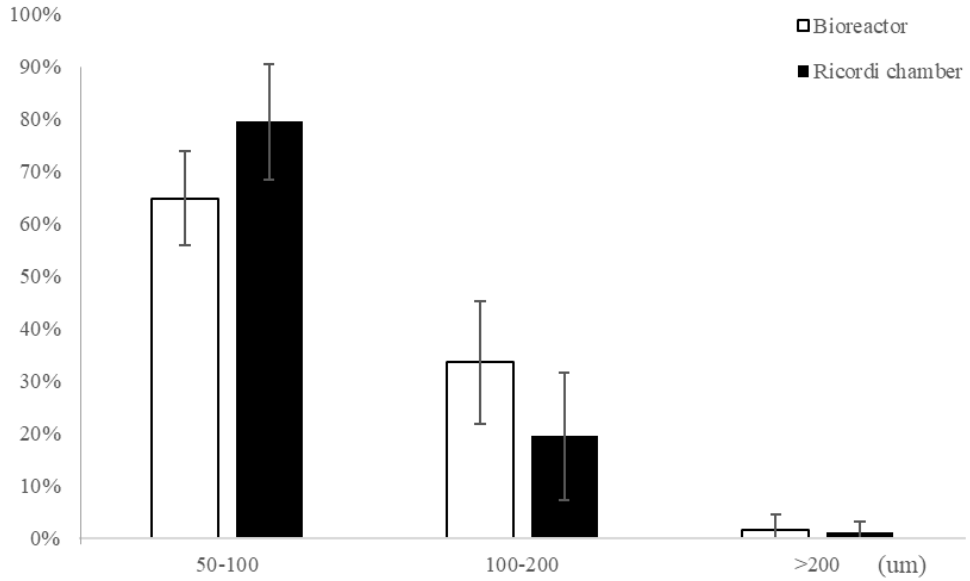

Figure 6.18 Size distribution of free islets for both methods. As shown, most islets fell in the 50-100μm, which is in accordance with previous studies [226]. Compared to islets isolated using the Ricordi chamber, there are more 100-200μm islets isolated using the new device (p<0.01).

6.4 Discussion

Although decades have passed since the introduction of Ricordi chamber, the isolation of islets was still conducted using the same device and method. Improvements have been made for enzyme dosage and purification [133], but there has been little research focus on the device itself. With the increasing demand in islet transplantation, there is an urgent requirement to develop an efficient and economic device to improve isolation yield.

As discussed in **Chapter 3**, isolated islets from younger donor are often mantled with exocrine tissue due to insufficient digestion [168]. This results in an increase in the density and poor isolation yields after purification [101]. In **Chapter 5**, the results suggested that prolonged digestion time may aid in complete digestion of pancreas from young donors. Nevertheless, exposing isolated pancreatic cells to the toxic enzymatic environment increases the risk of fragmentation and impairment of islet function [217]. Furthermore, the basement membrane is also digested during islet isolation [13], [209] and this is linked with pancreatic cell apoptosis [220]. Consequently, a prompt removal of released islets from enzymatic solution is desirable.

In this study, we have designed a mastication bag with spiky plates in connection to early separation system allowing complete digestion without further fragmentation. The digestive process involves little human intervention, reducing the risk of contamination and toxicity. Overall, this device meets the requirement of safe operation and easy sterilization.

The performance of this newly designed device was tested with pig pancreas

digestion. Juvenile pigs were used as these are the most common market pigs in the United Kingdom. Compared to human islets, the basement membrane at peri-islet interface for pigs is weakly expressed [221], [222]. This results in fragile porcine islets [218] and extra care is required to avoid fragmentation. Prolonged digestion with reduced enzyme concentration and static digestion with minimized mechanical agitation have been suggested [223]–[225]. Here with an early-separation system, we showed an improvement in preserving larger porcine islets after prolonged isolations.

Unfortunately, due to the problem in contamination, no comparisons on islet function could be conducted. However, as islets with 100-200μm were mostly present in digest using the new bioreactor, it was expected that with reduced fragmentation, the functionality of islets isolated using the new bioreactor system is at least comparable, if not superior than the islets isolated from the Ricordi chamber.

As shown in **Figure 6.15** and **6.16**, free islets were observed after 10min of digestion using the new bioreactor and an increase of free islets was observed at the collection point suggesting the continuous separation of cell clusters from the digestion system. Fee islets isolated from juvenile pigs tended to be smaller than human islets. Most islets fell in a size range of 50-200μm and islets larger than 200μm were seldom observed. This shows accordance with literature, where juvenile porcine islets tends to be smaller and 59.8-68.9% of porcine islets are 50-100μm [226].

After 35 minutes of digestion, the percentage of digestion, islet viability and purity were found to be the same with either new bioreactor or the Ricordi chamber. The IEQ and IEQ/g pancreas, on the other hand, were found to be higher using the new device.

The increased isolation yield might be a result from improved digestion with shearing forces. As discussed in **Chapter 2**, **Section 2.4.2.3**, compared to uncontrolled battering, shearing forces are more suitable in the dissociation of lobular fibrous tissue. The lobular ECM fibres could be torn apart and this might reduce destructions to the tissue. Not only does this increase the isolation yield but also protect the viability and functionality of the islets. Consequently it helps to relieve the shortage of transplantable islets and benefits outcomes of clinical transplantations.

As suggested in **Chapter 3** and **Chapter 5**, prolonged digestion was conducted, where the digestion time was extended to 35min. With an early-separation system, the islet number using the new device was found to be significantly lower than using the Ricordi chamber. A close look at the size distribution revealed that most islets isolated from Ricordi chamber were <100μm, indicating increased fragmentation. On the contrast, more islets in the size range of 50-200μm were obtained in the digest from the new bioreactor, suggesting its advantages in protecting early-released islets for prolonged digestion. This proves the protective effects of the early-separation system in prolonged digestions, which would help to achieve complete digestion, especially for pancreas from young and lean donors.

6.5 Conclusion

In summary, a bioreactor for prolonged pancreas isolation was successfully designed and built. This new device provided a method to achieve prolonged digestion with limited islet fragmentation. With subsequent animal testing, this device overcame some

of the shortcomings of the conventional Ricordi chamber, showing comparable quality and improved yield of islets. With a significant improvement in preserving the integrity of isolated islets, it is proposed that this device could provide researchers and clinicians with an alternative option for islet isolation.

Chapter 7

Conclusions and future work

7.1 Conclusions and contributions

Diabetes mellitus is a metabolic disorder associated with life-threatening hypoglycaemia events and other chronic complications [22]. Insulin administration is the mainstay method to control normal glycaemia [3]. However, for certain T1DM patients, swings of blood glucose occur regardless of their blood glucose control, leading to life-threatening complications [4]–[6], [50]. As a viable treatment strategy for T1DM, islet transplantation has become a clinical option for those patients suffering from severe hypoglycaemia unawareness [8]. Islets isolated from donated pancreas can significantly improve patients' blood glucose level and quality of life [8]. Nevertheless, the isolation yield is always less than half of the number of islets the pancreas potentially contains, and generally multiple infusions are required for one patient to reverse hypoglycaemic events [11], [44]. As the demand for islets for transplantation outstrips supply, actions need to be taken to improve the availability of islets for transplant.

As discussed in **Chapter 2.4**, there are many approaches to expand islet source [135], [136], [140], [144]. However, the most effective and immediate method is to improve current isolation results. For this purpose, this thesis aimed to use biological and engineering techniques to investigate and improve islet isolation with respect to donor-rated variables. The main objective seeks to deepen the understanding of digestion phase and to develop engineering tools promoting research on the improvement of isolation yield for specific donor groups.

To achieve this, an analysis of current isolation situation was conducted, as shown

in **Chapter 2.4.2.1**. Age and BMI are two of the most common factors associated with variations in clinical isolations [159]–[161]. The isolation yield from older and obese donors tends to be much higher [165], [166]. However, isolated islets from older donors are found to be associated with worse function and poor transplantation results [166]–[169]. Consequently, improving the isolation yields from younger and/or lean donors is of particular interest. Throughout the literature, investigations in the substrate, the ECM network [13], [80], [89], and development of new enzyme blends [12], [133], [179], [185] were conducted but the dynamic digestion process at molecular level has yet to be elucidated. Further to this, the equipment used for current clinical isolation remains unchanged for over 30 years. Modifications of this apparatus based on better understanding of the digestion process may provide a better approach to improve the isolation efficiency.

The first step to solve the above problems was to improve current understanding of pancreatic ECM and the influences of donor characteristics, as shown in **Chapter 3**. Revealing the 3D molecular ultrastructure of the islet-ECM interface and the impact of donor variables on it could also enable the development of tailored isolation strategies. For this purpose, multiphoton microscopy was used due to its long penetration depth. A new protocol for staining an intact islet embedded in pancreatic tissue was developed. The presence of common ECM proteins, including collagen I, collagen III, collagen IV, collagen VI, laminin and perlecan, was studied within donors of different age and BMI. Quantification analyses were conducted to reveal the effects of these two donor characteristics.

Unlike studies where donors were grouped into “older” (usually >45 years old) and “younger” (usually <35 years old), here a continuous range of donor age and BMI was investigated. Results from 3D images showed that collagen and laminin were prevalent in islet ECM, forming a network-like structure in exocrine part and a sheet-like membrane wrapping the entire islet. Quantification analyses showed the content of collagen I and laminin decreased with donor age rather than BMI, while perlecan increased with both donor age and BMI. In terms of clinical significance, these results suggest a specific enzyme blend in islet isolation for different donor groups, rather than an “all-in-one” solution, for the improvement in isolation efficiency and use of resources.

With an understanding of the ECM network, investigations into the digestion process at molecular level were conducted in **Chapter 4**. As clinical isolation is a continuous process, it was desirable to investigate the process in a similar environment. To achieve this, a perfusion system with an inverted microscope was developed. Building the chamber holding the tissue was challenging, as it needed to (1) hold tissue and perfused solution without leaking; (2) have a thin bottom to allow light to pass through; (3) allow even flow of solutions over the tissue surface and (4) be easily manufacturable and reproducible. PDMS was chosen due to its availability, biocompatibility, transparency and deformability. To fulfil condition (2), a very thin PDMS layer was produced and attached to the PDMS wall to finish the making of this observation chamber. When slides with tissue samples were placed in, a sink could be formed at the entrance surrounded by the glass slide and the chamber wall. This

allowed accumulation of solutions which could subsequently flow evenly over the slides.

With the built chamber, digestions of one stromal ECM protein, collagen VI, and one basement membrane protein, collagen IV, were conducted. The effects of individual enzymes as well as their combinations and one donor characteristic, age, were investigated in **Chapter 5**.

The digestion process was fastest when only collagenase was involved. With the introduction of neutral protease, a competitive effect was observed. This was obvious for the digestion of collagen IV in pancreatic samples obtained from older donors, where greater extent of digestion was achieved when only collagenase was used. Part of the reason was attributed to a change in the composition and quality of ECM proteins in relation with donor age. The results suggest that a change in enzyme dosage pattern or prolonging the digestion time should be conducted in younger donors for optimized human islet isolation and consistently better islet yields. Considering the time and effort required to find optimal enzyme dosage pattern for each individual donor, prolonging the digestion is more feasible and practical. This calls for prompt removal of early-released islets, which is currently absent in clinical isolation.

With the above drawn conclusion, a new digestion system was designed, built and tested in **Chapter 6**. The new system composed of a mastication bag and an early separation system to remove isolated islets the from toxic enzymatic environment. This allowed the preservation of islet integrity in prolonged islet isolations. Challenges were encountered in the designing process and three systems were proposed. With a

comparison of feasibility and operationality, a filtration tank system was adopted. Moreover, unlike the Ricordi chamber, which uses silicon nitride marbles to induce mechanical agitation, the new system uses shearing forces induced by two spiky plates to tear the tissue apart. Compared to uncontrolled battering caused by marbles, the shearing forces are more suitable in digestion of lobular ECM fibres. The plates were 3D-printed and assembled into the mastication bag. Furthermore, the mastication bag is attached to an enzyme introduction port, where additional enzymes could be added at any desired time point. This allows adjustment of enzyme concentrations in prolonged isolations.

To investigate the performance of this device, animal tests using porcine pancreases were conducted. Juvenile pig pancreases were obtained from an abattoir and transported in an ice box. After enzyme infusion, the pancreas was placed in the digestion chamber for 35min. With dithizone staining, the morphology, yield and viability of isolated islets were analysed. The performance of this new device compared to the original Ricordi chamber were also tested with porcine pancreases.

The new system was successful in the digestion of juvenile pig pancreases. With the early separation system, it helped to achieve complete digestion with limited islet fragmentation. Overall, the bioreactor allowed the separation of more than 100,000IEQ islet with >38% purity from each juvenile pig pancreas. Compared to Ricordi chamber, insignificant differences were found for purity (55% for both methods) and viability (42%±4% and 43%±6% for bioreactor and Ricordi chamber respectively). However, total IEQ and IEQ/g pancreas were significantly higher using the bioreactor

(221,000±50,000IEQ and 162,000±50,000IEQ, 1533±70IEQ/g pancreas and 1332±80IEQ/g pancreas for the bioreactor and Ricordi chamber respectively). Furthermore, about 40,000±8,000 free islets were obtained using the bioreactor and 78,000±4,000 were obtained using the Ricordi chamber. This significant increase in islets number, especially the number of those in the range of 50-100μm in diameter, suggested that more fragmentation occurred using this traditional device. The results favour the use of this new system in prolonged digestion.

To conclude, this thesis contributed to a deepened understanding of the 3D structure of pancreatic ECM network and indicated the dynamic digestion process of the matrix in an enzymatic environment. Further to this, several engineering tools were built to improve the digestion efficiency and to allow further improvements of this process.

7.2 Limitations and future perspectives

In **Chapter 3**, the 3D structure of ECM proteins surrounding an intact islet was revealed. Although efforts were put into the staining process, penetration of antibodies into the tissue sample proved to be difficult. Prolonging the incubation time results in excess antibodies attached to the surface of the sample. This severely affected image quality, where the surface of the sample was always much brighter than the inner core. Fine tuning of the microscope and programmed laser scanning strategy helped to relieve but not resolve the problem. As a result, only qualification analyses were conducted using the 200μm-thick samples. Further improvements of image quality rely

on the development of microscopy, such as new filters and spectral detection systems.

In **Chapter 4** a new system for real-time observation of the digestion system was developed. The new system allowed imaging of the digestion process on a sample-loaded slide where enzymatic solution was perfused over the surface. However, in clinical isolations, enzyme solutions are injected into the ducts rather than perfused to the surface of tissue. This was hard to reproduce as (1) it is hard to fix a large chunk of tissue sample at a certain place in a perfusion system; (2) imaging of thick tissue samples proved to be difficult using fluorescence microscopy while long-time imaging using laser-induced microscopy resulted in burning of the sample. Consequently, only slides loaded with thin samples (<15μm-thick) were used. The results may not reflect the real digestion process in a clinical isolation, and this was considered in the interpretation of the results.

For real-time observation, as the tissue sample was placed in a perfusion environment, manual adjustment of the focus was sometimes necessary. To further improve the efficiency, it is recommended that an automated programme based on image tracking and machine learning to be developed. This could massively reduce human intervention and consequently improve the accuracy of the results.

Another limitation needs to be mentioned is the intrinsic variations among and within humans, as discussed in **Chapter 3** and **Chapter 5**. The presence of these large variations leads to difficulties not only in the experimental design but also in statistical analyses. Methods to reduce these variations were proposed and the extra care was taken in the interpretation of the results.

In **Chapter 6** a new digestion system was developed. Bags instead of a solid chamber was used due to its flexibility and disposability. To achieve mechanical agitation, spiked plates were designed and assembled into a Y-shape to hold the pancreas. Consequently, the bag needs to have a wide opening allowing the assembling of internal designs as well as connections to a perfusion system. Difficulties were encountered in the bag-making process and therefore a commercially available bladder bag was used. This limits the layout of internal structures and may affect the isolation efficiency.

Juvenile pig pancreases were used for the proof-of-principle experiments. Compared to the human pancreas, porcine islets are much more fragile, and the dissociation of a pig pancreas is relatively rapid. Their islets were also smaller compared to human islets. Consequently, the digestion process may differ from clinical isolation and this was considered in results interpretation.

Despite the above-mentioned limitations, methods and tools designed in this thesis could be applied in many other studies. Although complicated and time-consuming, 3D imaging of an intact islet enabled detailed studies at the islet-exocrine interface. Compared to image sets obtained from serial thin sections, the integrity and continuity of structural features are perfectly preserved. This allows studies on the interaction between islet and surrounding ECM, which could provide valuable information not only for islet isolation but also for 3D islet culture. Unlike conventional 2D cell culture system, where cells are grown in a flat layer, 3D cell culture involves scaffolds to support cell adhesion and growth and could mimic *in vivo* histoarchitecture

more closely [227]. The scaffolds are engineered to provide high surface area or coated with specific cues which promote cell growth and differentiation. Moreover, its porous structure allows easy access to nutrients for cells at centre [228]. In fact, 3D culture of islets has been conducted, where isolated islets are attached to scaffolds made of various materials such as polyactic-co-glycolic acid (PLGA) [229], [230], poly-L-lactide acid (PLA) [231], chitosan [232], collagen [231], [233], hyaluronic acid [234] and decellularized mouse pancreas [235]. It was found that islets after 3D culture functioned generally more efficiently than those cultured in a 2D system [227]. A better understanding of the 3D structure of peri-islet ECM and its interaction with islets will form a firm foundation for scaffolds design.

Using the 15μm-thick samples, a large image set of various pancreatic ECM proteins from donors of different age and BMI were obtained in **Chapter 3**. Here, as the research interest for this thesis was placed on properties related to digestion phase, only the presence and abundance of ECM proteins at the ECM-islet interface was analysed. This is only the first step to understand donor-related variations in isolation outcomes. The information-rich image set obtained in this thesis could also be used for the study of other ECM properties such as variations of protein porosity among different donor groups. Detailed mechanisms, such as interactions of these proteins and their deformations along with ageing and fat accumulation are also important and could be studied in a similar manner.

In **Chapter 4** and **5**, to achieve real-time observation, the ECM proteins were firstly antibody-labelled. It was found that the digestions of collagen IV and collagen

VI were not interfered by this labelling technique. However, the results for perlecan and laminin were significantly different from the control group. Part of the reason was attributed to the block or shield of enzyme-protein binding sites by antibody labelling. As a result, only the digestion of collagen IV and collagen VI were conducted for further perfusion experiments. For further analyses for perlecan and laminin, a change and selection of antibodies is recommended.

To improve the understanding on the digestion process and donor-related variations, it is recommended that a thorough analyses of other common pancreatic ECM proteins and effects of other donor characteristics to be carried out. Due to its small volume, the system provides a cost-effective approach for such analyses. Similarly, the performance of other enzymes and even lot-to-lot variations could also be directly compared with this system.

In **Chapter 6**, the performance of the new system was compared with the Ricordi chamber with a focus on islet yield and purity. The next step is to test the performance of this bioreactor using human pancreases rejected from clinical transplantation with appropriate ethical approval. This includes a comparison of isolation time, yield, purity, viability and islet functionality between the bioreactor and the Ricordi chamber using clinical standards.

7.3 Summary

The research presented in this thesis focused on development of techniques and engineering tools to promote research on the improvement of isolation yield for specific

donor groups. This task was approached from 3D imaging of the peri-islet ECM with a focus on donor-related variables, real-time observation of the dynamic digestion process and development of a bioreactor for prolonged digestions. Challenges were encountered during the development of these techniques but were overcome by specific modifications and careful adjustment. Future work could aim to investigate the islet-ECM interface and its digestion process using the presented approaches. With potential for clinical and research use, the performance of designed devices on digestion of human pancreases is also interesting and might be examined in the future.

Reference

[1] P. In't Veld and M. Marichal, "Microscopic anatomy of the human islet of Langerhans.," *Adv. Exp. Med. Biol.*, vol. 654, pp. 1–19, Jan. 2010.

[2] D. Zipris, "Toll-like receptors and type 1 diabetes.," *Adv. Exp. Med. Biol.*, vol. 654, pp. 585–610, Jan. 2010.

[3] American Diabetes Association, "Standards of Medical Care in Diabetes--2014," *Diabetes Care*, vol. 37, no. Supplement_1, pp. S14–S80, Jan. 2014.

[4] A. N. Dixon, E. B. Jude, A. K. Banerjee, and S. C. Bain, "Simultaneous pulmonary and cerebral oedema, and multiple CNS infarctions as complications of diabetic ketoacidosis: a case report," *Diabet. Med.*, vol. 23, no. 5, pp. 571–573, May 2006.

[5] R. Tattersall, R. Gregory, C. Selby, D. Kerr, and S. Heller, "Course of brittle diabetes: 12 year follow up.," *BMJ*, vol. 302, no. 6787, pp. 1240–3, May 1991.

[6] N. T. Christina Voulgari, "Brittle Diabetes: A Contemporary Review of the Myth and Its Realization," in *Diabetes - Damages and Treatments*, E. Rigobelo, Ed. InTech, 2011.

[7] G. P. Forlenza *et al.*, "Fully Closed-Loop Multiple Model Probabilistic Predictive Controller Artificial Pancreas Performance in Adolescents and Adults in a Supervised Hotel Setting," *Diabetes Technol. Ther.*, vol. 20, no. 5, pp. 335–343, May 2018.

[8] F. B. Barton *et al.*, "Improvement in outcomes of clinical islet transplantation: 1999-2010.," *Diabetes Care*, vol. 35, no. 7, pp. 1436–45, Jul. 2012.

[9] A. C. Gruessner, "2011 Update on Pancreas Transplantation: Comprehensive Trend Analysis of 25,000 Cases Followed Up Over the Course of Twenty-Four Years at the International Pancreas Transplant Registry (IPTR)," *Rev. Diabet. Stud.*, vol. 8, no. 1, pp. 6–16, 2011.

[10] Collaborative Islet Transplant Registry, "2010 CIRT Annual Report," 2011.

[11] A. N. Balamurugan *et al.*, "Islet Isolation from Pancreatitis Pancreas for Islet Autotransplantation," in *Islets of Langerhans*, Dordrecht: Springer Netherlands, 2015, pp. 1199–1227.

[12] R. C. McCarthy, A. G. Breite, M. L. Green, and F. E. Dwulet, "Tissue dissociation enzymes for isolating human islets for transplantation: factors to consider in setting enzyme acceptance criteria.," *Transplantation*, vol. 91, no. 2, pp. 137–45, Jan. 2011.

[13] R. M. Spiers *et al.*, "Development of a Simple *In Vitro* Assay to Assess Digestion of the Extracellular Matrix of the Human Pancreas by Collagenase Enzyme Blends," *Cell Transplant.*, p. 096368971877977, Jun. 2018.

[14] C. Ricordi, "Lilly Lecture 2002: Islet Transplantation: A Brave New World," *Diabetes*, vol. 52, no. 7, pp. 1595–1603, Jul. 2003.

[15] D. W. R. Gray, N. Sudhakaran, T. T. Titus, P. McShane, and P. Johnson, "Development of a novel digestion chamber for human and porcine islet

isolation.," *Transplant. Proc.*, vol. 36, no. 4, pp. 1135–8, May 2004.

[16] S. J. Hughes, P. McShane, H. H. Contractor, D. W. R. Gray, A. Clark, and P. R. V Johnson, "Comparison of the collagen VI content within the islet-exocrine interface of the head, body, and tail regions of the human pancreas.," *Transplant. Proc.*, vol. 37, no. 8, pp. 3444–5, Oct. 2005.

[17] W. Gepts, "Pathologic anatomy of the pancreas in juvenile diabetes mellitus.," *Diabetes*, vol. 14, no. 10, pp. 619–33, Oct. 1965.

[18] P. Newsholme, C. Gaudel, and N. H. McClenaghan, "Nutrient regulation of insulin secretion and beta-cell functional integrity.," *Adv. Exp. Med. Biol.*, vol. 654, pp. 91–114, Jan. 2010.

[19] P. Marchetti, R. Lupi, S. Del Guerra, M. Bugliani, L. Marselli, and U. Boggi, "The beta-cell in human type 2 diabetes.," *Adv. Exp. Med. Biol.*, vol. 654, pp. 501–14, Jan. 2010.

[20] W. Gepts and P. Lecompte, "The pancreatic islets in diabetes," *Am. J. Med.*, vol. 70, no. January, pp. 105–115, 1981.

[21] D. Voet and J. G. Voet, *Biochemistry*. John Wiley & Sons, 2011.

[22] K. G. M. M. Alberti and P. Z. Zimmet, "Definition, diagnosis and classification of diabetes mellitus and its complications. Part 1: diagnosis and classification of diabetes mellitus. Provisional report of a WHO Consultation," *Diabet. Med.*, vol. 15, no. 7, pp. 539–553, Jul. 1998.

[23] E. Selvin *et al.*, "Meta-Analysis: Glycosylated Hemoglobin and Cardiovascular Disease in Diabetes Mellitus," *Ann. Intern. Med.*, vol. 141, no. 6, p. 421, Sep. 2004.

[24] H. C. Gerstein *et al.*, "The relationship between dysglycaemia and cardiovascular and renal risk in diabetic and non-diabetic participants in the HOPE study: a prospective epidemiological analysis," *Diabetologia*, vol. 48, no. 9, pp. 1749–1755, Sep. 2005.

[25] World Health Organization and International Diabetes Federation, "Definition and diagnosis of diabetes mellitus and intermediate hyperglycaemia : report of a WHO/IDF consultation," 2006.

[26] R. Alejandro, F. B. Barton, B. J. Hering, S. Wease, and Collaborative Islet Transplant Registry Investigators, "2008 Update From the Collaborative Islet Transplant Registry," *Transplantation*, vol. 86, no. 12, pp. 1783–1788, Dec. 2008.

[27] World Health Organization and International Diabetes Federation, "Use of glycated haemoglobin (HbA1c) in the diagnosis of diabetes mellitus Abbreviated report of a WHO consultation," World Health Organization, 2011.

[28] D. Daneman, "State of the world's children with diabetes," *Pediatr. Diabetes*, vol. 10, no. 2, pp. 120–126, Mar. 2009.

[29] B. O. Roep, "The role of T-cells in the pathogenesis of Type 1 diabetes: From

cause to cure," *Diabetologia*, vol. 46, no. 3, pp. 305–321, Mar. 2003.

[30] H. Kolb and R. B. Elliott, "Increasing incidence of IDDM a consequence of improved hygiene?," *Diabetologia*, vol. 37, no. 7, p. 729, Jul. 1994.

[31] Y. Shi and F. B. Hu, "The global implications of diabetes and cancer.," *Lancet*, vol. 383, no. 9933, pp. 1947–8, Jun. 2014.

[32] DiABETES UK, "Diabetes: facts and stats October 2016," 2016.

[33] International Diabetes Federation, "IDF Diabetes Atlas," International Diabetes Federation, Brussels, 2013.

[34] B. D. Association, "Diabetes in the UK," London, United Kingdom, 1996.

[35] N. Hex, C. Bartlett, D. Wright, M. Taylor, and D. Varley, "Estimating the current and future costs of Type 1 and Type 2 diabetes in the UK, including direct health costs and indirect societal and productivity costs," *Diabet. Med.*, vol. 29, no. 7, pp. 855–862, Jul. 2012.

[36] JDRF, "Facts and figures about type 1 diabetes," 2018. [Online]. Available: https://jdrf.org.uk/information-support/about-type-1-diabetes/facts-and-figures/. [Accessed: 30-Aug-2019].

[37] NHS, "Diabetes: cases and costs predicted to rise," 2012. [Online]. Available: https://www.nhs.uk/news/diabetes/diabetes-cases-and-costs-predicted-to-rise/. [Accessed: 30-Aug-2019].

[38] M. Boland, M. Golding, H. Singh, and D. and H. (Conference) (1st : 2012 P. N. Food Structures, *Food structures, digestion and health*. .

[39] M. Riddell and B. A. Perkins, "Exercise and glucose metabolism in persons with diabetes mellitus: perspectives on the role for continuous glucose monitoring.," *J. Diabetes Sci. Technol.*, vol. 3, no. 4, pp. 914–23, Jul. 2009.

[40] O. P. Adams, "The impact of brief high-intensity exercise on blood glucose levels.," *Diabetes. Metab. Syndr. Obes.*, vol. 6, pp. 113–22, 2013.

[41] Diabetes Control and Complications Trial Research Group *et al.*, "The Effect of Intensive Treatment of Diabetes on the Development and Progression of Long-Term Complications in Insulin-Dependent Diabetes Mellitus," *N. Engl. J. Med.*, vol. 329, no. 14, pp. 977–986, Sep. 1993.

[42] D. M. Nathan *et al.*, "Intensive Diabetes Treatment and Cardiovascular Disease in Patients with Type 1 Diabetes," *N. Engl. J. Med.*, vol. 353, no. 25, pp. 2643–2653, Dec. 2005.

[43] T. D. C. and C. T. of D. I. and C. R. Diabetes Control and Complications Trial/Epidemiology of Diabetes Interventions and Complications Research Group, J. M. Lachin, S. Genuth, P. Cleary, M. D. Davis, and D. M. Nathan, "Retinopathy and nephropathy in patients with type 1 diabetes four years after a trial of intensive therapy.," *N. Engl. J. Med.*, vol. 342, no. 6, pp. 381–9, 2000.

[44] P. R. V Johnson and K. E. Jones, "Pancreatic islet transplantation.," *Semin.*

Pediatr. Surg., vol. 21, no. 3, pp. 272–80, Aug. 2012.

[45] P. Cravedi, I. M. van der Meer, S. Cattaneo, P. Ruggenenti, and G. Remuzzi, "Successes and Disappointments with Clinical Islet Transplantation," in *Advances in experimental medicine and biology*, vol. 654, 2010, pp. 749–769.

[46] A. L. McCall, "Insulin therapy and hypoglycemia.," *Endocrinol. Metab. Clin. North Am.*, vol. 41, no. 1, pp. 57–87, Mar. 2012.

[47] P. E. Cryer *et al.*, "Evaluation and Management of Adult Hypoglycemic Disorders: An Endocrine Society Clinical Practice Guideline," *J. Clin. Endocrinol. Metab.*, vol. 94, no. 3, pp. 709–728, Mar. 2009.

[48] P. E. Cryer, "Diverse Causes of Hypoglycemia-Associated Autonomic Failure in Diabetes," *N. Engl. J. Med.*, vol. 350, no. 22, pp. 2272–2279, May 2004.

[49] P. E. Cryer, "The barrier of hypoglycemia in diabetes.," *Diabetes*, vol. 57, no. 12, pp. 3169–76, Dec. 2008.

[50] G. Shafiee, M. Mohajeri-Tehrani, M. Pajouhi, and B. Larijani, "The importance of hypoglycemia in diabetic patients.," *J. Diabetes Metab. Disord.*, vol. 11, no. 1, p. 17, Oct. 2012.

[51] M. S. Ho *et al.*, "Prevalence of Structural Central Nervous System Abnormalities in Early-Onset Type 1 Diabetes Mellitus," *J. Pediatr.*, vol. 153, no. 3, pp. 385–390, Sep. 2008.

[52] F. M. Cameron *et al.*, "Closed-Loop Control Without Meal Announcement in Type 1 Diabetes," *Diabetes Technol. Ther.*, p. dia.2017.0078, Aug. 2017.

[53] M.-C. Vantyghem *et al.*, "Intraperitoneal Insulin Infusion Versus Islet Transplantation: Comparative Study in Patients with Type 1 Diabetes," *Transplantation*, vol. 87, no. 1, pp. 66–71, Jan. 2009.

[54] J. J. Meier *et al.*, "Beta-Cell Replication Is the Primary Mechanism Subserving the Postnatal Expansion of -Cell Mass in Humans," *Diabetes*, vol. 57, no. 6, pp. 1584–1594, Jun. 2008.

[55] A. Rojas, A. Khoo, J. R. Tejedo, F. J. Bedoya, B. Soria, and F. Martín, "Islet cell development.," *Adv. Exp. Med. Biol.*, vol. 654, pp. 59–75, Jan. 2010.

[56] E. Lammert, O. Cleaver, and D. Melton, "Induction of pancreatic differentiation by signals from blood vessels.," *Science*, vol. 294, no. 5542, pp. 564–7, Oct. 2001.

[57] J. M. Slack, "Developmental biology of the pancreas.," *Development*, vol. 121, no. 6, pp. 1569–80, Jun. 1995.

[58] K. A. Y. J. Gordon Betts, Peter Desaix, Jody E. Johnson, Oksana Korol, Dean Kruse, Brandon Poe, James Wise, Mark D. Womble, "The Endocrine System," in *Anatomy and Physiology*, 12th Media Services, 2016.

[59] P. H. Smith, "Structural modification of Schwann cells in the pancreatic islets of the dog.," *Am. J. Anat.*, vol. 144, no. 4, pp. 513–7, Dec. 1975.

[60] M. Feldman, L. S. Friedman, and L. J. Brandt, *Sleisenger and Fordtran's Gastrointestinal and Liver Disease: Pathophysiology, Diagnosis, Management, Expert Consult Premium Edition - Enhanced Online Features, Volume 1*. Elsevier Health Sciences, 2010.

[61] X. Wang *et al.*, "Regional differences in islet distribution in the human pancreas--preferential beta-cell loss in the head region in patients with type 2 diabetes.," *PLoS One*, vol. 8, no. 6, p. e67454, 2013.

[62] H. R. Kimmel JR, Pollock HG, "A new pancreatic polypeptide," *Fed Proc*, vol. 30, p. 1318, 1971.

[63] W. Bloom, "A new type of granular cell in the islets of Langerhans of man," *Anat. Rec.*, vol. 49, no. 4, pp. 363–371, Jun. 1931.

[64] M. A. Lane, "The cytological characters of the areas of langerhans," *Am. J. Anat.*, vol. 7, no. 3, pp. 409–422, Nov. 1907.

[65] N. Wierup, H. Svensson, H. Mulder, and F. Sundler, "The ghrelin cell: a novel developmentally regulated islet cell in the human pancreas.," *Regul. Pept.*, vol. 107, no. 1–3, pp. 63–9, Jul. 2002.

[66] D. Kawamori, H. J. Welters, and R. N. Kulkarni, "Molecular pathways underlying the pathogenesis of pancreatic alpha-cell dysfunction.," *Adv. Exp. Med. Biol.*, vol. 654, pp. 421–45, Jan. 2010.

[67] J. Koska, A. DelParigi, B. de Courten, C. Weyer, and P. A. Tataranni, "Pancreatic polypeptide is involved in the regulation of body weight in pima Indian male subjects.," *Diabetes*, vol. 53, no. 12, pp. 3091–6, Dec. 2004.

[68] M. Z. Strowski, R. M. Parmar, A. D. Blake, and J. M. Schaeffer, "Somatostatin Inhibits Insulin and Glucagon Secretion via Two Receptor Subtypes: An *in Vitro* Study of Pancreatic Islets from Somatostatin Receptor 2 Knockout Mice [1]," *Endocrinology*, vol. 141, no. 1, pp. 111–117, Jan. 2000.

[69] M. R. DiGruccio *et al.*, "Comprehensive alpha, beta and delta cell transcriptomes reveal that ghrelin selectively activates delta cells and promotes somatostatin release from pancreatic islets," *Mol. Metab.*, vol. 5, no. 7, pp. 449–458, Jul. 2016.

[70] A. Rabiee, P. Galiatsatos, R. Salas-Carrillo, M. J. Thompson, D. K. Andersen, and D. Elahi, "Pancreatic polypeptide administration enhances insulin sensitivity and reduces the insulin requirement of patients on insulin pump therapy.," *J. Diabetes Sci. Technol.*, vol. 5, no. 6, pp. 1521–8, Nov. 2011.

[71] L. Orci and R. Unger, "Functional Subdivision of Islets of Langerhans and Possible Roles of D cells," *Lancet*, vol. 306, no. 7947, pp. 1243–1244, Dec. 1975.

[72] D. Bosco *et al.*, "Unique arrangement of alpha- and beta-cells in human islets of Langerhans.," *Diabetes*, vol. 59, no. 5, pp. 1202–10, May 2010.

[73] O. Cabrera, D. M. Berman, N. S. Kenyon, C. Ricordi, P.-O. Berggren, and A.

Caicedo, “The unique cytoarchitecture of human pancreatic islets has implications for islet cell function.,” *Proc. Natl. Acad. Sci. U. S. A.*, vol. 103, no. 7, pp. 2334–9, Feb. 2006.

[74] A. Kim, K. Miller, J. Jo, G. Kilimnik, P. Wojcik, and M. Hara, “Islet architecture: A comparative study.,” *Islets*, vol. 1, no. 2, pp. 129–36, 2009.

[75] R. S. Heller, “The Comparative Anatomy of Islets,” in *Advances in experimental medicine and biology*, vol. 654, 2010, pp. 21–37.

[76] R. O. Hynes, “The extracellular matrix: not just pretty fibrils.,” *Science*, vol. 326, no. 5957, pp. 1216–9, Nov. 2009.

[77] J. K. Mouw, G. Ou, and V. M. Weaver, “Extracellular matrix assembly: a multiscale deconstruction.,” *Nat. Rev. Mol. Cell Biol.*, vol. 15, no. 12, pp. 771–785, Nov. 2014.

[78] R. Malik, P. I. Lelkes, and E. Cukierman, “Biomechanical and biochemical remodeling of stromal extracellular matrix in cancer.,” *Trends Biotechnol.*, vol. 33, no. 4, pp. 230–6, Apr. 2015.

[79] J. C. Stendahl, D. B. Kaufman, and S. I. Stupp, “Extracellular matrix in pancreatic islets: relevance to scaffold design and transplantation.,” *Cell Transplant.*, vol. 18, no. 1, pp. 1–12, Jan. 2009.

[80] S. J. Hughes, A. Clark, P. McShane, H. H. Contractor, D. W. R. Gray, and P. R. V Johnson, “Characterisation of collagen VI within the islet-exocrine interface of the human pancreas: implications for clinical islet isolation?,” *Transplantation*, vol. 81, no. 3, pp. 423–6, Feb. 2006.

[81] P. N. Venkatasubramanian, “Imaging the pancreatic ECM.” Transworld Research Network, 2012.

[82] M. K. Gordon and R. A. Hahn, “Collagens.,” *Cell Tissue Res.*, vol. 339, no. 1, pp. 247–57, Jan. 2010.

[83] M. D. Shoulders and R. T. Raines, “Collagen structure and stability.,” *Annu. Rev. Biochem.*, vol. 78, pp. 929–58, 2009.

[84] P. Szpak, “Fish bone chemistry and ultrastructure: implications for taphonomy and stable isotope analysis,” *J. Archaeol. Sci.*, vol. 38, no. 12, pp. 3358–3372, Dec. 2011.

[85] S. Ricard-Blum, “The collagen family.,” *Cold Spring Harb. Perspect. Biol.*, vol. 3, no. 1, p. a004978, Jan. 2011.

[86] K. Gelse, E. Pöschl, and T. Aigner, “Collagens--structure, function, and biosynthesis.,” *Adv. Drug Deliv. Rev.*, vol. 55, no. 12, pp. 1531–46, Nov. 2003.

[87] Jens Friedrichs, “Analyzing Interactions Between Cells And Extracellular Matrix By Atomic Force Microscopy,” Dresden University of Technology, 1980.

[88] S. P. McAdoo and C. D. Pusey, “Anti-Glomerular Basement Membrane

Disease.," *Clin. J. Am. Soc. Nephrol.*, vol. 12, no. 7, pp. 1162–1172, Jul. 2017.

[89] M. Kragl and E. Lammert, "Basement membrane in pancreatic islet function.," *Adv. Exp. Med. Biol.*, vol. 654, pp. 217–34, Jan. 2010.

[90] P. Laurila and I. Leivo, "Basement membrane and interstitial matrix components form separate matrices in heterokaryons of PYS-2 cells and fibroblasts.," *J. Cell Sci.*, vol. 104 (Pt 1), pp. 59–68, Jan. 1993.

[91] J. Y. C. Cheng, M. Raghunath, J. Whitelock, and L. Poole-Warren, "Matrix components and scaffolds for sustained islet function.," *Tissue Eng. Part B. Rev.*, vol. 17, no. 4, pp. 235–47, Aug. 2011.

[92] Y.-S. Cheng, M.-F. Champliaud, R. E. Burgeson, M. P. Marinkovich, and P. D. Yurchenco, "Self-assembly of Laminin Isoforms," *J. Biol. Chem.*, vol. 272, no. 50, pp. 31525–31532, Dec. 1997.

[93] K. Beck, I. Hunter, and J. Engel, "Structure and function of laminin: anatomy of a multidomain glycoprotein.," *FASEB J.*, vol. 4, no. 2, pp. 148–160, Feb. 1990.

[94] N. Turck *et al.*, "Laminin isoforms: biological roles and effects on the intracellular distribution of nuclear proteins in intestinal epithelial cells," *Exp. Cell Res.*, vol. 303, no. 2, pp. 494–503, Feb. 2005.

[95] T. Otonkoski, M. Banerjee, O. Korsgren, L.-E. Thornell, and I. Virtanen, "Unique basement membrane structure of human pancreatic islets: implications for beta-cell growth and differentiation.," *Diabetes. Obes. Metab.*, vol. 10 Suppl 4, pp. 119–27, Nov. 2008.

[96] I. Virtanen *et al.*, "Blood vessels of human islets of Langerhans are surrounded by a double basement membrane.," *Diabetologia*, vol. 51, no. 7, pp. 1181–91, Jul. 2008.

[97] G. Nikolova *et al.*, "The Vascular Basement Membrane: A Niche for Insulin Gene Expression and β Cell Proliferation," *Dev. Cell*, vol. 10, no. 3, pp. 397–405, Mar. 2006.

[98] K. Sigmundsson *et al.*, "Culturing functional pancreatic islets on α5-laminins and curative transplantation to diabetic mice," *Matrix Biol.*, vol. 70, pp. 5–19, Sep. 2018.

[99] Georgia Purdom, "Laminin and the Cross Is There a Connection?," *Answers in genesis*, Oct-2008. [Online]. Available: http://www.fasebj.org/doi/10.1096/fasebj.4.2.2404817. [Accessed: 08-Mar-2019].

[100] E. Hohenester and P. D. Yurchenco, "Laminins in basement membrane assembly," *Cell Adh. Migr.*, vol. 7, no. 1, pp. 56–63, Jan. 2013.

[101] A. N. Balamurugan *et al.*, "Suitability of human juvenile pancreatic islets for clinical use.," *Diabetologia*, vol. 49, no. 8, pp. 1845–54, Aug. 2006.

[102] S. E. Cross *et al.*, "Key Matrix Proteins Within the Pancreatic Islet Basement

Membrane Are Differentially Digested During Human Islet Isolation," *Am. J. Transplant.*, vol. 17, no. 2, pp. 451–461, Feb. 2017.

[103] W. D. Kelly, R. C. Lillehei, F. K. Merkel, Y. Idezuki, and F. C. Goetz, "Allotransplantation of the pancreas and duodenum along with the kidney in diabetic nephropathy.," *Surgery*, vol. 61, no. 6, pp. 827–37, Jun. 1967.

[104] D. Tedesco and L. Haragsim, "Cyclosporine: a review.," *J. Transplant.*, vol. 2012, p. 230386, 2012.

[105] J.-P. Squifflet, R. W. G. Gruessner, and D. E. R. Sutherland, "The history of pancreas transplantation: past, present and future.," *Acta Chir. Belg.*, vol. 108, no. 3, pp. 367–78, 2008.

[106] A. C. Gruessner and R. W. G. Gruessner, "Long-term outcome after pancreas transplantation," *Curr. Opin. Organ Transplant.*, vol. 21, no. 4, pp. 377–385, Aug. 2016.

[107] W. Steurer, J. Malaise, W. Mark, A. Koenigsrainer, and R. Margreiter, "Spectrum of surgical complications after simultaneous pancreas–kidney transplantation in a prospectively randomized study of two immunosuppressive protocols," *Nephrol. Dial. Transplant.*, vol. 20, no. suppl_2, pp. ii54–ii61, May 2005.

[108] M. Page *et al.*, "Early Relaparotomy After Simultaneous Pancreas-Kidney Transplantation," *Transplant. J.*, vol. 94, no. 2, pp. 159–164, Jul. 2012.

[109] A. Manrique *et al.*, "Relaparotomy After Pancreas Transplantation: Causes and Outcomes," *Transplant. Proc.*, vol. 41, no. 6, pp. 2472–2474, Jul. 2009.

[110] R. W. G. Gruessner, D. E. R. Sutherland, and A. C. Gruessner, "Mortality Assessment for Pancreas Transplants," *Am. J. Transplant.*, vol. 4, no. 12, pp. 2018–2026, Dec. 2004.

[111] L. W. Ssobolew, "Zur normalen und pathologischen Morphologie der inneren Secretion der Bauchspeicheldrüse," *Arch. für Pathol. Anat. und Physiol. und für Klin. Med.*, vol. 168, no. 1, pp. 91–128, May 1902.

[112] P. E. Lacy and M. Kostianovsky, "Method for the isolation of intact islets of Langerhans from the rat pancreas.," *Diabetes*, vol. 16, no. 1, pp. 35–9, Jan. 1967.

[113] J. S. Najarian, D. E. Sutherland, A. J. Matas, M. W. Steffes, R. L. Simmons, and F. C. Goetz, "Human islet transplantation: a preliminary report.," *Transplant. Proc.*, vol. 9, no. 1, pp. 233–6, Mar. 1977.

[114] D. E. R. Sutherland, "Pancreas and Islet Transplantation* II. Clinical Trials," 1981.

[115] D. E. Sutherland, "Report of International Human Pancreas and Islet Transplantation Registry Cases through 1981.," *Diabetes*, vol. 31 Suppl 4, pp. 112–6, Aug. 1982.

[116] A. M. Shapiro *et al.*, "Islet transplantation in seven patients with type 1

diabetes mellitus using a glucocorticoid-free immunosuppressive regimen.," *N. Engl. J. Med.*, vol. 343, no. 4, pp. 230–8, Jul. 2000.

[117] Y. Iwanaga, D. E. Sutherland, J. V Harmon, and K. K. Papas, "Pancreas preservation for pancreas and islet transplantation," *Curr. Opin. Organ Transplant.*, vol. 13, no. 4, pp. 445–451, Aug. 2008.

[118] G. L. Warnock, D. Ellis, R. V. Rajotte, I. Dawidson, S. Baekkeskov, and J. Egebjerg, "Studies of the isolation and viability of human islets of langerhans," *Transplantation*, vol. 45, no. 5, pp. 957–963, May 1988.

[119] J. R. T. Lakey *et al.*, "Intraductal Collagenase Delivery into the Human Pancreas Using Syringe Loading or Controlled Perfusion," *Cell Transplant.*, vol. 8, no. 3, pp. 285–292, May 1999.

[120] C. Ricordi, P. E. Lacy, E. H. Finke, B. J. Olack, and D. W. Scharp, "Automated method for isolation of human pancreatic islets.," *Diabetes*, vol. 37, no. 4, pp. 413–20, Apr. 1988.

[121] A. M. J. Shapiro *et al.*, "International Trial of the Edmonton Protocol for Islet Transplantation," *N. Engl. J. Med.*, vol. 355, no. 13, pp. 1318–1330, Sep. 2006.

[122] M. McCall and A. M. J. Shapiro, "Update on islet transplantation.," *Cold Spring Harb. Perspect. Med.*, vol. 2, no. 7, p. a007823, Jul. 2012.

[123] H. Noguchi *et al.*, "Islet Culture/Preservation Before Islet Transplantation.," *Cell Med.*, vol. 8, no. 1–2, pp. 25–9, Dec. 2015.

[124] T. Yamamoto *et al.*, "Quality control for clinical islet transplantation: organ procurement and preservation, the islet processing facility, isolation, and potency tests," *J. Hepatobiliary. Pancreat. Surg.*, vol. 16, no. 2, pp. 131–136, Mar. 2009.

[125] N. J. London, H. Contractor, S. P. Lake, G. C. Aucott, P. R. Bell, and R. F. James, "A microfluorometric viability assay for isolated human and rat islets of Langerhans.," *Diabetes Res.*, vol. 12, no. 3, pp. 141–9, Nov. 1989.

[126] A. Gamble, A. R. Pepper, A. Bruni, and A. M. J. Shapiro, "The journey of islet cell transplantation and future development," *Islets*, vol. 10, no. 2, pp. 80–94, Mar. 2018.

[127] Collaborative Islet Transplant Registry, "2017 CIRT Annual Report," 2017.

[128] D. van Dellen *et al.*, "Mortality in diabetes: pancreas transplantation is associated with significant survival benefit," *Nephrol. Dial. Transplant.*, vol. 28, no. 5, pp. 1315–1322, May 2013.

[129] T. Nir, D. A. Melton, and Y. Dor, "Recovery from diabetes in mice by β cell regeneration," *J. Clin. Invest.*, vol. 117, no. 9, pp. 2553–2561, Sep. 2007.

[130] T. Berney and A. Secchi, "Rapamycin in islet transplantation: friend or foe?," *Transpl. Int.*, vol. 22, no. 2, pp. 153–161, Feb. 2009.

[131] P. F. Halloran, "Immunosuppressive Drugs for Kidney Transplantation," *N.*

Engl. J. Med., vol. 351, no. 26, pp. 2715–2729, Dec. 2004.

[132] D. E. R. Sutherland *et al.*, "Islet Autotransplant Outcomes After Total Pancreatectomy: A Contrast to Islet Allograft Outcomes," *Transplantation*, vol. 86, no. 12, pp. 1799–1802, Dec. 2008.

[133] A. R. Pepper, B. Gala-Lopez, and T. Kin, "Advances in Clinical Islet Isolation," in *Islets of Langerhans*, Dordrecht: Springer Netherlands, 2015, pp. 1165–1197.

[134] W. Bennet, C.-G. Groth, R. Larsson, B. Nilsson, and O. Korsgren, "Isolated Human Islets Trigger an Instant Blood Mediated Inflammatory Reaction: Implications for Intraportal Islet Transplantation as a Treatment for Patients with Type 1 Diabetes," *Ups. J. Med. Sci.*, vol. 105, no. 2, pp. 125–133, Jan. 2000.

[135] "ANNUAL REPORT ON PANCREAS AND ISLET TRANSPLANTATION PRODUCED IN COLLABORATION WITH NHS ENGLAND Contents," 2015.

[136] A. Andres *et al.*, "Clinical islet isolation and transplantation outcomes with deceased cardiac death donors are similar to neurological determination of death donors," *Transpl. Int.*, vol. 29, no. 1, pp. 34–40, Jan. 2016.

[137] D. Dufrane and P. Gianello, "Pig islet for xenotransplantation in human: structural and physiological compatibility for human clinical application," *Transplant. Rev.*, vol. 26, no. 3, pp. 183–188, Jul. 2012.

[138] R. B. Elliott, L. Escobar, P. L. J. Tan, M. Muzina, S. Zwain, and C. Buchanan, "Live encapsulated porcine islets from a type 1 diabetic patient 9.5 yr after xenotransplantation," *Xenotransplantation*, vol. 14, no. 2, pp. 157–161, Mar. 2007.

[139] R. A. Valdés-González *et al.*, "Xenotransplantation of porcine neonatal islets of Langerhans and Sertoli cells: a 4-year study," *Eur. J. Endocrinol.*, vol. 153, no. 3, pp. 419–427, Sep. 2005.

[140] O. Garkavenko *et al.*, "The first clinical xenotransplantation trial in New Zealand: Efficacy and safety," *Xenotransplantation*, vol. 19, no. 1, pp. 6–7, Jan. 2012.

[141] S. Wynyard, D. Nathu, O. Garkavenko, J. Denner, and R. Elliott, "Microbiological safety of the first clinical pig islet xenotransplantation trial in New Zealand," *Xenotransplantation*, vol. 21, no. 4, pp. 309–323, Jul. 2014.

[142] B. F. Salama and G. S. Korbutt, "Porcine Islet Xenografts: a Clinical Source of ß-Cell Grafts," *Curr. Diab. Rep.*, vol. 17, no. 3, p. 14, Mar. 2017.

[143] H. Ungefroren and F. Fändrich, "The programmable cell of monocytic origin (PCMO): a potential adult stem/progenitor cell source for the generation of islet cells.," *Adv. Exp. Med. Biol.*, vol. 654, pp. 667–82, Jan. 2010.

[144] A. A. Tomei, C. Villa, and C. Ricordi, "Development of an encapsulated stem

cell-based therapy for diabetes.," *Expert Opin. Biol. Ther.*, pp. 1–16, Jul. 2015.

[145] Y.-J. Chen *et al.*, "De novo formation of insulin-producing 'neo-β cell islets' from intestinal crypts.," *Cell Rep.*, vol. 6, no. 6, pp. 1046–58, Mar. 2014.

[146] K. L. Sinagoga and J. M. Wells, "Generating human intestinal tissues from pluripotent stem cells to study development and disease.," *EMBO J.*, vol. 34, no. 9, pp. 1149–1163, Mar. 2015.

[147] C. Talchai, S. Xuan, T. Kitamura, R. A. DePinho, and D. Accili, "Generation of functional insulin-producing cells in the gut by Foxo1 ablation.," *Nat. Genet.*, vol. 44, no. 4, pp. 406–12, S1, Apr. 2012.

[148] H. A. Russ *et al.*, "Controlled induction of human pancreatic progenitors produces functional beta-like cells in vitro.," *EMBO J.*, vol. 34, no. 13, pp. 1759–72, Apr. 2015.

[149] H. Okura *et al.*, "Transdifferentiation of human adipose tissue-derived stromal cells into insulin-producing clusters," *J. Artif. Organs*, vol. 12, no. 2, pp. 123–130, Jun. 2009.

[150] J. B. Sneddon *et al.*, "Stem Cell Therapies for Treating Diabetes: Progress and Remaining Challenges.," *Cell Stem Cell*, vol. 22, no. 6, pp. 810–823, Jun. 2018.

[151] A. Veres *et al.*, "Charting cellular identity during human in vitro β-cell differentiation," *Nature*, vol. 569, no. 7756, pp. 368–373, May 2019.

[152] D. Balboa, J. Saarimäki-Vire, and T. Otonkoski, "Concise Review: Human Pluripotent Stem Cells for the Modeling of Pancreatic β-Cell Pathology," *Stem Cells*, vol. 37, no. 1, pp. 33–41, Jan. 2019.

[153] M. Goto *et al.*, "Refinement of the automated method for human islet isolation and presentation of a closed system for in vitro islet culture.," *Transplantation*, vol. 78, no. 9, pp. 1367–75, Nov. 2004.

[154] D. O'Gorman *et al.*, "The standardization of pancreatic donors for islet isolation.," *Transplant. Proc.*, vol. 37, no. 2, pp. 1309–10, Mar. 2005.

[155] T. Kin, "Islet isolation for clinical transplantation.," *Adv. Exp. Med. Biol.*, vol. 654, pp. 683–710, Jan. 2010.

[156] I. Matsumoto *et al.*, "Improvement in islet yield from obese donors for human islet transplants.," *Transplantation*, vol. 78, no. 6, pp. 880–5, Sep. 2004.

[157] S. C. Hanley, S. Paraskevas, and L. Rosenberg, "Donor and isolation variables predicting human islet isolation success.," *Transplantation*, vol. 85, no. 7, pp. 950–5, Apr. 2008.

[158] R. Nano *et al.*, "Islet isolation for allotransplantation: variables associated with successful islet yield and graft function.," *Diabetologia*, vol. 48, no. 5, pp. 906–12, May 2005.

[159] T. Berney and P. R. V Johnson, "Donor pancreata: evolving approaches to

organ allocation for whole pancreas versus islet transplantation.," *Transplantation*, vol. 90, no. 3, pp. 238–43, Aug. 2010.

[160] D. E. Hilling, E. Bouwman, O. T. Terpstra, and P. J. Marang-van de Mheen, "Effects of donor-, pancreas-, and isolation-related variables on human islet isolation outcome: a systematic review.," *Cell Transplant.*, vol. 23, no. 8, pp. 921–8, Jan. 2014.

[161] A. N. Balamurugan *et al.*, "Islet product characteristics and factors related to successful human islet transplantation from the Collaborative Islet Transplant Registry (CITR) 1999-2010.," *Am. J. Transplant*, vol. 14, no. 11, pp. 2595–606, Nov. 2014.

[162] D. Ridgway, D. Manas, J. Shaw, and S. White, "Preservation of the donor pancreas for whole pancreas and islet transplantation.," *Clin. Transplant.*, vol. 24, no. 1, pp. 1–19, Jan. 2010.

[163] H. Miyake *et al.*, "Association of fatty pancreas with pancreatic endocrine and exocrine function," *PLoS One*, vol. 13, no. 12, p. e0209448, Dec. 2018.

[164] P. Y. Benhamou *et al.*, "Human islet isolation in 104 consecutive cases. Factors affecting isolation success.," *Transplantation*, vol. 57, no. 12, pp. 1804–10, Jun. 1994.

[165] H. Brandhorst, D. Brandhorst, B. J. Hering, K. Federlin, and R. G. Bretzel, "Body Mass Index of Pancreatic Donors: A Decisive Factor for Human Islet Isolation," *Exp. Clin. Endocrinol. Diabetes*, vol. 103, no. S 02, pp. 23–26, Jul. 1995.

[166] S.-H. Ihm, "Effect of Donor Age on Function of Isolated Human Islets," *Diabetes*, vol. 55, no. 5, pp. 1361–1368, May 2006.

[167] C. Reers *et al.*, "Impaired islet turnover in human donor pancreata with aging.," *Eur. J. Endocrinol.*, vol. 160, no. 2, pp. 185–91, Feb. 2009.

[168] N. Niclauss *et al.*, "Influence of donor age on islet isolation and transplantation outcome.," *Transplantation*, vol. 91, no. 3, pp. 360–6, Feb. 2011.

[169] U. Boggi *et al.*, "Pancreas transplants from donors aged 45 years or older.," *Transplant. Proc.*, vol. 37, no. 2, pp. 1265–7, Mar. 2005.

[170] R. P. H. Meier *et al.*, "Islet of Langerhans isolation from pediatric and juvenile donor pancreases.," *Transpl. Int.*, vol. 27, no. 9, pp. 949–55, Sep. 2014.

[171] G. H. Wolters, G. H. Vos-Scheperkeuter, H. C. Lin, and R. van Schilfgaarde, "Different roles of class I and class II Clostridium histolyticum collagenase in rat pancreatic islet isolation.," *Diabetes*, vol. 44, no. 2, pp. 227–33, Feb. 1995.

[172] U. Eckhard, E. Schönauer, D. Nüss, and H. Brandstetter, "Structure of collagenase G reveals a chew-and-digest mechanism of bacterial collagenolysis.," *Nat. Struct. Mol. Biol.*, vol. 18, no. 10, pp. 1109–14, Oct. 2011.

[173] S. E. Cross, S. J. Hughes, C. J. Partridge, A. Clark, D. W. R. Gray, and P. R. V

Johnson, “Collagenase penetrates human pancreatic islets following standard intraductal administration.,” *Transplantation*, vol. 86, no. 7, pp. 907–11, Oct. 2008.

[174] M. J. Barnett, X. Zhai, D. F. LeGatt, S. B. Cheng, A. M. J. Shapiro, and J. R. T. Lakey, “Quantitative assessment of collagenase blends for human islet isolation.,” *Transplantation*, vol. 80, no. 6, pp. 723–8, Sep. 2005.

[175] T. Kin, X. Zhai, T. B. Murdoch, A. Salam, A. M. J. Shapiro, and J. R. T. Lakey, “Enhancing the success of human islet isolation through optimization and characterization of pancreas dissociation enzyme.,” *Am. J. Transplant*, vol. 7, no. 5, pp. 1233–41, May 2007.

[176] T. Kin, X. Zhai, D. O’Gorman, and A. M. J. Shapiro, “Detrimental effect of excessive collagenase class II on human islet isolation outcome,” *Transpl. Int.*, vol. 21, no. 11, p. ???-???, Jul. 2008.

[177] H. Brandhorst *et al.*, “The ratio between collagenase class I and class II influences the efficient islet release from the rat pancreas.,” *Transplantation*, vol. 85, no. 3, pp. 456–61, Feb. 2008.

[178] G. H. Wolters, G. H. Vos-Scheperkeuter, J. H. van Deijnen, and R. van Schilfgaarde, “An analysis of the role of collagenase and protease in the enzymatic dissociation of the rat pancreas for islet isolation.,” *Diabetologia*, vol. 35, no. 8, pp. 735–42, Aug. 1992.

[179] H. Brandhorst, M. D. Brendel, M. Eckhard, R. G. Bretzel, and D. Brandhorst, “Influence of neutral protease activity on human islet isolation outcome.,” *Transplant. Proc.*, vol. 37, no. 1, pp. 241–2, Jan. 2005.

[180] T. Kin *et al.*, “Nonsimultaneous Administration of Pancreas Dissociation Enzymes During Islet Isolation,” *Transplantation*, vol. 87, no. 11, pp. 1700–1705, Jun. 2009.

[181] Y.-Z. Zhang, L.-Y. Ran, C.-Y. Li, and X.-L. Chen, “Diversity, Structures, and Collagen-Degrading Mechanisms of Bacterial Collagenolytic Proteases.,” *Appl. Environ. Microbiol.*, vol. 81, no. 18, pp. 6098–107, Sep. 2015.

[182] A. J. Barrett, N. D. Rawlings, and J. F. Woessner, *Handbook of proteolytic enzymes*. Elsevier Academic Press, 2004.

[183] T. Berney *et al.*, “Endotoxin-mediated delayed islet graft function is associated with increased intra-islet cytokine production and islet cell apoptosis.,” *Transplantation*, vol. 71, no. 1, pp. 125–32, Jan. 2001.

[184] J. R. Lakey, T. J. Cavanagh, M. A. Zieger, and M. Wright, “Evaluation of a purified enzyme blend for the recovery and function of canine pancreatic islets.,” *Cell Transplant.*, vol. 7, no. 4, pp. 365–72, 1998.

[185] J. Caballero-Corbalán *et al.*, “Vitacyte collagenase HA: a novel enzyme blend for efficient human islet isolation.,” *Transplantation*, vol. 88, no. 12, pp. 1400–2, Dec. 2009.

[186] A. N. Balamurugan *et al.*, "A New Enzyme Mixture to Increase the Yield and Transplant Rate of Autologous and Allogeneic Human Islet Products," *Transplantation*, vol. 93, no. 7, pp. 693–702, Apr. 2012.

[187] G. L. Szot *et al.*, "Successful clinical islet isolation using a GMP-manufactured collagenase and neutral protease.," *Transplantation*, vol. 88, no. 6, pp. 753–6, Sep. 2009.

[188] H. Brandhorst, P. R. V Johnson, O. Korsgren, and D. Brandhorst, "Quantifying the Effects of Different Neutral Proteases on Human Islet Integrity.," *Cell Transplant.*, vol. 26, no. 11, pp. 1733–1741, 2017.

[189] Y. Zongyi, Z. Funian, L. Hao, C. Ying, Z. Jialin, and L. Baifeng, "A rapid, efficient, and economic device and method for the isolation and purification of mouse islet cells.," *PLoS One*, vol. 12, no. 2, p. e0171618, 2017.

[190] T. Alanentalo *et al.*, "Tomographic molecular imaging and 3D quantification within adult mouse organs.," *Nat. Methods*, vol. 4, no. 1, pp. 31–3, Jan. 2007.

[191] U. Ahlgren and M. Gotthardt, "Approaches for imaging islets: recent advances and future prospects.," *Adv. Exp. Med. Biol.*, vol. 654, pp. 39–57, Jan. 2010.

[192] W. R. Zipfel, R. M. Williams, R. Christie, A. Y. Nikitin, B. T. Hyman, and W. W. Webb, "Live tissue intrinsic emission microscopy using multiphoton-excited native fluorescence and second harmonic generation.," *Proc. Natl. Acad. Sci. U. S. A.*, vol. 100, no. 12, pp. 7075–80, Jun. 2003.

[193] Z. Huang, S. Zhuo, J. Chen, R. Chen, and X. Jiang, "Multiphoton microscopic imaging of adipose tissue based on second-harmonic generation and two-photon excited fluorescence.," *Scanning*, vol. 30, no. 6, pp. 452–6, Jan. 2008.

[194] M. Strupler *et al.*, "Second harmonic imaging and scoring of collagen in fibrotic tissues," *Opt. Express*, vol. 15, no. 7, p. 4054, 2007.

[195] G. A. Blab, P. H. . Lommerse, L. Cognet, G. S. Harms, and T. Schmidt, "Two-photon excitation action cross-sections of the autofluorescent proteins," *Chem. Phys. Lett.*, vol. 350, no. 1–2, pp. 71–77, Dec. 2001.

[196] L. Gailhouste *et al.*, "Fibrillar collagen scoring by second harmonic microscopy: a new tool in the assessment of liver fibrosis.," *J. Hepatol.*, vol. 52, no. 3, pp. 398–406, Mar. 2010.

[197] K. König, K. Schenke-Layland, I. Riemann, and U. A. Stock, "Multiphoton autofluorescence imaging of intratissue elastic fibers.," *Biomaterials*, vol. 26, no. 5, pp. 495–500, Feb. 2005.

[198] J. Chen *et al.*, "Spectroscopic characterization and microscopic imaging of extracted and in situ cutaneous collagen and elastic tissue components under two-photon excitation.," *Skin Res. Technol.*, vol. 15, no. 4, pp. 418–26, Nov. 2009.

[199] Y. Wu and J. Y. Qu, "Two-photon autofluorescence spectroscopy and second-harmonic generation of epithelial tissue," *Opt. Lett.*, vol. 30, no. 22, p. 3045,

Nov. 2005.

[200] C. Pitsillides, J. M. Runnels, D. Côté, and C. P. Lin, “Multiphoton Microscopy of Live Tissues With Ultraviolet Autofluorescence,” *IEEE J. Sel. Top. Quantum Electron.*, vol. 16, no. 3, pp. 516–523, 2010.

[201] J. C. Stendahl, D. B. Kaufman, and S. I. Stupp, “Extracellular Matrix in Pancreatic Islets: Relevance to Scaffold Design and Transplantation,” *Cell Transplant.*, vol. 18, no. 1, pp. 1–12, Jan. 2009.

[202] J. Daoud, M. Petropavlovskaia, L. Rosenberg, and M. Tabrizian, “The effect of extracellular matrix components on the preservation of human islet function in vitro.,” *Biomaterials*, vol. 31, no. 7, pp. 1676–82, Mar. 2010.

[203] P. Bedossa, G. Lemaigre, J. Bacci, and E. Martin, “Quantitative Estimation of the Collagen Content in Normal and Pathologic Pancreas Tissue,” *Digestion*, vol. 44, no. 1, pp. 7–13, 1989.

[204] A. J. Bailey, R. G. Paul, and L. Knott, “Mechanisms of maturation and ageing of collagen.,” *Mech. Ageing Dev.*, vol. 106, no. 1–2, pp. 1–56, Dec. 1998.

[205] G. Loganathan *et al.*, “Improved recovery of human islets from young donor pancreases utilizing increased protease dose to collagenase for digesting peri-islet extracellular matrix,” *Am. J. Transplant.*, vol. 19, no. 3, pp. 831–843, Mar. 2019.

[206] H. Brandhorst *et al.*, “The importance of tryptic-like activity in purified enzyme blends for efficient islet isolation.,” *Transplantation*, vol. 87, no. 3, pp. 370–5, Feb. 2009.

[207] J. A. M. S. A. M. James Shapiro, *Islet Transplantation and Beta Cell Replacement Therapy*. CRC Press, 2007.

[208] S. E. Cross, S. J. Hughes, A. Clark, D. W. R. Gray, and P. R. V Johnson, “Collagenase does not persist in human islets following isolation.,” *Cell Transplant.*, vol. 21, no. 11, pp. 2531–5, Jan. 2012.

[209] H. S., C. S., G. D., C. A., and J. P., “Development of an assay for the detailed study of collagenase-digestion within the islet-exocrine interface of the human pancreas,” *Xenotransplantation*, vol. 14, pp. 485–485, 2007.

[210] M. Shimoda *et al.*, “Improved method of human islet isolation for young donors.,” *Transplant. Proc.*, vol. 42, no. 6, pp. 2024–6, Jul. 2010.

[211] P. Bucher *et al.*, “Optimization of neutral protease to collagenase activity ratio for islet of langerhans isolation,” *Transplant. Proc.*, vol. 36, no. 4, pp. 1145–1146, May 2004.

[212] L. Shi, R. Ermis, A. Garcia, D. Telgenhoff, and D. Aust, “Degradation of human collagen isoforms by *Clostridium* collagenase and the effects of degradation products on cell migration,” *Int. Wound J.*, vol. 7, no. 2, pp. 87–95, Apr. 2010.

[213] R. A. Heller-Harrison and W. G. Carter, “Pepsin-generated type VI collagen is

a degradation product of GP140.," *J. Biol. Chem.*, vol. 259, no. 11, pp. 6858–64, Jun. 1984.

[214] F. Hayase, R. H. Nagaraj, S. Miyata, F. G. Njoroge, and V. M. Monnier, "Aging of proteins: immunological detection of a glucose-derived pyrrole formed during maillard reaction in vivo.," *J. Biol. Chem.*, vol. 264, no. 7, pp. 3758–64, Mar. 1989.

[215] T. Kin, D. O'Gorman, P. Senior, and A. J. Shapiro, "Experience of islet isolation without neutral protease supplementation," *Islets*, vol. 2, no. 5, pp. 278–282, Sep. 2010.

[216] P. A. Piemonti L., "25 Years of the Ricordi Automated Method for Islet Isolation," *CellR4*, vol. 1, no. (1), p. e128, 2013.

[217] A. N. Balamurugan, Y. Chang, J. J. Fung, M. Trucco, and R. Bottino, "Flexible management of enzymatic digestion improves human islet isolation outcome from sub-optimal donor pancreata.," *Am. J. Transplant.*, vol. 3, no. 9, pp. 1135–42, Sep. 2003.

[218] C. Ricordi, E. H. Finke, and P. E. Lacy, "A method for the mass isolation of islets from the adult pig pancreas.," *Diabetes*, vol. 35, no. 6, pp. 649–53, Jun. 1986.

[219] C. Ricordi *et al.*, "Islet isolation assessment in man and large animals.," *Acta Diabetol. Lat.*, vol. 27, no. 3, pp. 185–95.

[220] S. Paraskevas, D. Maysinger, R. Wang, W. P. Duguid, and L. Rosenberg, "Cell Loss in Isolated Human Islets Occurs by Apoptosis," *Pancreas*, vol. 20, no. 3, pp. 270–276, Apr. 2000.

[221] J. H. M. Van Deijnen, P. T. R. Van Suylichem, G. H. J. Wolters, and R. Van Schilfgaarde, "Distribution of collagens type I, type III and type V in the pancreas of rat, dog, pig and man," *Cell Tissue Res.*, vol. 277, no. 1, pp. 115–121, Jul. 1994.

[222] J. H. M. van Deijnen, C. E. Hulstaert, G. H. J. Wolters, and R. van Schilfgaarde, "Significance of the peri-insular extracellular matrix for islet isolation from the pancreas of rat, dog, pig, and man," *Cell Tissue Res.*, vol. 267, no. 1, pp. 139–146, Jan. 1992.

[223] Y. Yonekawa *et al.*, "Effective Islet Isolation Method with Extremely High Islet Yields from Adult Pigs," *Cell Transplant.*, vol. 14, no. 10, pp. 757–762, Nov. 2005.

[224] J. J. O'neil, J. P. Stegemann, D. T. Nicholson, K. A. Gagnon, B. A. Solomon, and C. J.-P. Mullon, "The Isolation and Function of Porcine Islets from Market Weight Pigs," *Cell Transplant.*, vol. 10, no. 3, pp. 235–246, Apr. 2001.

[225] H. Brandhorst, P. R. V. Johnson, and D. Brandhorst, "Pancreatic Islets: Methods for Isolation and Purification of Juvenile and Adult Pig Islets," in *Advances in experimental medicine and biology*, vol. 938, 2016, pp. 35–55.

[226] K. Ulrichs *et al.*, “Histomorphological characteristics of the porcine pancreas as a basis for the isolation of islets of Langerhans,” *Xenotransplantation*, vol. 2, no. 3, pp. 176–187, Aug. 1995.

[227] B. E. Tuch, S. Y. Gao, and J. G. Lees, “Scaffolds for islets and stem cells differentiated into insulin-secreting cells.,” *Front. Biosci. (Landmark Ed.*, vol. 19, pp. 126–38, Jan. 2014.

[228] J. P. Vacanti and R. Langer, “Tissue engineering: the design and fabrication of living replacement devices for surgical reconstruction and transplantation.,” *Lancet (London, England)*, vol. 354 Suppl, pp. SI32-4, Jul. 1999.

[229] R. F. Gibly, X. Zhang, W. L. Lowe, and L. D. Shea, “Porous scaffolds support extrahepatic human islet transplantation, engraftment, and function in mice.,” *Cell Transplant.*, vol. 22, no. 5, pp. 811–9, Jan. 2013.

[230] H. Blomeier *et al.*, “Polymer scaffolds as synthetic microenvironments for extrahepatic islet transplantation.,” *Transplantation*, vol. 82, no. 4, pp. 452–9, Aug. 2006.

[231] J. T. Daoud *et al.*, “Long-term in vitro human pancreatic islet culture using three-dimensional microfabricated scaffolds.,” *Biomaterials*, vol. 32, no. 6, pp. 1536–42, Feb. 2011.

[232] T. L. Y. Murat Elçin, A. Eser Elçin, Reinhardt G. Bretzel, *Tissue Engineering, Stem Cells, and Gene Therapies*, vol. 534. Boston, MA: Springer US, 2003.

[233] H. Baharvand, S. M. Hashemi, S. Kazemi Ashtiani, and A. Farrokhi, “Differentiation of human embryonic stem cells into hepatocytes in 2D and 3D culture systems in vitro.,” *Int. J. Dev. Biol.*, vol. 50, no. 7, pp. 645–52, Jan. 2006.

[234] B. Zavan, R. Cortivo, C. Tonello, and G. Abatangelo, “Gland cell cultures into 3D hyaluronan-based scaffolds.,” *J. Mater. Sci. Mater. Med.*, vol. 14, no. 8, pp. 727–9, Aug. 2003.

[235] S.-K. Goh *et al.*, “Perfusion-decellularized pancreas as a natural 3D scaffold for pancreatic tissue and whole organ engineering.,” *Biomaterials*, vol. 34, no. 28, pp. 6760–72, Sep. 2013.

Appendices

7.1 Antibodies used in staining experiments

Primary Antibody	Supplier	Host	Dilution	Secondary Antibody
Collagen I	Abcam: Ab34710	Polyclonal Rabbit	1:500	Polyclonal goat anti-rabbit Alexa 488 (Invitrogen: A11034) 1:500
Collagen III	Abcam: Ab7778	Polyclonal Rabbit	1:500	
Collagen IV	Abcam: Ab6588	Polyclonal Rabbit	1:500	
Collagen VI	Abcam: Ab6588	Polyclonal Rabbit	1:500	
Pan-Laminin	Abcam: Ab11575	Polyclonal Rabbit	1:300	
Perlecan (HSPG2)	Abcam: Ab23418	Monoclonal Mouse	1:500	Horse anti-mouse FITC (Vectorlabs: DK-8828) 1:50
Insulin	Dako: IR002	Polyclonal Guinea Pig	1:100	Polyclonal goat anti-Guinea pig Texas Red (Vectorlabs: TI-1000) 1:100
CD31	Dako: M0823	Monoclonal mouse	1:25	AMCA-conjugated horse anti-mouse IgG (Vectorlab: CI-2000) 1:50

7.2 Macros used for image analyses

```
//B&C control
run("Duplicate...", "title=Base duplicate");
run("32-bit");
run("HiLo");
setSlice(40);
run("Brightness/Contrast...");
waitForUser("Adjust Brightness/Contrast");
selectWindow("B&C");
run("Close");

//Background
setSlice(40);
setTool("freehand");
waitForUser("Select all ROI");
roiManager("Add");
run("Clear Outside", "stack");
selectWindow("ROI Manager");
roiManager("Delete");
run("Select None");
run("Close");

setTool("Line");
waitForUser("Draw an line to measure background");
run("Measure");
selectWindow("Results");
c=getResult("Mean", 0);
print(c);

waitForUser("Subtract value");
run("Grays");
selectWindow("Log");
run("Close");
selectWindow("Results");
run("Clear Results");

//Threshold
run("Duplicate...", "title=[For Threshold] duplicate");
run("8-bit");
run("Auto Threshold", "method=Default white stack");

//Analysis
run("Make Binary", "method=Default background=Light calculate");
run("Invert", "stack");
run("Analyze Particles...", "size=15.00-50000.00 show=Outlines display include summarize add stack");

//Close
selectWindow("For Threshold");
run("Close");
```

Figure 7.1 Macro for start/preparation stage

```
//Merge & Measure
selectWindow("Base")
run("Duplicate...", "title=Binary duplicate");
run("Subtract...", "value=254 stack");
selectWindow("ROI Manager")
run("Select All");
run("Enlarge...", "enlarge=0.05");
setForegroundColor(255, 255, 255);
roiManager("Draw");
roiManager("Fill");
roiManager("Show None");

run("Invert", "stack");
run("Merge Channels...", "c1=Base c2=Binary keep");
imageCalculator("Subtract create stack", "RGB","Binary");

//Close
selectWindow("Base");
run("Close");
selectWindow("RGB");
run("Close");
selectWindow("Result of RGB");
rename("Whole Islet Threshold");

//Save
waitForUser("Save Image window for intensity measurement");

//Detailed Analysis
selectWindow("Results");
run("Clear Results");
selectWindow("ROI Manager");
run("Close");
selectWindow("Summary of For Threshold");
run("Close");

//Threshold
run("Duplicate...", "title=[For Measurement] duplicate");
run("8-bit");
run("Auto Threshold", "method=Default white stack");

//Analysis
run("Make Binary", "method=Default background=Light calculate");
run("Invert", "stack");
run("Analyze Particles...", "size=15.00-50000.00 show=Outlines display include summarize add stack");
selectWindow("ROI Manager");
run("Close");

//Save data
waitForUser("Save summary window");
waitForUser("Save results window");
selectWindow("For Measurement");
run("Close");

```

Figure 7.2 Macro for islet area & intensity measurement

```
//2ND Channel
waitForUser("Select Protein Channel");

//B&C control
run("Duplicate...", "title=Base duplicate");
run("32-bit");
run("HiLo");
setSlice(40);
run("Brightness/Contrast...");
waitForUser("Adjust Brightness/Contrast");
selectWindow("B&C");
run("Close");

//Background
setSlice(40);

setTool("Line");
waitForUser("Draw an line to measure background");
run("Measure");
selectWindow("Results");
c=getResult("Mean", 0);
print(c);

waitForUser("Subtract value");
run("Grays");
selectWindow("Log");
run("Close");
selectWindow("Results");
run("Clear Results");

//Merge
run("Merge Channels...", "c1=Base c2=Binary keep");
imageCalculator("Subtract create stack", "RGB","Binary");
run("32-bit");
run("Green");
run("RGB Color");

//Close
selectWindow("Base");
run("Close");
selectWindow("RGB");
run("Close");
selectWindow("Result of RGB");
rename("Whole Protein Threshold");

//Save
waitForUser("Save Image window for intensity measurement");

//Threshold
run("Duplicate...", "title=[For Measurement] duplicate");
run("8-bit");
run("Auto Threshold", "method=Default white stack");


//Analysis
run("Make Binary", "method=Default background=Light calculate");
run("Invert", "stack");
run("Analyze Particles...", "size=15.00-50000.00 show=Outlines display include summarize add stack");
selectWindow("ROI Manager");
run("Close");

//Save data
waitForUser("Save summary window");
waitForUser("Save results window");
selectWindow("For Measurement");
run("Close");
```

Figure 7.3 Macro for protein area & intensity measurement

7.3 Performance of bioreactor & comparison with Ricordi chamber

Isolation ID	CIT (h)	Pancreas weight (g)	Tests	Digested tissue (%)	Yield (*1000 IEQ)	Islet number (*1000)	IEQ/g Pancreas	Purity (%)	Viability (%)
1	5	207	Bioreactor	54	236±49	40±8	1143±238	60	45±5
2	5	62	Bioreactor	58	200±44	29±5	3226±703	40	45±5
3	7	61	Bioreactor	56	160±34	35±5	2623±568	40	43±3
4	7	177	Bioreactor	52	290±44	45±5	1638±246	55	42±6
5	9	104	Bioreactor	53	150±44	27±5	1442±419	55	42±3
6	6	147	Bioreactor	46	223±50	48±8	1519±335	55	42±6
7	10	121	Ricordi chamber	47	160±10	72±8	1322±83	50	42±8
8	5	108	Ricordi chamber	48	156±15	69±12	1451±141	55	45±5
9	7	139	Ricordi chamber	52	170±26	80±21	1223±190	60	38±3